Renewable hydrogen production by aqueous phase reforming of oxygenated biomass over hydrotalcite derived Ni/Mg/Al catalysts

AMAN NAGORI

Renewable hydrogen production by aqueous phase reforming of oxygenated biomass over hydrotalcite derived Ni/Mg/Al catalysts

Department of Chemistry, Durham University

2021 – 2022

Thesis submitted for the degree of master's by research

By

Aman Nagori

Under the supervision of

Dr. Simon Beaumont

(Associate Professor, Department of Chemistry, Durham University)

Abstract

The conversion, selectivity for hydrogen, and stability of different Ni based hydrotalcite derived catalysts were studied in aqueous phase reforming of ethylene glycol and phenol and were benchmarked against Ni/γ-Al_2O_3 and commercial 5 wt.% Pt/C and 5 wt.% Pd/C. Hydrotalcite catalysts were given a nomenclature as aNib, were 'a' is M^{2+}/M^{3+} ratio and 'b' is Ni loading. The highest conversion obtained was for 3Ni20 catalyst giving a mass activity of 24.4 mmol of substrate per g of catalyst (38% conversion), which was similar to the mass activity of commercial 5 wt.% Pt/C and 5 wt.% Pd/C catalyst. However, selectivity for hydrogen of commercial catalysts was at least 1.5 times more than 3Ni20. The highest selectivity for hydrogen for hydrotalcite derived catalyst was obtained with 8Ni15 catalyst, which was similar to the selectivity obtained by Pt/C, however, mass activity of 8Ni15 was only 11.5 mmol of substrate per g of catalyst. With an increase in Ni loading in Ni-hydrotalcite derived catalysts (keeping the M^{2+}/M^{3+} ratio constant) conversion of ethylene glycol increased (3Ni5 < 3Ni10 < 3Ni15 < 3Ni20) but the selectivity towards hydrogen decreased (3Ni5 > 3Ni10 > 3Ni15 > 3Ni20). With an increase in $M^{2+}/^{3+}$ ratio (keeping Ni loading constant) conversion of ethylene glycol decreased (2Ni15 > 3Ni15 > 6Ni15 > 8Ni15) but the selectivity to hydrogen increased (2Ni15 < 3Ni15 < 6Ni15 < 8Ni15). Monometallic Ni/γ-Al_2O_3 demonstrated poorer selectivity compared to all hydrotalcite derived catalysts. Post reaction pXrd patterns showed that the hydrotalcite structure was changed to a spinel structure (in case of hydrotalcite derived catalysts) and boehmite in case of Ni/γ-Al_2O_3. Ni leaching was lower in hydrotalcite derived catalysts as compared to monometallic Ni/γ-Al_2O_3, except for sample 8Ni15, indicating that higher Mg content can negatively affect catalyst stability. Spent 2Ni15, 3Ni20 and Pd/C were re-tested in APR of ethylene glycol. For hydrotalcite derived catalysts, conversion dropped by 50% as compared to fresh catalyst while conversion remained almost same in Pd/C. Selectivity for hydrogen of spent and fresh catalysts were almost same. The major reason for deactivation was leaching of Ni. With the increase in reduction temperature, conversion increased but the selectivity dropped. In case of aqueous phase reforming of phenol, no conversion of phenol was observed with any catalyst and consequently, no hydrogen was produced, in contrast to literature reports.

Declaration

This thesis is based on work carried out by the author in the Department of Chemistry at Durham University, during the period January 2021 – May 2022. All of the work detailed in this thesis is original, unless specifically acknowledged in the text or references. None of this work has been submitted for another degree in this or any other university.

Copyright

Acknowledgment

I would like thank Dr. Simon Beaumont for helping me throughout the project. I would also like to thank Beaumont group lab members (Dr. Kathryn, Dr. Andrea, Dr. Li Li, Nargiz, Amy, Zixuan, Majed, Eder) for their endless support whenever I needed it and keeping the environment of the lab cheerful. I would also like to thank Dr.Philip W. Dyer and Dr. Russell A. Taylor for their advice and safety cover in absence of Dr. Beaumont. I would also like to thank the management and analytical staff members at Durham University for their support and running the samples when I needed.

Lastly, I would like to thank my family for the endless love and support they provided during this project and beyond.

This thesis is dedicated to my late grandfather Mr. Shantilal Nagori who unfortunately passed away in my absence, when I was working on this project abroad.

Index

List of figures

List of tables

Chapter 1: Introduction

Ever increasing energy demand and rising global pollution level means there's an urgent need to develop more sustainable energy sources. Hydrogen as a fuel is light, colourless and odourless, has a high calorific value and theoretically gives clean emissions. However, before hydrogen can be used as a mainstream fuel, it needs to be produced sustainably. Currently 95% of the total hydrogen is produced from fossil fuels.[1] One of the methods to produce clean, renewable hydrogen from sustainable resources is aqueous phase reforming. Aqueous phase reforming is a method of producing a gaseous mixture rich in hydrogen alongside light liquid hydrocarbons from dilute aqueous waste streams of oxygenated biomass (e.g., ethylene glycol, glycerol, sorbitol, ethanol etc.) over heterogeneous catalysts in liquid phase at high pressure (30-60 bar) and moderate temperatures (220-280 °C). However, currently there are two challenges in aqueous phase reforming which limits its scalability. Firstly, hydrogen can only be produced through a very selective route. Competing pathways produce more liquid hydrocarbons (which have insignificant economic value), and also consumes the produced hydrogen in-side reactions such as methanation, Fischer-Tropsch reactions and hydrogenation of liquid hydrocarbons, thus decreasing the selectivity for hydrogen. Secondly, the hydrothermal conditions of the reaction affect the stability of catalyst. Hence, there's a need to design a stable and hydrogen selective catalyst for aqueous phase reforming. Most reports reported that Pt/Al_2O_3 is a stable and selective catalyst. However, the cost of platinum makes the whole APR process expensive and difficult to scale-up. Recent attention has been drawn to nickel-based catalysts because of their high activity in C-C bond scission, promotion of the water-gas shift reaction and low cost. However, monometallic Ni/Al_2O_3 catalysts suffered from stability issues (leaching, sintering and carbonaceous deposits) and are not selective towards hydrogen production. Hence, there is a need to incorporate a basic metal and make a matrix that can help the nickel to be more stable and selective towards hydrogen production. Layered double hydroxide (LDH) / hydrotalcites provide an excellent route to incorporate nickel into a matrix of oxides of Mg and Al in a controlled way. Layered double hydroxides (LDHs), also known as hydrotalcite-like materials, are a class of two-dimensional (2D) anionic clays consisting of positively charged host layers and exchangeable interlayer anions. The structure is like brucite [$Mg(OH)_2$], where Mg^{2+} ions occupy octahedral positions and form infinite layers connected by hydrogen bonds.[2] In Mg-Al LDH, some Mg^{2+} ions are substituted by Al^{3+} ions and produced an excess positive charge which is compensated by carbonate anions present in the interlayer space. The general formula of LDH is $[M^{2+}_{1-x}M^{3+}_{x}(OH)_2]^{x+}$ $[A^{n-}_{x/n}]\cdot mH2O$,

where M^{2+} is a divalent cation, M^{3+} is a trivalent cation, and A^{n-} is the anion. Further, some of the Mg in the layered double hydroxide structure is isomorphously replaced by Ni, hence no extra phase is observed in pXrd. When these double hydroxides are calcined and reduced, they yield a hydrotalcite derived catalyst Ni/MgO-Al_2O_3 with high surface area. The basicity of the catalyst and particle size of nickel can be adjusted by varying the Ni wt% and molar ratio of bivalent (Mg+Ni) to trivalent (Al) metals (M^{2+} /M^{3+}) in the LDH. Changing the concentration of metals have effect on its basicity, reducibility, and stability, which in turn effects activity and selectivity of the catalysts. These catalysts are proven to be highly stable and active in various reforming reactions.[3-5] There is some literature available for use of hydrotalcite derived catalysts in aqueous phase reforming, mostly concentrating on adding a fourth metal or using a different preparation route as compared to the much-used co-precipitation method. However, there is a lack of systematic study on effect of M^{2+}/M^{3+} ratio on APR catalyst activity and selectivity, catalyst deactivation, quantification and importantly (given nickel catalysts in general for APR) comparison of leaching and effect of reduction temperature on catalyst activity and selectivity.

1.1 Literature review

1.1.1 Energy Demand

From the beginning of the industrial revolution in the mid-eighteenth century until today, steam powdered trains and ships and later, internal combustion engines aided people to produce and export goods around the world. This transition from horse-power to horsepower was derived largely from our ability to exploit fossil fuels. Coupling this with the increase in population from around 700 million at the beginning of industrial revolution to 7 billion today, has resulted in massive energy demands. To meet the energy demands, the consumption of fossil fuels increased year-by-year as evident from Figure 1. According to the International Energy Agency (Paris), the energy demand will increase from 12 billion tonne oil equivalents in 2009 to 18 billion tonne oil equivalents by 2035.[6] Currently, 65% of energy demand is satisfied by liquid and gaseous fossil fuels (petroleum, natural gas etc.).[7] In 2014, the transportation sector accounted for 18% energy usage with oil being the primary fuel source accounting for 95% of transport energy demand.[8] Sadly, when fossil fuels are burned, they emit harmful and polluting gases. A major part of the released gas is CO_2. Swedish Nobel prize winner, Svante Arrhenius was among those to theorize about the harmful impact of CO_2 on earth's climate. However, the theory initially met criticism and was not realised until the 1950s.[9] The temperature of the

Earth depends on a balance between incoming energy from the Sun and the energy that bounces back into space. Carbon dioxide absorbs heat that would otherwise be lost to space. Some of this energy is re-emitted back to Earth, causing additional heating of the planet. Carbon-dioxide emissions are expected to increase from 29 gigatonnes per year around 2009 to 43 gigatonnes per year around 2035.[6] In 2014, 17% of global CO_2 emissions came alone from the transportation sector.[8]

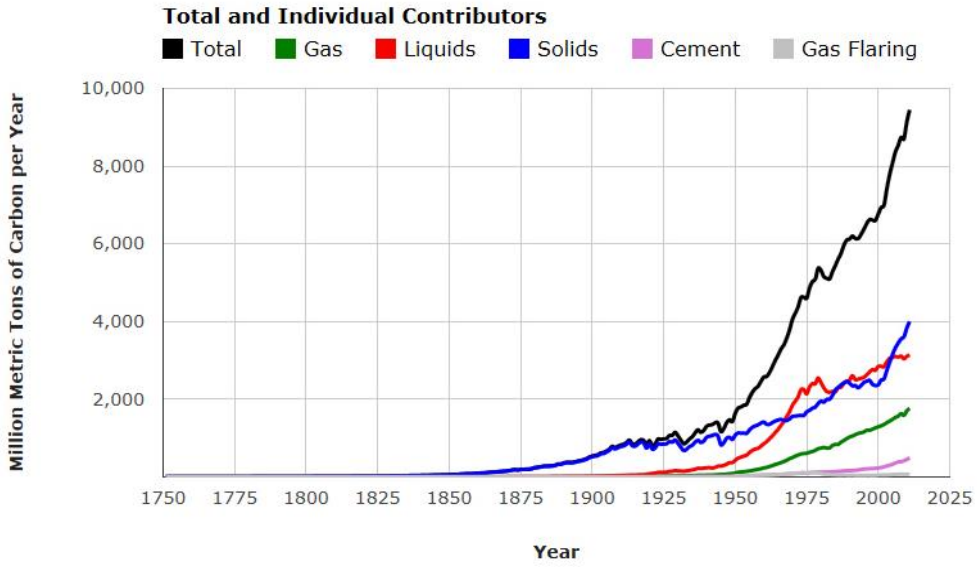

Figure 1: Global carbon emission from 1750 to 2010 , reproduced (without permission) from Boden et al.[10].

Using fossil fuels to fulfil the ever-growing energy demand, has created certain concerns:[11]

1. large CO_2 emissions from carbon-based fossil fuels resulting in anthropogenically induced climate change.
2. international vexing issue of fuel poverty and energy inequality due interconnected energy supply and political instability.
3. strong reliance between fossil fuels and economic growth.
4. depletion and extinction of the conventional fossil resources.

1.1.2 Hydrogen as fuel

To overcome these drawbacks and meet future energy demands, there is considerable international interest in the possibility of developing a hydrogen economy. Hydrogen energy use is hardly a novel idea, with interest in applications dating back to the 1800s. However, the confluence of factors including urban air pollution, CO_2 emissions and global climate change has resulted in a recent increase in attractions for hydrogen energy.[12] The main reasons for the growth of interest of hydrogen as fuel are clean (CO_2 and air pollutant free) emissions, it is the

lightest fuel, reasonably easy storage (colourless, odourless and non-toxic gas), high calorific value (34.0Kcal g^{-1}), and widespread availability.[13] Moreover, advances in fuel cell technology and direct use of H_2 in internal combustion engines have attracted significant attention.[7] Versatility of Hydrogen allows it to be converted into different forms of energy:

1. combustion.
2. conversion into steam.
3. conversion into heat through catalytic conversion.
4. as a heat source/sink through chemical reactions.
5. conversion into electricity through electrochemical processes.

However, before hydrogen can be used as a widespread energy source, there are major scientific, technical, and socio-economic challenges to overcome related to production, storage, and transportation of hydrogen.

1.1.3 Global hydrogen production

One of the major challenges in realizing a hydrogen economy is today over 95% of world hydrogen production is from fossil fuels (see Figure 2, 48% from natural gas, 30% from heavy oils and naphtha, and 18% from coal).[1] There are several technologies for producing hydrogen from fossil fuels, the main ones of which are hydrocarbon reforming, partial oxidation and pyrolysis.[1]

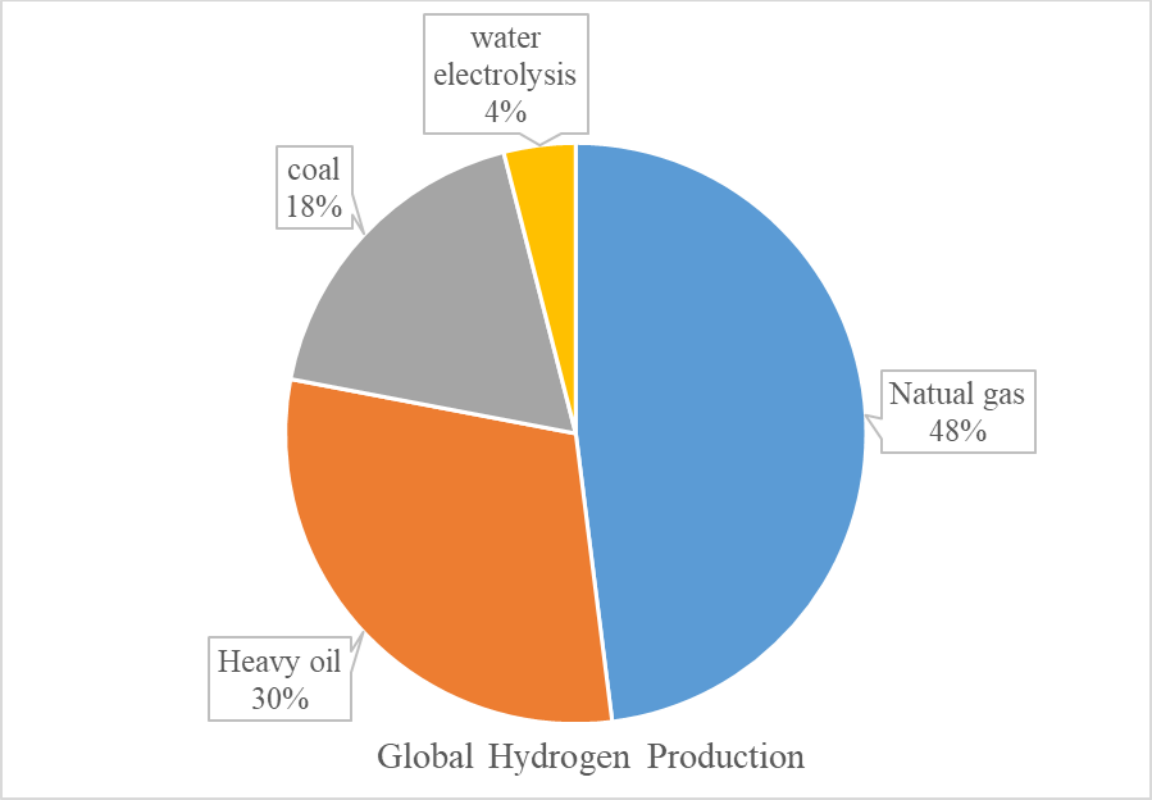

Figure 2: Global hydrogen production adapted from Nikolaidis et al.[1]

Hydrocarbon reforming is a process by which the hydrocarbon fuel is converted into hydrogen through reforming techniques. There are three main techniques used to produce hydrogen from hydrocarbon fuels: steam reforming (SR), partial oxidation (POX), and autothermal reforming (ATR).[1]

The process of SR involves a catalytic conversion of the hydrocarbon and steam to hydrogen and carbon oxides and consists of the main steps of reforming or synthesis gas (syngas) generation, water-gas shift (WGS) and methanation or gas purification.[14] Raw materials includes methane, natural gas, and other methane containing gases through various combinations of light hydrocarbons including ethane, propane, butane, pentane, and light and heavy naphtha.[15] The POX method involves the conversion of steam, oxygen and hydrocarbons to hydrogen and carbon oxides. The catalytic process occurs at about 950 °C, whereas the non-catalytic process occurs at 1150 °C–1315 °C. Feedstocks include methane, heavy oil and coal.[16] The ATR method uses the exothermic partial oxidation to provide the heat and endothermic steam reforming to increase the hydrogen production. Steam and oxygen or air, are injected into the reformer, causing the reforming and oxidation reactions to occur simultaneously.[1]

Hydrocarbon pyrolysis is a process in which the hydrocarbon undergoes thermal decomposition to produce hydrogen. Thermo-catalytic decomposition of light liquid hydrocarbons produces elemental carbon and hydrogen, whereas in the case of heavy residual fractions hydrogen is produced in a two-step scheme namely, hydrogasification and cracking of methane.[1]

1.1.4 Catalysts

Catalysts are an important class of materials, which can improve the overall sustainability of the above types of processes. A catalyst is a substance that increases the rate of chemical reaction without being consumed in the reaction or being part of the final products.[17] Catalytic processes were known to humans from dawn of civilization, for example fermentation of sugar to produce alcohol. The first documented use of an inorganic catalyst is by Valerius Cordus in 1552 when he used sulfuric acid to catalyse the conversion of alcohol to ether.[18] In early 19th Century Humphry Davy and his invention of the mining safety lamp, is considered to be the first clear indication of a chemical reaction occurring on a metal surface between two gaseous reactants, without the metal being affected.[19] Many other such processes were studied around that time by contemporary scientists including Antoine Augustin Parmentier (1737-1813) , Johann Wolfgang Döbereiner (1780-1849), Sigismund Konstantin Kirchhoff (1764-1833), Anselme Payen (1795-1871) Jean-François Persoz (1805-1868), Johann Rudolph Deiman (1743-1808), Adrien Paets von Trootswijk (1752-1837), Anthoni Lauwerenburg (1758-1820), Nicolas Bondt (1765-1796), Pieter Nieuwland (1764-1794) and many others.[20] The first time a catalyst was used in the industry was in 1746 by J. Hughes in the manufacture of lead chamber sulfuric acid.[21]

However, there were no significant efforts made to explain these phenomena. Jöns Jakob Berzelius (1779-1848) systematically investigated the recorded observations and proposed the term catalysis (Greek words kata meaning down and lyein meaning loosen) in 1835.[22] In his own words: “the property of exerting on other bodies an action which is very different from chemical affinity. By means of this action, they produce decomposition in bodies, and form new compounds into the composition of which they do not enter”.[20, 22] This resulted in the start of systematic research and discovery of new catalytic processes. It became quite evident that catalysis was useful in most chemical processes and financial gains was realized. By the end of the 19th century academic knowledge was translated into industrial applications. Today, catalysts have direct involvement in the production of 80% of industrially important chemicals

and involved in more than $10 trillion in goods and services of the global gross domestic product (GDP) annually with an estimate that the global demand on catalysts is more than $30 billion.[23] With the increasing energy and environmental concerns, one can expect a further rapidly expanding market for catalysts.

The importance of catalysis can be realized by the industrial example of essential nonsteroidal, anti-inflammatory painkillers. When Ibuprofen was initially developed in 1962, the production route consisted for six stoichiometric steps with overall atom economy of 40%. Later, it was replaced by a three-step catalytic process with overall atom economy of 77% and acetic acid as only by product. When methods for recovering and recycling acetic acid were developed, the atom utilization increased to 99% and it revolutionised the process pharmaceutical industry forever.[24]

Catalysts cannot change the thermodynamic equilibrium (thermal equilibrium, chemical equilibrium and mechanical equilibrium), but it changes the way equilibrium is reached. Hence catalysis is a kinetic phenomenon. The energy needed to start a reaction is called activation energy. A catalyst lowers the activation energy of a reaction as represented in Figure 3. [25-26]

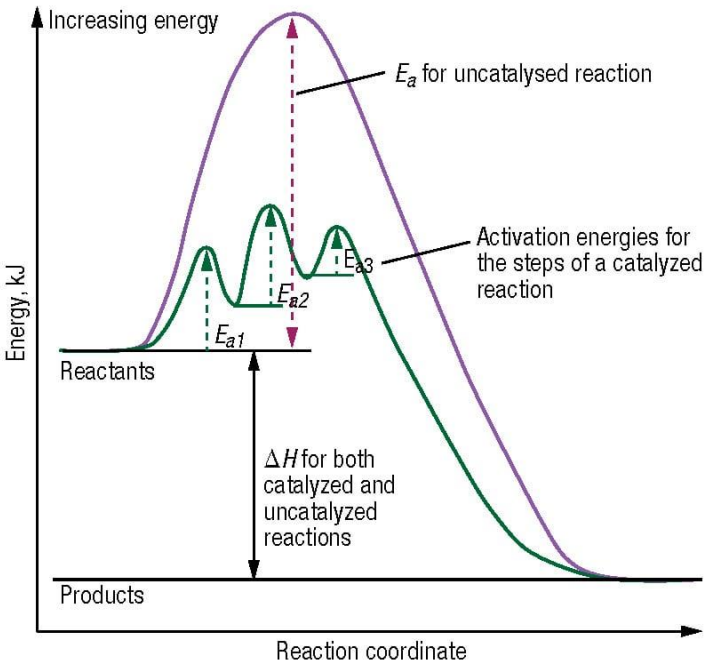

Figure 3: Energy vs. reaction coordinate for uncatalyzed and catalysed reaction reproduced (without permission) from Chorkendorff et al.[25].

A catalyst acts by lowering the activation energy by providing an alternative path to the reaction. Catalysts facilitate this by forming new temporary bonds between the reactants and catalyst

and breaking the existing bonds. After that new bonds are made, and the product is released by breaking of temporary bonds between reactants and catalyst. A catalytic route is made up of several steps and the product of each step between products and reactants is known as a catalytic intermediate. Since the bonds between the catalyst and reactants are broken at the end of the cycle, the catalyst is regenerated and ready for the next conversion. Thus only a small amount of catalyst is used in each reaction and is often recovered at the end of the reaction.[25-26] Since a catalyst lowers the activation energy, more molecular collisions have the energy needed to reach the transition state, which increases the reaction rate, selectivity of pathways with lowered activation energy, and enables the reaction at lower temperatures.[25-26]

Some important terminology in catalysis is highlighted as follows.

1. Activity: the ability of a catalyst to increase the rate of a chemical reaction is called its activity, and usually measured as mass activity – the moles of reactant converted per g of catalyst.

2. Selectivity: the ability of the catalyst to direct a reaction to yield a particular product is referred to as the selectivity of the catalyst.

3. Promotors: promoters are substances that increase the catalytic activity, even though they are not catalysts by themselves.

4. Inhibitors: added substances which reduce the reaction rate are reaction inhibitors.

5. Poisons: catalyst poisoning refers to the partial or total deactivation of a catalyst by a chemical compound.

6. Sintering: sintering is broadly termed as a physical and/or thermal phenomenon that leads to agglomeration of an active phase, a reduction in the surface to volume ratio of the catalyst. It normally results in the loss of active sites due to alteration of the catalyst's structure. Depending on the catalyst's type, it can either result in loss of active sites due to agglomeration of dispersed metal or crystallites to larger ones or partial to total collapse of the internal pore structure and a corresponding loss of surface area.

7. Leaching: leaching refers to the loss of active species from the solid that are transferred into the liquid medium, causing eventually a deactivation of the catalyst.

In homogeneous catalysis, the catalyst is in the same phase as the reactants and/or products. Homogeneous catalysis reactions are typically liquid phase, where both reactants and the catalysts are in liquid state.[27] Homogeneous catalysts are mostly organic or organometallic compounds. Homogeneous catalysis provides excellent atom efficiency, reactivity and selectivity towards one product but it's separation and reusability can be very difficult.[28]

When the catalysts and the reactants/products are in different phases it is called heterogeneous catalysis. The catalyst is typically solid, and the reactants/products are in the liquid or gaseous phase. Heterogeneous catalysts dominate over 80% of the catalysis reactions used in industry, resulting in sales over 12 billion USD out of total 15 billion USD catalysis market.[29] For the preparation of supported catalysts (typically a metal on metal oxides), precursor of active metal species is deposited on the surface of a support. The precursor is then converted to nanocrystallites or amorphous nanoparticles of an active species usually through thermal treatment. Supports are usually oxides, or carbons with different surface characteristics. The supported particles are in oxidic, metallic or sulfidic state. Catalytic properties of the material are governed by the nature of active sites and the support, interaction between active sites and support and size of the active sites can all play a role. Active sites should be highly dispersed as small nanoparticles with high loading to obtain a high-area active surface.[29-30]

1.1.5 Aqueous phase reforming

There is an urgent demand for production of renewable hydrogen using sustainable feedstocks. Aqueous Phase Reforming (APR) is a novel method of using the aqueous phase obtained from waste biomass streams (mostly oxygenated hydrocarbons) to produce a hydrogen-rich gas mixture (alongside light alkanes) over heterogeneous catalysts at mild reaction conditions.[31] APR was first proposed by the research group of Prof. Dumesic in 2002 to produce hydrogen from biomass derived hydrocarbons (sugar and alcohols) in liquid water using a platinum-based catalyst at 225 °C temperature.[32] APR is potentially advantageous over the high temperature vapour-phase steam reforming process of oxygenated hydrocarbons (500 °C <T<800 °C) because it provides additional H_2 through WGS by using water as solvent and reactant and reducing CO levels in the product gases. Since APR produces H_2 with little or no CO, it is especially suitable for producing renewable H_2 for PEM fuel cells in portable

devices.[31] APR also saves energy by not vaporizing the feed (and is especially valuable where feeds are already in dilute aqueous form) and lowers cost by excluding an extra WGS reactor.[33] APR can be used to sustainably produce liquid fuels by reforming over bi-functional catalysts, e. g., dehydration on acid catalyst and hydrogenation on metal catalyst.[34] APR can be potentially applied where the installation of a small-scale methane steam reforming unit is not economically attractive, for example at a standalone green diesel production plant located close to a pulp mill.[35]

In early studies, ethylene glycol was mainly a feed molecule for the APR process. It possesses the typical structure of alcohols including C-C, C-O, C-H, O-H bonds, and OH groups. Dumesic et al. in their first report about APR outlined the possibility of APR of ethylene glycol on platinum catalysts, the H_2 formation paths and the production of alkanes from alcohols as shown in Figure 4.[32] First, the alcohols transform into the adsorbed intermediates on the catalyst surface after dehydrogenation steps, followed by cleavage of the C-C or C-O bonds. After that, the optimal situation is the scission of the C-C bonds is followed by the WGS reaction, which will produce H_2. However, the scission of C-O bonds will make organic acids, which are stable and cannot be reformed easily. Moreover, the produced organic acids can corrode the equipment and deactivate catalysts by leaching and poisoning. Organic acids can be formed by dehydrogenation reactions catalysed by the metal, followed by rearrangement reactions that take place in solution or on the catalyst. These organic acids lead to the formation of alkanes from carbon atoms that are not bonded to oxygen atoms.[32]

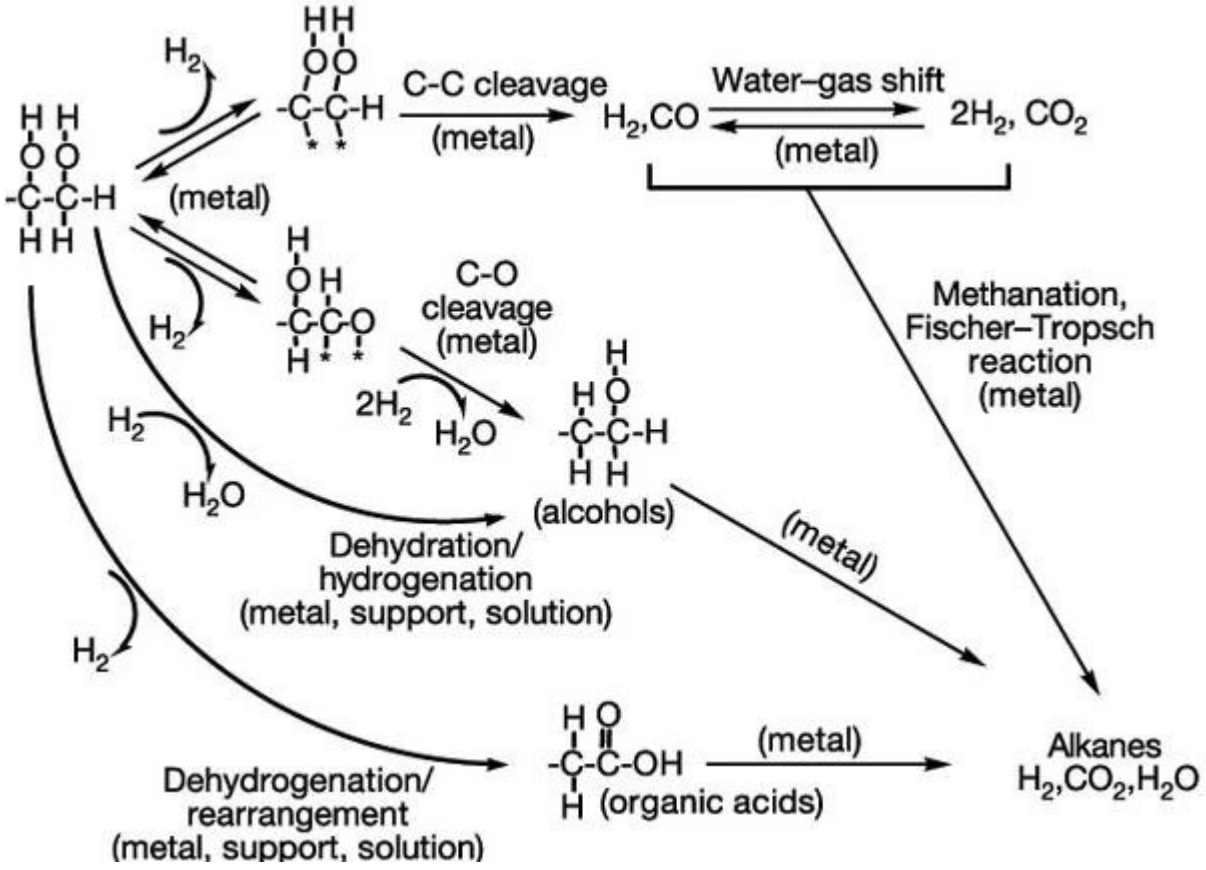

Figure 4: Reaction pathways for production of H_2 by reactions of oxygenated hydrocarbons with water, reproduced from[32]

Therefore, effective catalysts for the APR process should demonstrate high activity in cleaving C-C bonds, low affinity for C-O bond cleavage, high capacity to promote the subsequent WGS reaction, and low activity in the methanation reactions.[31] Activity and selectivity of hydrogen in APR can be modified by using different active metal, support type, and reaction conditions (pressure, temperature, acidic or basic additives, presence of the carrier gas, reactor type).

1.1.5.1 Operating conditions for aqueous phase reforming

In the review published by Dumesic et al. after some initial studies, they concluded that milder operating temperatures are thermodynamically favourable to reforming oxygenated hydrocarbons with C:O stoichiometry with a ratio of 1:1 to hydrogen compared to the chemical equilibrium of the hydrocarbons with an equivalent carbon number.[33] The operating conditions applied in APR involve temperatures in the range of 225 °C - 280 °C and pressures above the bubble point of the feedstock at the reaction temperature.[31, 33] A comparative study carried out by the group of Dumesic, reported that reforming in the liquid phase resulted in lower production rates of hydrogen compared to those obtained in SR.[36] In the APR of methanol at 150 °C, changing the reactor pressure from 0.45 MPa to 0.58 MPa changed the operation from

vapour phase to liquid phase, the methanol conversion dropped from 31.8% to 4.9% and the turnover frequency (TOF) of H_2 decreased from 0.23 min^{-1} to 0.03 min^{-1}. Hence methanol reforming is more kinetically limited in the liquid phase than in the vapour phase. Similarly, Roy and co-workers compared APR and SR of butanol. The results showed an increase in conversion at higher temperatures and lower pressures. However, the selectivity with respect to hydrogen increased at lower temperatures and higher pressure under SR conditions. The H_2 selectivity was highest at the vapour pressure of the feedstock, and it decreased at higher pressures under APR conditions.[37] Hence, the range of possible APR operating conditions is limited. Once the temperature is fixed, the pressure should be as close as possible to the bubble point to maximise conversion and H_2 yield and high enough to avoid evaporation of the feedstock. Low temperatures applied in APR are favourable for the chemical equilibrium of the WGS reaction that converts CO into CO_2 and additional H_2 and are thermodynamically unfavourable for undesirable carbon formation.[33]

Reaction rates are lower at lower temperatures, which can be rectified by increasing the contact time of reactants and catalysts. However, a longer contact will give higher conversions but decrease H_2 selectivity. The research group of Dumesic in 2004 reported that higher space velocities which involve shorter residence times, increased the hydrogen selectivity while they decreased the alkane selectivity in the APR of oxygenated hydrocarbons over a Sn modified Ni catalyst.[38] This provides evidence that production of hydrogen from aqueous phase reforming is a kinetically controlled and there should be a balance between desirable conversion and contact time due to the desired hydrogen product being only metastable.

1.1.5.2 Reactors in aqueous phase reforming

Aqueous-phase reforming experiments are commonly conducted in fixed bed reactors[32, 39-40] or in batch autoclaves reactors[41-46]. The inventors of aqueous phase reforming used a fixed bed reactor with feed flowing from bottom to top using a HPLC pump. They pressurized the system using N_2 gas. The reactor effluent was cooled using a double-pipe heat exchanger and separated using a gas-liquid separator and the pressure was regulated using a back pressure relief valve.[39]

Some alternative reactors are also reported in the literature. The research group of Nijhuis conducted aqueous phase reforming in a boehmite-washcoated microchannel reactor.[47-49] In their first report, higher conversion and selectivity of hydrogen in APR of ethylene glycol was seen over Pt/boehmite catalyst in a coated-wall microchannel reactor (ID = 320 μm) than in a packed fixed-bed reactor (ID = 250 μm). Moreover, the washcoated reactor allowed for

efficient hydrogen removal from the catalyst due to the thin catalyst layer (1–5 μm) and short diffusion path, avoiding undesired hydrogenation reactions, which improved H_2 production efficiency.[48] The same group published another study where they evaluated mass transfer in the APR of sorbitol in washcoated microchannel and fixed-bed reactors.[47] Comparable conversions at different residence times were obtained in the fixed-bed reactor, indicating that intra-particle mass transfer was not the rate-limiting step in the reaction. The hydrogen selectivity was higher in the microchannel reactor due to an improved mass transfer that allowed for the removal of hydrogen from the catalyst surface, avoiding its participation in the side reactions.[47] In a third study hydrogen stripping further improved its selectivity by a factor of 5.2 in addition to the feedstock conversion, which was 2.4 times higher.[49] Another type of reactor used was carbon coated ceramic membrane reactor, used for APR of sorbitol. The hydrogen removal in a membrane reactor increased the hydrogen productivity by avoiding its consumption in side reactions.[50]

1.1.5.3 Catalysts in aqueous phase reforming

Metals form Groups 8–10 have been applied in the reforming reactions of $>C_2$ hydrocarbons because of their efficiency for C-C bond cleavage, necessary for H_2 production.[32, 39] The results obtained in one of the first studies on APR showed that the catalytic activity in the APR of EG decreased over silica-supported catalysts with metals in the order of Pt ~ Ni > Ru > Rh ~ Pd > Ir.[39] After Pt was found to be the most efficient metal to produce H_2, the role of different support materials was assessed in the APR of EG. A comparison between a silica-supported catalyst and an alumina-supported catalyst demonstrated poor selectivity of silica towards hydrogen due to the dehydration pathways to alkanes.[39] The production rate of hydrogen over different supported Pt catalysts decreased in the order of TiO_2 > γ-Al_2O_3 > carbon > Pt-black > SiO_2-Al_2O_3 ~ ZrO_2 > CeO_2 ~ ZnO ~ SiO_2.[40] Using mixed oxides of CeO_2 and ZrO_2 to support Pt doubled the catalytic activity and the H_2 selectivity compared to the single zirconium and cerium oxides in aqueous phase reforming of ethylene glycol.[51] The improvement is a result of higher Pt dispersion, strong metal-support interaction and a larger number of oxygen vacancies.[51] The inventors of aqueous phase reforming proposed the Pt/Al_2O_3 catalyst as the most suitable for conducting APR due to its lower alkane selectivity and suggested the use of alloys and dopants to further improve H_2 selectivity.[33] Although, in most reports Pt is shown to be highly active and selective to hydrogen, a certain number of attempts were made to find a replacement for this expensive noble metal by a cheaper alternative, e.g. nickel, cobalt or iron. Nickel based systems in particular have received considerable attention, given the capability

of Ni for cleaving C-C bonds and for promoting the water gas shift reaction (WGS), which increases hydrogen production. However, they suffered from selectivity and stability issues. Deactivation studies of Ni based catalyst supported on γ-Al_2O_3 suggested that a significant part of γ-Al_2O_3 was converted into γ-AlOOH under glycerol APR conditions. The formation of γ-AlOOH significantly changed the textural properties of these catalysts, decreasing the surface area/porosity and metal dispersion, and increasing their surface acidity. The agglomeration and re-oxidation of the Ni particles reduced the number of metallic Ni active sites, which results in decrease of catalyst activity. These phenomena, together with the adsorption of the carbonaceous molecules/organic compounds were the main reasons for deactivation of Ni/γ-Al_2O_3 catalysts.[52] Monometallic Ni/C catalyst was found not stable at APR conditions due to the metal leaching.[53] Haasterecht et al. prepared Ni supported over carbon nanofibers and tested them in APR of ethylene glycol. They reported Ni to have poor selectivity compared to Pt and Co and metal particle growth and coke deposition were responsible for the deactivation of Ni catalysts.[54] The group of James Dumesic reported that the use of bimetallic catalysts can increase activity and selectivity due to geometric, electronic, stabilising, synergistic and bi-functional effects.[55] Hence the successful use of nickel-based catalysts demanded use of another basic metal oxide.

A bimetallic Pt-Ni catalyst supported on Al_2O_3, was tested in APR by Dumesic et al.[56] and resulted in higher conversions and H_2 selectivity than the monometallic catalysts. When Lu and co-workers[57] studied the metal support interaction for APR of sorbitol, they observed a similar phenomenon only when the Pt and Ni catalysts were co-impregnated, which resulted in an alloy with improved reducibility. In contrast, the sequential impregnation of the Pt and Ni catalysts resulted in separate metal phases with higher catalytic activity than the monometallic Ni-based catalyst, though lower than that obtained over the co-impregnated catalyst. The formation of a Pt-Ni alloy also resulted in lower coke deposition in addition to higher activity. The H_2 activity decreased in the following order of the supports: Al_2O_3 > ZrO_2 > CZS (C= ceria, Z=Zirconia, S= Silica). Bimetallic Pt-Ni/C also showed better activity compared to monometallic Pt and Ni in aqueous phase reforming of glucose.[58] Raney nickel and alumina-supported Ni and Sn catalysts were tested in the APR of different oxygenated hydrocarbons and compared to Al_2O_3-supported Pt and Ni catalysts.[38] Compared to Pt/Al_2O_3, the Raney-NiSn catalyst was more active and selective in terms of hydrogen production, and more stable as well.[38] The improved stability was result of addition of Sn, which was found to minimise sintering, leaching and coking of the metal particles under APR conditions.[59] However with time, the Raney NiSn

catalysts got deactivated due to oxidation and leaching.[59] In the study of APR of EG by Xie et al., the H_2 selectivity increased over the Raney Ni catalyst doped with Sn as Sn could activate the water molecules and promote the WGS reaction.[60] A non-pyrophoric Ni catalyst prepared by alkali leaching of a $Ni_{50}Al_{50}$ alloy using small amounts of NaOH as compared to conventional Raney Ni catalyst showed a 50% higher EG conversion rate in APR and higher H_2 selectivity. The improved performance was attributed to a higher concentration of hydrated alumina in the support and its positive effect on the WGS reaction.[61] The research group of Lu showed nickel-boron alloy to be 50% more active and 31% more selective toward H_2 as compared to Raney Ni in aqueous phase reforming of glycerol.[62]

Iriondo et al. modified an Al_2O_3 support with the oxides of La, Mg, Zr and Ce, were selected to improve the performance of a Ni/Al_2O_3 catalyst in the APR of glycerol.[63] The catalysts were prepared by sequential impregnation of promotor oxide followed by Ni nitrate. The H_2 production rate over those catalysts, promoted with cerium and lanthanum oxides, was higher than over the non-promoted catalysts.[63] This effect of the Ce and La catalytic promotion was attributed to geometric effects which poisoned the Ni sites responsible for CO methanation.[63] APR of glycerol over Ni supported on Ce and Zr mixed oxide support showed higher activity as compared to single Ce and Zr oxide supported catalyst.[64] Ni supported over mixed oxides of Ce and Zr, La and Zr, and Ce, Zr and La resulted in higher conversion rates and H_2 selectivity compared to single-oxide CeO_2 and ZrO_2 supports in APR of methanol.[65] Rahman reported using bimetallic Pt-Ni supported on Multiwalled carbon nanotubes (MWNT) showed higher activity and selectivity towards hydrogen than corresponding monometallic catalysts in the APR of glycerol.[66] Park et al. prepared $X–Ni/LaAlO_3$ (X = Cu, Co, Fe) by precipitation to test in aqueous phase reforming of glycerol. The small size and high dispersion of Ni particles in the $Cu–Ni/LaAlO_3$ catalyst showed the highest glycerol conversion and hydrogen selectivity, which can be attributed to the synergistic effect of the nickel and copper components in the catalyst and also suppressed carbon deposition.[67] Coronado et al. prepared nickel-based catalysts with dopants copper and cerium and supports α-Al_2O_3, β-SiC, ZrO_2, γ-Al_2O_3 and tested for APR of methanol. $NiCe/\gamma$-Al_2O_3 exhibited the highest values of methanol conversion and hydrogen yield.[68] The effect of supports improved in the order α-Al_2O_3 < β-SiC < ZrO_2 < γ-Al_2O_3.[68] Ni-Cu bimetallic supported on mesoporous CeO_2 was successfully synthesized to investigate the catalytic performance in APR of glycerol. The results showed that the Cu in the catalysts can effectively improve water–gas shift (WGS) reaction and inhibit the formation of

methane, which increased the H_2 production. The higher reaction temperature is beneficial to the H_2 production rate, but not to H_2 selectivity.[69]

The basicity of supports were studied for influence on catalytic performance for APR of glycerol over Pt based catalysts. The APR tests showed that the selectivity for hydrogen followed the order $Pt/MgO > Pt/Al_2O_3 > Pt/CeO_2 > Pt/TiO_2 > Pt/SiO_2$. These results indicated that the APR of glycerol is more favourable for catalysts with more basic supports. However, Pt/MgO showed the worst stability in hydrothermal conditions.[70]

Hence, there is a need to incorporate MgO into a stable matrix with Ni, which will not only provide basicity but also be resistant to carbonaceous depositions and leaching.

1.1.6 Hydrotalcite derived catalysts

An excellent way of incorporating different metals and metal oxides of both support and active species in a matrix is preparing it through a layered double oxide / hydrotalcite derived route.

Layered double hydroxides (LDHs), also known as hydrotalcite-like materials, are a class of two-dimensional (2D) anionic clays consisting of positively charged host layers and exchangeable interlayer anions. The structure is like brucite [$Mg(OH)_2$], where Mg^{2+} ions occupy octahedral positions and form infinite layers connected by hydrogen bonds. In Mg-Al LDH, some Mg^{2+} ions are substituted by Al^{3+} ions and produced an excess positive charge which is compensated by carbonate anions present in the interlayer space. The general formula of LDH is $[M^{2+}_{1-x}M^{3+}_x(OH)_2]^{x+}\ [A^{n-}_{x/n}]\cdot mH_2O$, where M^{2+} is a divalent cation, M^{3+} is a trivalent cation, and A^{n-} is the anion. Most of the LDH corresponds to that of Mg-Al LDH, a natural magnesium-aluminium hydroxycarbonate, $Mg_6Al_2(OH)_{16}CO_3\cdot 4H_2O$.[2] However, both Mg^{2+} and Al^{3+} can also be substituted by other divalent cations(Ni^{2+} [46, 71], Sn^{2+} [72], Mn^{2+} [73], Cu^{2+} [41, 74], Zn^{2+} [43]) and trivalent cations (Co^{3+} [75-76], Fe^{3+} [77-78], Cr^{3+} [79,80]) and the interlayer anion can also be varied.

LDH are usually prepared by coprecipitation, a solution containing M^{2+} and M^{3+} metal salts are coprecipitated with an alkaline solution. The product crystallinity is affected by experimental parameters such as reaction pH and temperature, concentration of used solutions, flow rate during addition of reactants.[81]

An attractive feature of LDHs as far as catalysis is concerned, is that the M^{2+} and M^{3+} cations are distributed in a uniform manner in the hydroxide layers, without clusters of like cations. They can be used as precursors or templates for the formation of mixed metal oxides with high

surface area and high dispersion. This conversion from precursors to mixed metal oxides is initiated by thermal decomposition of LDH, leading to a high-surface-area Mg(Al)O mixed oxide with Lewis basic sites. The research group of Prof. Mokhtar reported that thermal decomposition of Mg-Al LDH led to the formation of a dehydrated intermediate phase at 200 °C, followed by crystalline MgO formation at 450 °C. Finally, the products were converted to an MgO-like structure where Al^{3+} ions are dissolved in the lattice to form a solid solution at 500 °C.[82] LDH-derived mixed oxides typically possess high surface area, phase purity, basic surface properties, and structural stability.

LDH-derived oxides containing other metal cations exhibit not only their original acid-basic properties of the Mg-Al system but also the properties of other cations that have substituted Mg and Al. LDH derived mixed oxides containing transition metal ions can be reduced to give catalytically active metal particles supported on the remaining metal oxide phase. The supported catalysts prepared from hydrotalcite often exhibit greater catalytic activity because of their small metal crystallite size, high surface area, basic properties, high dispersion of metal, and the ability to form homogeneous complex oxides.[72]

The mixed oxides have been reported in various literature to exhibit a property termed as the "memory effect".[83-87] The original layered structure can be reconstituted when the mixed oxides are contacted with aqueous solution containing many different anions or even with vaporized water. This will help in regeneration of catalysts that can be calcined and reduced to be used again and should theoretically give the same activity and selectivity.

Di Cosimo and co-workers prepared five samples with Mg–Al ratios of 0.5–9.0 in order to study the nature, density, and strength of surface basic sites of Mg-Al mixed oxide obtained by calcination and concluded that the surface basicity largely depends on the Al content. On pure MgO, strong basic sites consisted predominantly of O^{2-} anions but calcined LDH contains surface sites of weak (OH^- groups), medium (Mg-O pairs), and strong (O^{2-} anions) basicity. The addition of small amounts of Al to MgO diminished drastically the density of surface basic sites because of a significant Al surface enrichment. Formation of surface amorphous AlO_y structures in samples with low Al content (Mg/Al > 5) partially covered the Mg-O pairs and decreased the concentration of surface O^{2-} anions. At higher Al contents (5 > Mg/Al > 1), the basic site density increased because the Al^{3+} cations within the MgO lattice created a defect to compensate the positive charge generated, and the adjacent oxygen anions became co-ordinatively unsaturated. In samples with Mg/Al < 1, segregation of bulk $MgAl_2O_4$ spinels

occurred and caused the basic site density to diminish.[88] However, pure MgO support was proved to be unstable in aqueous phase reforming[70], but adding Al decreases the basicity of the catalyst.[88] Hence there will be a trade-off between basicity and stability, which calls for a need to systematically study the effect of Mg/Al ratios in aqueous phase reforming.

The conventional way to prepare nickel-containing Mg–Al mixed oxide catalysts via LDH precursor includes co-precipitation of Ni^{2+}, Mg^{2+}, and Al^{3+} with a carbonate counterion at basic pH. Due to their nearly equal cation size, nickel(II) isomorphously replaces magnesium(II) within the brucite-like layers of LDH, thus giving a structure very similar to that of hydrotalcite.[3]

1.1.6.1 Hydrotalcite derived catalyst used in Aqueous Phase reforming

Table 1 shows different hydrotalcite derived catalysts used previously in aqueous phase reforming of various feeds. Cruz et. al. tested Ni/Mg/Al with different Ni wt% in the APR of ethanol in a batch reactor.[44] Ni/Mg/Al hydrotalcites showed an isomorphous substitution of Mg by Ni cations in the brucite layers. Hence no other phases were detected, suggesting that both nickel and aluminum are well dispersed in MgO matrix. Hydrotalcite derived catalyst with highest Ni loading exhibited 70% ethanol conversion, 78% H_2 selectivity and less than 1% of CO formation at 230 °C. All their catalysts showed lower selectivity for methane than alumina supported nickel, hence improving selectivity for hydrogen. However, the effect of varying M^{2+}/M^{3+} was not studied and the stability of catalysts was not reported.[44] Bastan et al. tested Ni/Mg/Al with different Ni wt.% in the APR of glycerol in a fixed bed reactor. The 5 wt% Ni/Al_2O_3-MgO showed the highest catalytic activity of 92% total conversion as well as 76% selectivity towards the hydrogen production. The XRD and TEM characterizations of the spent catalysts showed no evidence of deactivation in terms of phase change or any carbon depositions. It was demonstrated that the APR activity lowered in the following Ni content order: 5 > 3 > 1 > 7 >10 wt% Ni/Al_2O_3-MgO.[89] Both the papers didn't study the effect of M^{2+}/M^{3+} ratio on conversion and selectivity of hydrogen in APR of substrate.

Pan et al. synthesised Ni/Sn/Al hydrotalcite derived catalyst by coprecipitation method. However, Sn^{2+} didn't substitute Mg isomorphously due to large ionic radii of Sn.[72] Their material consisted of two different phases: a hydrotalcite phase and a SnO phase. For APR of EG, they reported their catalyst was active over 120 h, however, no post mortem of catalysts characterization was done.[72] Pendem et al. promoted Pt/Mg/Al with K and tested in APR of

glycerol[42]. With the incorporation of K, the morphology of hydrotalcites were changed to the needle-like structure. Potassium enhanced the basicity of the catalyst which resulted in increased conversions and hydrogen yield. However, when the loading of K was increased above 28% Pt species became agglomerated and K blocked the active sites of Pt nanoparticles, which resulted in the decrease of conversion and H_2 selectivity. They observed no leaching in their catalyst and the catalyst retained its activity in 4 cycles.[42] Boga et al. used commercial LDH with varying Mg/Al as support for impregnating Pt and Pt-Cu to study APR of glycerol in a semi-batch reactor system.[90] Hydrogen selectivity increased with increasing Mg/Al ratio. The addition of Cu as a promoter increased the hydrogen selectivity and suppressed methane formation.[90] Cesar et al. compared a co-precipitated Ni/Mg/Al catalyst to Pt–Ni bimetallic catalyst derived from Ni LDH synthesized using surface organometallic chemistry on metals for the APR of ethylene glycol.[45] They reported the addition of Pt increased the activity but found the Ni/Mg/Al catalyst to be more selective than Pt-Ni bimetallic catalyst. They indicated this might be due to C-O bond cleavage.[45] However, this is the only report which suggested adding Pt decreased hydrogen selectivity

APR of glycerol over Ni/Cu/Mg/Al were tested by Manfro et al.[74] and Tuza et al.[41] in a fixed bed reactor and batch autoclave respectively. In batch reactor, with increase in temperature the selectivity for hydrogen decreased while in the fixed bed reactor with increase in temperature the selectivity for H_2 increased.[41, 74] In both reports, with the increase of Cu content the selectivity for the liquid products increased.[41, 74] Sintering of metal particles was reported in both papers.[41, 74]

Ni/Zn/Al was used by Chen et al. for the aqueous phase refroming of ethylene glycol in a batch autoclave. There was a ZnO phase shown alongside hydrotalcite phase in their pXrd pattern suggesting Zn was not incorporated into the layers. They reported over 99% conversion and 100% selectivity for their catalysts. However, it is important to note that the formula used to calculate the selectivity for hydrogen was different from usually reported in literature. H_2 selectivity was calculated by: $\frac{Hydrogen\ amounts\ of\ H_2}{Total\ carbom\ amounts\ of\ gas\ products\ \times\frac{1}{R}}$

Where *R* was the H_2/CO_2 reforming ratio of 5/2 for ethylene glycol.

Due to the use of this equation, the hydrogen selectivity reached 100%. No data for deactivation was reported.[43]

Despite suggesting that Ni hydrotalcite derived catalysts have better activity and selectivity than monometallic Ni, none of the papers study the effect of M^{2+}/ M^{3+} ratio, quantify deactivation, relate reducibility to activity and report the effect of reduction temperature.

Table 1: Hydrotalcite derived catalysts in Aqueous phase reforming

LDH based catalyst	Feed	Reactor type	Parameters	Reference
Ni/Cu/Mg/Al	Glycerol	Batch autoclave	250mL of 10 wt.% glycerol, 400mg catalyst, 38.5 bars at 250 °C and 52.6 bars at 270 °C. (autogenous pressures)	[41]
K promoted Pt/Mg/Al	Glycerol	Batch autoclave	20 mL of 10 wt.% glycerol. 200 mg catalyst. 10-60 bar pressure in 100-300 °C temperature range.	[42]
Ni/Sn/Al	Ethylene glycol	Fixed bed reactor	5 wt% ethylene glycol, flowrate: 0.05-1.00 mL min^{-1}, 1.5 g catalyst, 25.8 to 30 bars in 210-240 °C temperature range	[72]
Ni/Cu/Mg/Al	Glycerol	Fixed bed reactor	10 vol% of glycerol, flowrate: 0.102 mL min^{-1}, 1.25 g catalyst, 35.5 bars at 250 °C and 50.5 bars at 270 °C	[74]
Ni/Zn/Al	Ethylene glycol	Batch autoclave	20 wt% of 100mL ethylene glycol, 200mg catalyst, 19.5 – 34.5 bars pressure in 210-240 °C	[43]

			temperature range	
Ni/Mg/Al	Ethanol	Batch autoclave	200 mL of 1 wt%. ethanol, 100 mg catalyst, 15.2 bars at 200 °C , 28.3 at 230 °C and 39.5 at 250 °C temperature	[44]
Ni/Mg/Al And Ni-Pt/Mg/Al	Ethylene glycol	Batch autoclave	100 mL of 10 wt% ethylene glycol, 44 bar pressure at 250 °C temperature	[45]
Ni/Mg/Al, Ni/Cu/Al, Ni/Zn/Al, Ni/Sn/Al, and Ni/Mn/Al	Ethylene glycol	Batch autoclave	50 mL of 20 wt.% ethylene glycol, 100 mg of catalyst, 26 bar pressure at 225 °C temperature	[46]
Ni/Mg/Al	Glycerol	Fixed bed reactor	10 wt% Glycerol, flow 0.2mL min^{-1} 250 mg catalyst, 50 bars pressure at 250 °C.	[89]
Pt/Mg(Al)O and Pt-Cu/Mg(Al)O	Glycerol	Semi-batch reactor	10 mL of 10wt.% glycerol, 300 mg catalyst, 29 bar pressure at 225 °C temperature	[90]
Ni/Zn/Al	Phenol	Batch autoclave	50m:Lof 0.1-0.1mol L^{-1} phenol. 100mg catalyst. 40-70 bar pressure in 200-280 °C temperature range	[91]
Ni/Mg/Al , Ni/Mgo , Ni/Al2O3	Ethylene glycol	Fixed bed reactor	10 wt% ethylene glycol, flow 0.2mL $min^{-1,}$ 250 mg catalyst, 50 bars	[92]

			pressure at 250 °C.	

1.1.7 Aqueous phase reforming of Phenol

There is not much literature reported on APR of phenol. Commonly used feedstocks in APR are oxygenated hydrocarbons with C:O ratio close to 1:1 and different ratios can affect the process of APR and hydrogen selectivity.[33] The C:O ratio in phenol is 6:1 with a very stable structure, suggesting that APR of phenol is difficult. Groups studying APR of lignin wastewater excluded aromatic monomers (phenol and guaiacol) as they may be responsible for the decrease of hydrogen production.[93-94] However Yan et al.[95] and Li et al.[96] reported production of hydrogen by APR of phenol over Ni and NiCe catalysts, respectively, both supported on ZSM-5.[95-96] Li et al. conducted APR of phenol over hydrotalcite derived Ni/Zn/Al and reported the optimal conditions for hydrogen production are the concentration of 0.1 mol/L phenol under the pressure of 4 MPa at 270 °C.[91] Some reports studied in situ phenol hydrogenation by producing hydrogen from APR, suggesting that phenol did reform to produce hydrogen at APR conditions.[97-98] To mitigate phenol from waste-water Oliveira et al. degraded phenol into intermediates by oxidation and then converted the intermediates to valuable gases by an APR process in a second step.[99] This makes APR of phenol a debatable topic with no reliable evidence to confirm the production of hydrogen by APR of phenol.

1.2 Aims and objectives

During this project, Ni/Mg/Al hydrotalcite derived catalysts were prepared by co-precipitation with varying Ni wt% (5%, 10%, 15%, 20%) and molar ratio of bivalent (Mg + Ni) to trivalent (Al) metals (M^{2+}/M^{3+} = 2, 3, 6, 8). A detailed characterisation (H_2-TPR, CO_2-TPD, FTIR, pXrd, ICP-OES, BET, TGA) of these materials was carried out before testing them in a batch autoclave with ethylene glycol and phenol as feedstocks. The spent catalysts were dried in a vacuum oven at 120 °C for 4 h and were characterized for leaching, sintering and structural changes. Some of the spent catalysts were re-tested to check for activity and selectivity. These results were benchmarked against commercial catalysts and Ni/γ-Al_2O_3 incipient wet impregnation catalyst. The main questions this thesis tries to answer are:

1) How does the activity and selectivity for hydrogen in APR of ethylene glycol vary with Ni loading and M^{2+}/M^{3+}?

2) What is the effect of nickel reduction temperature on activity and selectivity of hydrogen in APR of ethlyene glycol?
3) How does the Ni loading and M^{2+}/M^{3+} influence the stability of catalyst (*e.g.* to leaching) in comparison to monometallic Ni and commercial catalysts?
4) How does the catalytic loading and temperature of reaction influence the activity and selectivity of hydrogen in APR of ethylene glycol?
5) What are the activity and selectivity of hydrogen on Ni/Mg/Al hydrotalcite derived catalysts for APR of phenol?

Chapter 2: Methodology and Experimental

2.1 Methodology

This section sets out key approaches and techniques used in this work, providing relevant underlying theory, and is followed by an experimental section that details the specific apparatus and procedures used.

2.1.1 Synthesis of Catalysts

A plethora of methods exist to prepare catalyst materials including supported metal catalysts, two are of specific importance to the work described here and so will be discussed in more detail, co-precipitation and incipient wetness impregnation.

2.1.1.1 Co-precipitation

One of the principal methods of synthesizing catalysts is co-precipitation. In this method, one or more metals are co-precipitated with the support using an alkaline solution. This method of preparation is widely used, including on an industrial scale. In this method of preparation, the chemical phase and dispersion is completed in a single step, hence, the surface area, porous structure and particle shape and size are governed by the precipitation parameters like method of dosing, mixing, and control of temperature. Hence, these process conditions need to be controlled accurately. An advantage of this technique is the high attainable metal loading, which is typically only limited by solubility of the precursor salt solution of metal in the solvent. A second benefit is high metal dispersion, usually resulting in higher weight and volume activities as a consequence of increased metal surface area. A third advantage is different mixtures of metals and non-metallic promoters can be deposited in a single process. A major disadvantage of using this method is large quantities of salt solution are required.[100]

This method is accomplished in a number of steps including precipitation, filtration, washing, drying and calcination. The major step to perform carefully is of precipitation as it controls the properties of the synthesized catalyst. Precipitation consists of several steps: liquid mixing, nucleation and crystal growth to form primary particles and aggregation of primary particles. Although nucleation and crystal growth usually proceed simultaneously, in the theory each step is treated separately from each other. The formation of monodisperse crystals is the key. Nucleation is a complex process especially in multicomponent systems. It starts with formation of clusters that are capable of spontaneous growth by further addition of monomers until a critical size is achieved. For nucleation to occur an energy barrier must be crossed (similar to

chemical reactions), hence it is necessary to create some degree of supersaturation before spontaneous crystallization. Below supersaturation concentration nucleation is very slow and above supersaturation concentration nucleation is very fast. Nucleation depends on both concentration and temperature.[100] The nucleation rate can be described as:

$$\frac{dN}{dt} = \beta \exp\left[\frac{-16\pi\sigma^3 v^2}{3\,(kT)^3\,ln^2 s}\right]$$

Equation 1: Rate of nucleation

Where, T is the temperature, s is supersaturation, v is solid molecular volume, β=pre exponential term, σ = solid/fluid interfacial energy.[100]

The supersaturation can be undertaken in a number of physical and chemical methods (cooling of reaction mixture, evaporation of solvents, hydrolysis etc.). However, the most common way is reaction of ions in aqueous media by which the solubility product is exceeded.

The crystal growth can then be explained by a simple equation:

$$K_g = a(c - c_{eq})^n$$

Equation 2: Rate of crystallization

Where, a is the growth rate constant, c = concentration and c_{eq} = solubility concentration, n = 1-2.

The key point to take from these equations is nucleation rate increases exponentially with supersaturation concentration, but crystallite growth rate is close to linear with concentration. Hence high supersaturation levels promote nucleation and favours the precipitation of highly dispersed materials while precipitation from more dilute solutions tends to produce fewer, but larger crystals. Therefore for those catalysts where the final dispersion and activity reflects the initial dispersion of the precipitate a high initial dispersion is desired.[100]

Aggregation is a process of formation of clusters of nanoscale primary particles into micrometer-scale secondary particles. Both physical and chemical forces hold these aggregates together. Porosity is then determined by how the primary particles are stacked, and pores can be considered as voids between the primary particles The primary precipitation products may not be thermodynamically stable and depending on the process conditions, counterions like carbonate, or chloride initially are incorporated, are later partially or largely displaced by

hydroxide. This displacement process is promoted by high pH and temperature, or by prolonged aging.[100]

In context to reduced metal catalysts, after co-precipitation, filtration and drying, often the materials are calcined to remove species other than metals and oxides and reduced to obtain metal particles on the oxide support.

2.1.1.2 Incipient Wetness impregnation

This is the most common route of catalyst preparation and is widely under in industry and the laboratory. It is accomplished in two steps: impregnation and drying.

The most common method to perform impregnation is contacting a dried support having pore volume V_p with V mL solution of precursor of the active phase, where $V = V_p$. The precursor solution is sucked up into the pores by capillary action. When this technique is performed properly, no solution is seen outside the pores and hence the method is called 'dry' or 'incipient wetness' impregnation. Sometimes the method is performed under vacuum to remove the air from pores, as air might affect the mechanical strength of the support while escaping during capillary suction. Heat is released when a solid/gas interface is replaced by solid/liquid interface. This might affect the impregnation, if solubility of precursor decreases with increase in temperature. This can be avoided by exposing the precursor to water vapour before impregnation.[101]

After impregnation, the solvent is eliminated by drying. Usually, the impregnated support is spread in a fine layer and is heated up to the boiling point of the solvent in an oven under static conditions or flow of gas. The elimination of solvent leads to an increase in precursor concentration up to saturation and crystallization. Both temperature and ramp rate play an important role in the distribution of the precursor species.[101]

Depending upon the precursor salt used, sometimes the material is calcined before reduction to achieve metal particles on the catalyst support.

2.1.2 Characterization techniques

2.1.2.1 IR spectroscopy

Infrared spectroscopy uses the vibrations of the atoms of a molecule to generate a spectrum. Infrared radiations are unable to excite electrons but can magnify the molecular and rotational vibrations. An infrared spectrum is generated by passing broadband infrared radiation through

a sample and the energy at which any peak in an absorption spectrum appears corresponds to the frequency of a vibration of a part of a sample.[102]

For infrared absorptions to be seen, molecules should change their electric dipole moment during vibration. Hence, homonuclear diatomic molecules (N_2, H_2, O_2) have no characteristic IR spectrum because their dipole moment remains zero on vibration. The far IR region of the IR spectrum records changes due to rotational vibrations while near IR region includes both vibrational-rotational vibrations. The absorption frequency varies with vibration mode, while intensity depends upon how effectively molecules absorb energy which again depends on the change in the dipole moment.[102]

IR spectra were recorded in the 1940s using dispersive instruments. From the 1950s, different modes of obtaining an IR spectrum have been explored. A very commonly used technique these days is Fourier-transform infrared spectrometers (FTIR). FTIR is derived from the idea of interference of radiations between two beans to yield an interferogram. The interferogram is a signal obtained as a function of the change of pathlength between the two beams. Fourier-transformation is than use to interconvert distance and frequency.[103]

The components of FTIR spectrometer includes a source, interferometer and detector. For mid-infrared region, a Globar or Nernst source is used and for the far infrared region a high-pressure mercury lamp is used. Tungsten-halogen lamps are used for the near-infrared region. A Michelson interferometer is commonly used for FTIR spectroscopy. The device has two perpendicular mirrors and a beamsplitter (chosen as per the region under examination) which bisects the planes of the two mirrors. The beamsplitter splits 50 % of incident radiation and reflects to one of the mirrors and the other half is transmitted to the second mirror. The two beans are reflected back to the beamsplitter from mirror where they recombine and interfere. This combined beam emerges at 90 degrees from the original beam and this beam is transmitted to the sample. Beyond the sample is a detector. The detector is usually mercury cadmium telluride or deuterium tryglycine sulfate. The signal is amplified, and high frequency contributions are filtered. The data is then converted to digital form using an analogue to digital converter and transferred to computer for fourier-transformation.[103]

Qualitative analysis: To interpret the spectrum recorded, the bands on the spectrum are assigned to specific parts of a molecule or material, called group frequencies. The mid infrared spectrum (4000-400 cm^{-1}) has four regions: X-H stretching region (O-H, C-H, N-H) (4000-2500 cm^{-1}), the triple bond region (C≡C, C≡N) (2500 -2000 cm^{-1}), the double bond region

(C=C, C=O) (2000-1500 cm^{-1}) and the fingerprint region (1500-600 cm^{-1}). In the fingerprint region, vibrations are not reliably positioned and vary by significant numbers of wavenumbers even for similar molecules. A spectrum of a molecule in fingerprint region may have a hundred or more absorption bands but there is no need to assign them.[104]

In the near-infrared region (13000-4000 cm^{-1}) the absorptions observed are overtones or combinations of basic stretching bands observed in the min-infrared region (generally due to C–H, N–H or O–H stretching). These bands are usually useless for qualitative analysis. The far infrared region (400-100 cm^{-1}) provides information about the vibration of molecules containing heavy atoms, molecular skeleton vibrations, molecular torsions and crystal lattice vibrations.[104]

It is important to note that hydrogen bonding effects infrared spectroscopy. This bonding influences the bond stiffness and hence alters the frequency of vibration. For example, for a hydrogen bond in an alcohol the O–H stretching vibration is observed in the 3500–2500 cm^{-1} range, rather than in the usual 3700–3600 cm^{-1} range.[104]

Quantitative analysis: The spectra obtained in absorbance or transmittance can be quantified by curve fitting at a particular wave number. The Beer-Lambert law (Equation 3) can be used to co-relate the intensity of an infrared band to the amount of analyte present. The absorbance of solution is directly proportional to the thickness and concentration of the sample:

$$A = \varepsilon cl$$

Equation 3: Beer-Lambert Law

Where, A = absorbance, c = concentration, l = pathlength and ε = molar absorptivity (constant of proportionality.

If a spectrum is obtained is in transmittance, it can be converted to absorbance to apply the Beer-Lambert law. Absorbance (A) is equal to difference between log of intensity of light entering (I) and log of intensity of light transmitted (I_o)

$$A = \log \frac{Io}{I}$$

Equation 4: Absorbance

Transmittance (T) is defined as

$$T = \frac{I}{Io}$$

Equation 5: Transmittance

Hence,

$$A = -\log\left(\frac{I}{Io}\right) = -\log T$$

Equation 6: Absorbance from Transmittance

Hence, the absorbance can be calculated using transmittance via Equation 6.

The Beer-Lambert law gives a linear plot of absorbance vs. concentration with gradient εl. Once a calibration curve of absorbance vs. known concentration is prepared, concentration of an unknown solution can be identified.[104]

2.1.2.2 Adsorption experiments for surface area (BET method)

Gas such as nitrogen or argon is used to carry out an equilibrium adsorption/desorption experiment at the liquified gas's boiling point temperature. There are two methodologies to perform equilibrium adsorption: manometric method and gravimetric method. In gravimetric method, the change in the weight of a solid is calculated after equilibrium is achieved at various gas pressures. This method has drawbacks, as the balance is at room temperature and sample is at liquid nitrogen temperature leading to significant temperature gradient. The manometric method considers pressure drop in a system of known volume to calculate adsorption at different gas pressures. This method is widely used and accurate as adsorption is favoured at low temperatures. This method is used for a total surface area of 40 m^2 or more. For materials with low surface area, a large amount of sample must be used, which can cause experimental error due to diffusion limitations in sample bed. The samples in this technique are pre-treated/degassed to remove any physically absorbed species like humidity, without changing the structure. Degassing is often carried out in vacuum and vacuum is applied slowly so no sample get sucked up into the pump. Once vacuum is reached, the sample is heated to a desired temperature. After degassing, the sample is weighed again and placed on the adsorption manifold. Firstly, a dead volume is calculated using helium. Helium is used as it does not get adsorbed on the sample.[105]

For measurements, a known amount of gas is filled in into the reference volume and then the reference volume is opened to the sample volume. The pressure is then monitored until an

equilibrium between the sample and the gas is reached. The equilibrium can be checked by establishing that there is no pressure change over a certain period. For each cycle the amount of gas in reference volume and sample volume is calculated by the ideal gas law (as deviation from nonideality is small for gases at 77 K and low pressures). The adsorbed amount of gas is typically given per gram of sample (mmol/g). The equilibrium pressure (p) is given in relation to the saturation vapor pressure (p^0), which is measured separately. Hence, the adsorption isotherm is presented as absorbed quantity (mmol g^{-1}) as a function of p/p^0. Similarly, a desorption isotherm is obtained by calculating amount of gas desorbed at equilibrium pressure.[105]

According to IUPAC, there are six types of isotherms possible: microporous solids (Type I) nonporous solids (Type II), nonporous and non-wetting solids (Type III), mesoporous solids (Type IV), mesoporous non-wetting solids (Type V), and extremely well-ordered nonporous systems such as graphite systems where adsorption occurs layer by layer (Type VI). A hysteresis loop is observed for the Type IV and Type V isotherms due to a capillary condensation phenomenon associated with the mesoporosity. This hysteresis loop was again classified into four types: 1) The H1 hysteresis loop is characterized by parallel adsorption and desorption branches and is due to adsorption in unconnected mesopores with a relatively narrow pore size distribution. 2) H2 hysteresis loop is almost of triangular shape and is due to pores which are interconnected, often with smaller entrances than bodies (like an ink bottle-shaped pores). 3) Hysteresis type H3 are due to non-rigid pore structures which can be between particle grains 4) Hysteresis type H4 are due to non-rigid pore structures which can be between flat plates. There's a type H5 loop but it's uncommon. It has a distinctive form associated with certain pore structures containing both open and partially blocked mesopores.[105-106]

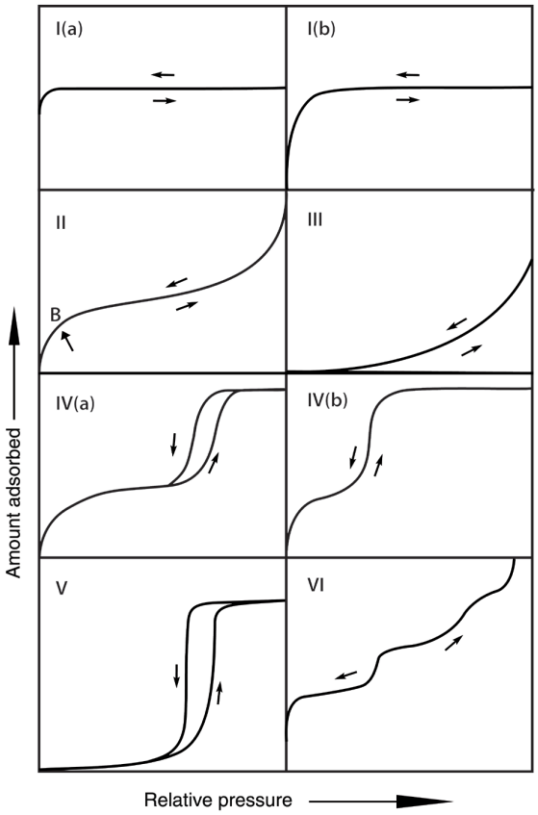

Figure 5: Different types of f physisorption isotherms as classified by IUPAC reproduced (without permission) from IUPAC technical report[106].

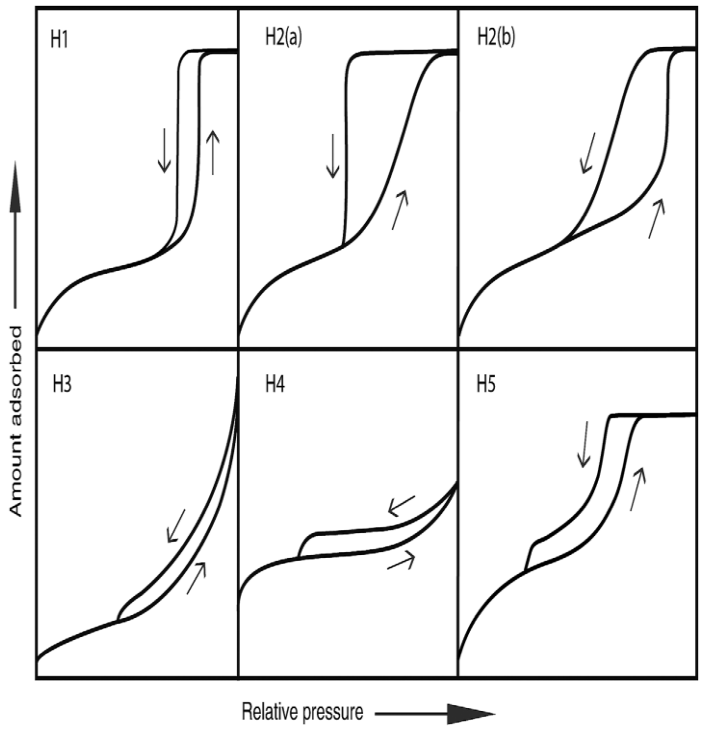

Figure 6: Different types of hysteresis loop as classified by IUPAC reproduced (without permission) from IUPAC technical[106].

The specific surface area is calculated using the Brunauer-Emmett-Teller (BET) equation (Equation 7). The BET equation is based on a modified Langmuir model.

$$\frac{1}{V[1-\left({}^{P_o}/_{P}\right)]} = \frac{C-1}{V_m C}\left({}^{P}/_{P_o}\right) + \frac{1}{V_m C}$$

Equation 7: BET equation

where C is the BET constant, P_o = saturation pressure, P = equilibrium pressure, V = volume of adsorbed gas, V_m = volume of monolayer adsorbed gas.

Thus, BET area is found via a plot of $\frac{1}{V[1-\left({}^{P_o}/_{P}\right)]}$ vs. $\left({}^{P}/_{P_o}\right)$. This is a linear relationship for the range of $0.05 < P/P_o < 0.35$. Solving for slope A and y-intercept I can be used to calculate V_m.

$$V_m = \frac{1}{A+I}$$

Once, V_m is calculated, the total surface area is calculated by

$$S_{total} = \frac{V_m N s}{V}$$

Where, N is Avogadro number and s is adsorption cross section of adsorbate.

Finally, the BET surface area is calculated by:

$$S_{BET} = \frac{S_{total}}{a}$$

Where, a is the mass of the sample.[105]

2.1.2.3 Powder X-ray diffraction (pXRD)

X-ray diffraction is a widely used technique in catalysis characterization. It is used to identify crystalline phases present and obtain an indication of particle size. X-ray diffraction happens due to the elastic scattering of X-ray photons by atoms in a periodic lattice. The scattering of monochromatic X-rays that are in same phase gives constructive interference. If the detector is at a suitable angle, this signal due to constructive interference will be detected. The lattice spacing can be derived using Bragg's relation:

$$n\lambda = 2dsin(\theta), n = 1,2,3 \ldots$$

Equation 8: Bragg's relation

where n = an integer (order of reflection), λ = wavelength of radiation, d = lattice spacing and θ = angle of incidence.[107]

If the angles 2θ are measured, under which constructively interfering X-rays leave the crystal, the Bragg relation gives lattice spacing, which are a characteristic for a particular compound. In the powered samples, constructive interference occurs when a small fraction of powder particlesare oriented such that a certain crystal plane is at angle θ to the incident beam.[107]

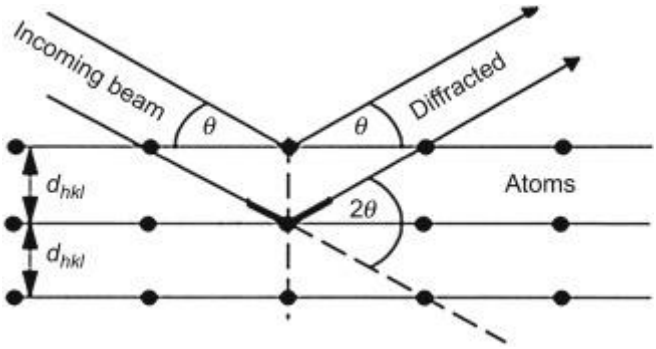

Figure 7:Geometrical condition for diffraction from lattice planes, reproduced (without permission) from Hübschen et al.[108]

The Scherrer equation can be used to approximately estimate the crystallite sizes. It relates the average crystal size in nm (*L*) to line width:

$$\beta(2\theta) = \frac{K\lambda}{Lcos(\theta)}$$

Equation 9: Scherrer Equation

where $\beta(2\theta)$ = peak width (FWHM) of reflection at angle 2θ in radians, *K* = dimensionless shape factor (~0.9), λ = wavelength of radiation in nm, and θ = angle of reflection in radians.[107]

The advantage of using X-rays is their penetrating power. pXRD can be used to study catalysis in dynamic conditions and even monitor changes in solid-state reactions such as reduction and oxidation with time. If the particles are too small or amorphous, they cannot be detected by pXrd. Hence pXRD does not guarantee absence of phases other than those detected in the pattern.[107]

2.1.2.4 Inductively coupled plasma – optical emission spectroscopy (ICP-OES)

ICP-OES is a proven technique for elemental analysis of a sample. It consists of two parts the ICP (plasma used as source of atomic excitation) and an optical spectrometer. A plasma is a

gas in which atoms are present in an ionised state, but overall, it is neutral. Usually, argon is used as the source of plasma (due to high ionisation energy and chemical inertness). Hence all elements other than argon can be determined. Basically, plasma is used as a source to excite the metal atoms in the solution and when these atoms return to their ground state, they emit a polychromatic light of their own characteristic wavelength. The major components of an ICP-OES consist of a nebulizer for sample introduction, ICP torch, high frequency generator, transfer optics, and spectrometer. A solution of an element whose concentration is to be known is introduced in the ICP torch as aqueous aerosol via nebulizer. The ICP torch is turned on creating an intense electromagnetic field. The argon gas is ionized in the intense electromagnetic field. The sample immediately collides with the electrons and charged ions in the plasma and is itself broken down into charged ions. The elements in the sample breaks up into atoms and losses electrons and re-combine repeatedly giving light of their characteristic wavelength. The polychromatic light is passed through a Rowland ring (monochromator) to separate the light of different wavelengths, which then falls on a photomultiplier tube which generates current proportional to the intensity of light and sends it to the data processor. A calibration curve is made with known concentration of element and subsequently the unknown concentration is identified.[109-110]

Several wavelengths are available for determination of any given element, hence ICP-OES works well for all concentrations. ICP uses a very small amount of sample but ICP is a destructive method and hence, sample is not recovered.[109-110]

2.1.2.5 H_2 Temperature programmed reduction (TPR) / CO_2 Temperature Programmed Desorption (TPD)

Temperature programmed techniques are a category of techniques in which a chemical reaction is monitored while the temperature increases linearly with time.

TPR is used to gather information on the temperature needed for completion of reduction of a catalyst. It is usually applied in the context of metal or metal oxide-based catalysts. The catalysts are typically heated at a constant rate in a reducing atmosphere (usually $H_2 – N_2$) and a thermal conductivity detector or mass spectrometer attached at the outlet, which is used to indicate the consumption of gas at temperature. The area under a TPR curve represents the total hydrogen consumption and is expressed in moles of hydrogen consumed per mol of metal atoms. Often, information about reduction mechanism can also be obtained from TPR curves (especially for bimetallic catalysts).[107, 111]

TPD is a technique that allows the study of the interaction of gases with solid surfaces and to evaluate active sites on catalysts, understand adsorption, surface reaction and desorption. In a TPD run, a small amount of catalyst is first degassed at high temperature under inert environment. Then a gas is adsorbed on the catalyst surface. In inert environment using a carrier gas (usually helium or a gas with different thermal conductivity to the gas of interest) the sample is linearly heated and at the outlet and the composition of gas is determined using a thermal conductivity detector or mass spectrometer. The evolution of adsorbed gas is plotted as a function of temperature.[112]

CO_2 is an acidic molecule which gets adsorbed on the basic sites of the catalyst. With increases in the temperature the CO_2 desorbs and the higher the temperature of desorption, the stronger are the basic sites.

2.1.2.6 Thermogravimetric analysis (TGA)

TGA is used to determine a material's thermal stability and the fraction of volatile components. This is done by heating the sample at a constant rate while monitoring the change in weight. The measurements are usually carried out in air or in inert environment. The weight of the sample is recorded as a function of increasing temperature. Information about phase transition, absorption, adsorption, desorption, chemisorption and thermal decomposition can be obtained by TGA.[113]

The construction of thermogravimetric analyser is simple and consists of a precision balance, a sample pan inside a furnace with temperature controller and mass flow controllers controlling the flow of gases. Often, a water-cooling system is attached with the analyser to quickly cool down the furnace after an experiment.

2.1.3 Batch reactor

In a typical batch reactor system, all the reactants and catalysts are charged into the vessel, and nothing is added or removed during the time of reaction. It is a perfectly mixed vessel where reactants are converted into products. All the reaction variables (concentrations, pressure) change with time. The concentration of reactants decreases, and products increases with the time of reaction. Since the reactant concentrations are initially large, this means that the reaction rate and heat transfer load is high initially and decreases with time. There is no steady state in batch reactors. Hence often, control parameters are changed with time.[114]

Batch reactors are usually large diameter, metallic cylinders with one end being welded. They are generally mounted vertically on a support structure. The heat is generally transfers through the wall either by furnace or jacket. Also, coils of pipes are installed inside a batch reactor to provide extra heating or cooling. These coils also act as a baffles. A shaft attached with a fixed or variable speed electrical motor runs through the top of the reactor. At the end of the shaft inside the cylinder it equipped with a stirrer, which is used to mix the contents of the reaction vessel. The speed and type of agitator depends on density, viscosity and state (slurry, gas-liquid, emulsion etc.) of the mixture. Advantages of using a batch reactor are simple construction, low installation cost, simple instrumentation and flexible operation. However, there operating cost is higher than continuous processes, requires more operating staff and have safety concerns due to unsteady-state processes.[115]

2.1.4 Chromatographic techniques

In chromatography, the components are separated by distribution between two phases. One of the phases is a stationary phase (solid or liquid) and the other phase is mobile phase (liquid, gas or fluid). A multi component mixture is introduced in chromatography into a moving phase. The moving phase is in contact with the stationary phase and a continuous supply of moving phase transports the mixture past the stationary phase. In the stationary phase, components of mixture are separated due to their relative affinities for the phases as determined by molecular structure and intermolecular forces. The components which have high affinity for the stationary phase spend longer in the stationary phase. Hence, the components with higher affinity for the stationary phase will move through the system slowly, while components with lower affinity move faster. This difference in the migration rate results in the separation of mixtures and forms the basis for chromatographic techniques.[116]

Even though the system is dynamic, it is operated close to equilibrium conditions by optimizing the mobile phase velocity and designing the stationary phase to allow achievement of rapid equilibrium. Under these conditions, the system can be characterized by a thermodynamic partition/ distribution coefficient K

$$K = \frac{C_s}{C_m}$$

Equation 10: Distribution coefficient

Where, C_s is concentration of analyte in stationary phase and C_m is concentration of analyte in mobile phase. Two components with same distribution coefficient will not be separated. The

separation may be improved by varying the mobile phase, the stationary phase or the temperature of the system.[116]

Chromatographic techniques can be used for both qualitative as well as quantitative applications. In qualitative analysis, presence or absence of a particular compound in a mixture can be confirmed by comparing a chromatogram of pure substance with that of the mixture under identical conditions. However, chromatograms are not unique for a particular compound and many other substances will exhibit same chromatographic behaviour under identical conditions. With the help of suitable standards and calibrations, chromatograms can be used to determine the amount of individual components in a sample. These techniques are widely used in the measurement of product distributions in the reaction mixtures.[116]

Depending upon the mobile phase, chromatographic techniques can be classified into three categories: Gas chromatography, Liquid chromatography and supercritical fluid chromatography depending on whether the mobile phase is a liquid, gas or supercritical fluid, respectively.[116]

2.1.4.1 Gas Chromatography (GC)

GC is a term used for the chromatographic methods in which the mobile phase is a gas. It has a capability of high resolution, selectivity and sensitivity. GC may involve either a solid stationary phase or a liquid stationary phase retained on a solid sorbent (packed column) or column wall (open tubular column). Gas-solid chromatography (GSC) comprises all techniques with an active solid as stationary phase and gas-liquid chromatography (GLC) those involving a liquid stationary phase.[117]

In a typical GC, there are three sperate heated zones for inlet, column and detector. Numerous GC have two different columns and detectors. The sample is injected into the chromatograph via the sample inlet into a continuous flow of mobile phase (also called carrier gas). The sample is vaporized in the inlet and transported by the carrier gas to the heated column where separation occurs. The individual components give rise to an electrical signal in the detector, which may have provision for inlet of additional makeup gases. After suitable amplification the detector signal is sent to a data processor. Pure components in the identical conditions give a characteristic retention time, which can be used to identify different components. With appropriate calibration, the amounts of the components can be calculated too. In GC, the basic requirement of the sample is that it should be thermally stable and should have a significant vapor pressure at column temperature, which will allow the sample to vaporize and move with

the carrier gas. Hence, GC can be applied to all permanent gases, non-ionizing small or medium sized organic molecules and many organometallic compounds. It cannot be used for macromolecules or salts. The carrier gases are usually cheap and non-reactive gases. Hydrogen, helium, and nitrogen are some commonly used carrier gases. However, it is important that the highest purity gas and oxygen and moisture traps are used to reduce deterioration of the stationary phase and lessen detector noise. The flow of carrier gas should be constant so that the retention times do not vary, and flow over a sensitive detector will not become nonlinear.[117]

The column is the key part of a GC for separation to occur. The column's tubing contains the stationary phase which determines the selectivity and efficiency of the separation. Columns in GC are reusable. The packed columns are usually 0.5m-3 m long with 3mm-6 mm OD and 2mm-4mm ID. Packed columns are inexpensive and require lesser technical expertise to obtain reproducible results. The less commonly used open tubular columns give higher resolution, greater sensitivity and reduced analysis time but are expensive. The ID of these column are 0.1-1.0 mm and column lengths are 5-50m and the thickness of stationary phase is 0.1-5 µm. With increase in the thickness of the stationary phase, the sample capacity increases, and efficiency decreases. The column tubing must be chemically inert, thermally stable, direct carrier gas, robust and flexible. Earlier materials such as stainless steel, copper, aluminium or nickel were commonly used, which were later replaced by glass columns due to greater chemical internes. Fused silica columns are also widely used but are weak and friable. Polysiloxanes are most commonly used as stationary phases, because a variety of groups can be incorporated into the structure, allowing a wide range of polarities as well as being robust and stable.[117]

The most commonly used detectors are thermal conductivity detector (TCD) and flame ionization detector (FID).

Thermal conductivity detector (TCD): TCD was the first detector to be used and is still widely used. The principal behind detection is reduction in heat loss of a hot wire because of the presence of solute molecules. The TCD is made up of four tiny coiled wires (filaments) in a Wheatstone bridge configuration. The wires are usually mounted concentrically in a cylinder cavity. These wires are electrically heated when the column effluent flows past two of the wires and reference gas flows past the other two. The gas carries away the excess heat at a rate dependent upon the thermal conductivity of the gas. A thermal equilibrium is established when the column effluent consists of carrier gas alone. When effluent consisting of solute molecules

enters the detector the heat loss alters, the temperature of the wires changes and resistance of the wires changes, causing a change in the Wheatstone bridge. The signal appears as a difference in current from the reference. Thus, TCD responds to any compound irrespective of it's structure whose thermal conductivity differs from that of the carrier gas. For this reason, hydrogen or helium are most often used as a carrier gas. Nitrogen is only used when analyte is hydrogen or helium as thermal conductivity of nitrogen is like most organic compounds. The TCD requires constant temperature control with good thermal insulation from the column oven and also should be protected from oxygen while they are hot.[117]

Flame ionization detector (FID): FID is the most common detector used in the GC.[117] In FID carrier gas exiting the column flows through a jet, mixes with hydrogen gas and flows to a micro burner, which is swept by a high flow of air for combustion. Ions produced by combustion are collected at a pair of polarized electrodes, constituting a small background current, which is the signal. The number of ions depends upon presence and absence of solute in carrier and thus the signal spikes when the carrier contains solute. FID gives no response to inorganic compounds (that do not burn). FID uses three gas (hydrogen, carrier and air) whose flowrates must be adjusted correctly with respect to one another. Large deviations from optimum values will produces noisy background, difficulty in flame ignition and might extinguish as the sample solvent peak is eluted. The FID often needs to be baked off at high temperature after extended use as they become contaminated by stationary phase and sample residues.[117]

2.1.4.2 HPLC

The basic components of an HPLC system are a solvent reservoir (mobile phase), a solvent delivery system (a pump), a sample introduction device (injector), a column, detectors and a data system. The column (containing stationary phase) is connected to the injector via a narrow bore tubing. The separated components are then passed via a narrow bore tubing to the detector where they generate a signal. Columns are usually packed with rigid solids (for example silica), resins (usually polystyrene divinylbenzene) and soft gels. Rigid solids based on silica are the most common HPLC packings. Some of the commonly used detectors are UV/Vis detectors, electrochemical detectors, refractive index detectors and conductivity detectors.[118]

UV/Vis detectors: This is the most common type of detector used these days. The detector operates on the same principals as a spectrophotometer. Light from a radiation source is passed through a monochromating device and then to a cell in which the mobile phase flows. The

amount of transmitted light is measured using an array of photodetectors. Using Beer-Lambert law absorbance is calculated. At a fixed wavelength a linear relationship exists between absorbance and concentration. UV/Visible detectors are operated typically as solute property detectors, wherein direct detection of the solute is achieved by selecting a wavelength at which the solute exhibits a high value of molar absorptivity. Using an appropriate calibration curve, concentration is obtained.[118]

2.2 Experimental

2.2.1 Materials

All gases used in this thesis (nitrogen, argon, hydrogen, carbon-dioxide, helium) were obtained from BOC and had a minimum purity of 99.99 %. Nickel nitrate hexahydrate, sodium hydroxide and nitric acid were purchased from Fisher Scientific. Aluminium nitrate nonahydrate and γ-Al_2O_3 were purchased from Alfa Aesar (Fisher Scientific). Magnesium nitrate hexahydrate and benzoic acid were purchased from Arcos Organics (Fisher Scientific).Nitric acid was purchased from SLR (Fisher Scientific),ethylene glycol and 1,2-butadiene were purchased from Sigma Aldrich. Phenol was purchased from TCI. A commercial 5% Pt/C catalyst was obtained from Johnson Matthey and 5% Pd/C catalyst was received from Koch laboratories. All the chemicals were used as received without any further purification. A Sorvall Legend centrifuge with 50 mL centrifuge tubes was used for all centrifugations. UHP water was obtained from a Purite Neptune and had a resistivity of 18.2 MΩ.

2.2.2 Synthesis of Catalysts

2.2.2.1 Synthesis of Hydrotalcite derived Ni/Mg/Al catalyst

The hydrotalcite derived catalysts with varying Ni wt.% (5%, 10%, 15%, 20%) and M^{2+}/M^{3+} (2, 3, 6, 8) were synthesized using co-precipitation method reported widely in the literature. Calculated amounts of nickel nitrate hexahydrate, magnesium nitrate hexahydrate and aluminium nitrate nonahydrate were weight and mixed in a beaker with 55 mL of UHP water (called solution A). In a second beaker, 250 mL 2M NaOH solution was prepared (called solution B). A 500 mL 3-neck round bottom flask was filled with 100 mL UHP water and was placed on a hot plate for stirring at room temperature. A magnetic stirrer bar was dropped in the flask. A Jenway 3510 pH meter was used to monitor the pH of the solution. Before every synthesis, the pH meter was calibrated at pH 4, 7 & 9 using standard pH buffer solutions. The probe of the Jenway 3510 pH meter was lowered in the flask until it was immersed in the water. Using a plastic syringe, solution B was dropped in the flask until the pH reached 10. Solution

A was filled in a dropping funnel and opened to give a flowrate of 0.3 mL min^{-1} and was placed in one of the openings of the flask. As solution A started to drop in the flask, solution B was manually injected dropwise using a plastic syringe in the flask to maintain the pH constant at 10±0.2. After the solution A was completely dosed at pH 10, the slurry was left to stir at room temperature for 24 h. After 24 h, the slurry was filtered using a sintered glass funnel in vacuum. The precipitate was washed with UHP water at 80 °C until the pH of the filtrate became 7.0. The residue on the filter was taken in a glass beaker and was dried overnight at 120 °C in a static air oven. The obtained material was nickel containing layered double hydroxide. This material was used as precursor for the preparation of Ni/Mg/Al catalysts.

Calcination: Calcination was carried out in air in a muffle furnace bought from Paragon Instruments equipped with a Sentry Xpress 4.0 microprocessor to control the temperature. All the samples were calcined at 800 °C for 5 h (ramp rate: 5 °C min^{-1}). Table 2 represents the nominal composition of LHD derived catalysts in calcined state. Samples are given a nomenclature of aNib, where a is M^{2+}/M^{3+} and b is Ni wt.%. The state of hydrotalcite material (precursor, calcined or reduced) is mentioned superficially where required.

Table 2: Nominal compositions of LDH derived catalysts (Ni wt.% in calcined state)

Sample name	Ni wt.%	M^{2+}/M^{3+}
3Ni5	5%	3
3Ni10	10%	3
3Ni15	15%	3
3Ni20	20%	3
2Ni15	15%	2
6Ni15	15%	6
8Ni15	15%	8

Reduction: All the reductions were carried out in an in-house built system. In a quartz tube (OD=1/2inch) a piece of quartz wool was placed in the centre. On the piece of wool, sample was dropped and after that another piece of quartz wool was used to pack the sample. A K-type thermocouple was attached using high temperature wire on the outside of the tube positioned in centre of the catalyst bed. The thermocouple was attached to a PID temperature controller (omega CN-7500), which took feedback from the thermocouple and controlled the temperature of furnace. The quartz tube was placed inside the furnace and positioned as such that the

catalyst bed is in the middle of furnace. Gases were supplied to the tube using MKS G series mass flow controllers. The gases were passed through filters of activated carbon and zeolite sieves to prevent hydrocarbon impurities and/or water from entering the MFCs. The quartz tubes were attached to the gas supply via Ultra-Torr vacuum fittings (Swagelok).

All the samples were reduced ex-situ in 60 mL min^{-1} of 20% H_2/N_2 at 800 °C for 30 min (ramp rate: 10 °C min^{-1}). Sample calcined 3Ni15 was also reduced at 650 °C, 700 °C, 750 °C (other conditions the same) to observe the effect of reduction temperature.

2.2.2.2 Ni/γ-Al_2O_3 incipient wetness impregnation (IWI) catalysts

Before impregnation, pore volume of γ-alumina was determined. About 500 mg of γ-alumina was dried overnight at 120 °C in an oven. After that, to ensure no water is retained inside the pores of the support, γ-alumina was dried in a vacuum oven for around 4 h at 120 °C. Whilst γ-alumina was above room temperature, UHP water of known mass was added dropwise and mixed using a vortex mixer frequently to ensure an even dispersion of the water. Once the γ-alumina was seen to be macroscopically wet, the pores were assumed to be filled. The mass (and volume) of water added was measured, and this was used to calculate the approximate apparent pore volume of the γ-alumina.

To prepare 15 wt.% Ni/γ-Al_2O_3 IWI catalyst, γ-alumina was first dried overnight at 120 °C in air in an oven followed by drying in a vacuum oven for around 4 h at 120 °C. Calculated amount of $Ni(NO_3)_2.6H_2O$ was dissolved in deionised water of volume equal to the pore volume of support. The $Ni(NO_3)_2.6H_2O$ solution was added dropwise to the γ-Al_2O_3 with frequent mixing using a vortex mixer to ensure an even distribution. The impregnated γ-Al_2O_3 was then dried overnight in an oven at 120 °C and then further dried in a vacuum oven for a minimum of 4 h at 120 °C. The catalyst was calcined at 500 °C for 4 h and was reduced at 800 °C for 30 min in the same setups mentioned above.

2.2.2.3 Reduction of commercial catalysts

Both the commercial catalysts (Pt/C & Pd/C) were reduced ex situ before reactions. The reduction was carried out in the same setup as described above. Pt/C was reduced at 400 °C (ramp rate = 10 °C min^{-1}) in 50mL flow of 20% H_2-N_2 for 4 h. Pd/C was reduced at 300 °C (ramp rate = 10 °C min^{-1}) in 50mL flow of 20% H_2-N_2 for 3 h.

2.2.3 Characterisation

2.2.3.1 H_2 Temperature programmed reduction (TPR) / CO_2 Temperature programmed desorption (TPD)

All the temperature programmed experiments were carried out in an in-house built system (Figure 8). In a quartz tube (OD=1/4inch) a piece of quartz wool was placed in the centre. On the piece of wool, pre-determined mass of sample was dropped and after that another piece of quartz wool was used to pack the sample. A K-type thermocouple was attached using high temperature wire on the outside of the tube positioned in centre of the catalyst bed. The thermocouple was attached to an omega CN-7500 temperature controller, which took feedback from the thermocouple and controlled the temperature of furnace. The quartz tube was placed inside the furnace and positioned as such that the catalyst bed is in the middle of furnace. Gases were supplied to the tube using MKS G series mass flow controllers. The gases were passed through filters of activated carbon and zeolite sieves to prevent hydrocarbon impurities and/or water prior from entering the MFCs. The quartz tubes were attached to the gas supply via Ultra-Torr vacuum fittings (Swagelok). The outlet of the quartz tube was connected to a calcium chloride column (via Ultra-Torr vacuum fittings (Swagelok)) to remove water before the gases were analysed with a homebuilt thermal conductivity detector (TCD).

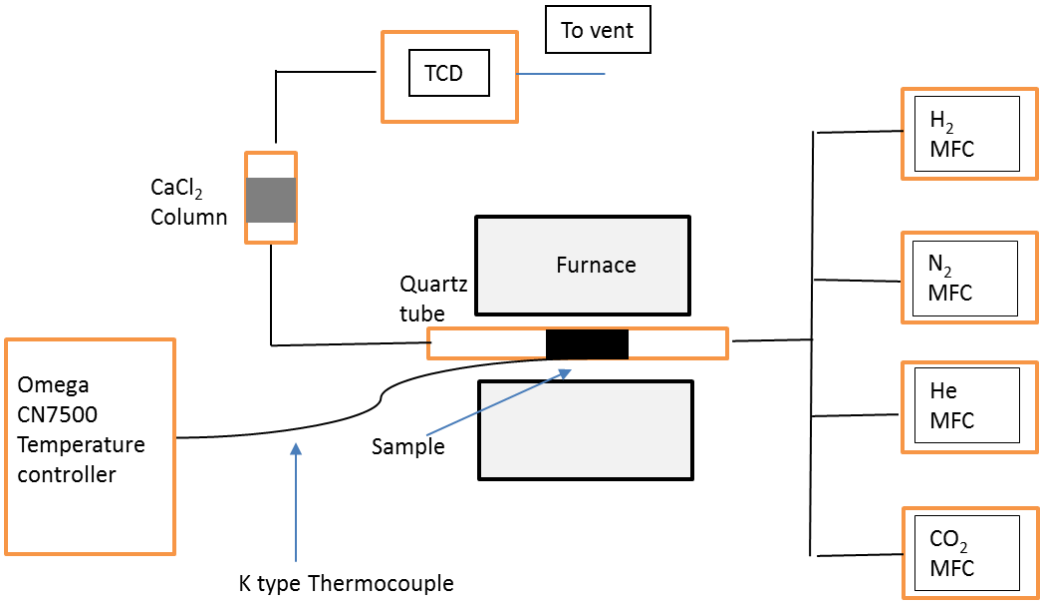

Figure 8: Schematic representation of set-up used in TPR/TPD (MFC: mass flow controller)

H_2 Temperature programmed reduction: Calcined hydrotalcite samples were subjected to TPR experiments to determine the reducibility of the samples. TPR experiments were conducted in 50 mL min^{-1} of 5% H_2/N_2. 70mg of sample was used in each run. First the temperature was

raised from room temperature to 120 °C (ramp rate = 10 °C min^{-1}) and held at 120 °C for 2 h to degas the sample. After that the temperature was increased from 120 °C to 900 °C at ramp rate of 7.5 °C min^{-1} and the gases were analysed via TCD.

CO_2 Temperature programmed desorption (TPD): Calcined hydrotalcite samples were subjected to TPD experiments to determine the basicity of the samples. Ideally the reduced sample should have been subjected to TPD experiments. However, it is believed that basicity of support wouldn't change much upon reduction. Hence due to time constraint and save time by not reducing, the calicned samples were used to determine bascitiy by TPD. First, 100mg of sample was degassed under helium environment (flowrate = 30mL min^{-1}) at 500 °C for 2 h and cooled to room temperature under helium. Once the sample was degassed the calcium chloride column was removed to prevent absorption of CO_2 on the column. After room temperature was reached, 30 mL min^{-1} of 50% CO_2/He mixture was flowed for 1 h. After that pure helium at a flowrate of 30 mL min^{-1} was flowed for 15 min to desorb any weakly absorbed CO_2. The helium flow rate was lowered to 10 mL min^{-1} and temperature was ramped from room temperature to 600 °C at ramp rate of 10 mL min^{-1}. The gases were analysed during the ramp using homebuilt TCD system. The amount of CO_2 represented by TPD peaks was calibrated by decomposition of known masses of Calcium carbonate diluted in SiC ($CaCO_3$ – ≥ $CaO + CO_2$; 3 different masses, each run-in duplicate) in helium environment (flow rate = 10 mL min^{-1}).

The total basicity was calculated by means of the integration of the overall desorption profile. The overall profile was de-convoluted into three gaussian peaks. The peak fit was performed by putting "bounds" on the centre of the peak. The gaussian peaks were fitted with bounds on centre as 50 °C to 160 °C (for weak basic sites), 160 °C to 260 °C (for medium basic sites) and 280 °C to 400 °C (for strong basic sites).[3] The main aim of this experiment was not to explicitly calculate the basicity of support but rather identify the trends on increase / decrease in basicity with addition of MgO.

2.2.3.2 Powder X-ray Diffraction (pXRD)

Precursors, calcined, reduced and spent catalysts were characterized by means of powder X-ray diffraction. All the pXRD diffractograms were acquired using a Bruker AXS D8 Advance diffractometer, fitted with a Lynxeye Soller PSD detector and controlled by Diffrac and XRD commander software. Samples were placed on a low background silicon sample holder (silicon wafer (100)-cut off orientation 9° towards (001), Sil'tronix Silicon Technologies, mounted in

a plastic puck) using Vaseline as adhesive. Copper $K\alpha_1$ (λ = 1.5406 Å) and $K\alpha_2$ (λ = 1.5444 Å) radiation was used. Diffractograms were recorded in open air environment with a 2θ range of 10 – 90^o and a typical scan lasted ~110 min.

The average crystallite size was estimated using the Scherrer equation given in the methodology section. Origin software was used to fit a Gaussian function at different reflections for a given set of samples. This gave the full width at half maximum (FWHM) of the reflection, permitting crude estimation of the crystallite size using the Scherrer equation (Equation 9)

2.2.3.3 ICP-OES

Elemental analysis of calcined samples and spent catalysts was carried out to determine the amount of Ni, Mg, and Al in the samples. Digestion was carried out by boiling a pre-calculated and weighed amount of sample in around 3 mL of aqua regia (3:1 v/v conc. HCl: conc. HNO_3) at 80 °C for 1 h. After digestion was complete and the solutions were cooled to room temperature, they were diluted with deionised water using volumetric flasks to achieve a solution with the appropriate metal concentration (Ni: 8 mg L^{-1}; Mg: 16 mg L^{-1}, Al: 16 mg L^{-1}). Controls were prepared from the water-soluble salt precursor $Ni(NO_3)_2.6H_2O$ for Ni, $Mg(NO_3)_2.6H_2O$ for Mg and $Al(NO_3)_3.9H_2O$ for Al. These standards were used to confirm the absence of any significant deviations on a given run. The required amount of the salt was dissolved and diluted in aqua regia and deionised water, ensuring both the metal and acid concentrations matched that of the digested samples. All samples were prepared in duplicate.

A Thermo iCAP 6000 series instrument was used. The instruments has a cyclonic spray chamber, a concentric nebuliser, and a vertical torch. The nickel content was determined from the emission line at 361.9 nm, the magnesium content was determined from the emission line at 279.0 nm and the aluminium content was determined from the emission line at 236.7 nm. The instrument was calibrated before the samples were measured using commercial Ni, Mg and Al calibration standards of known metal content.

2.2.3.4 BET

The BET surface area of reduced Ni/Mg/Al hydrotalcite derived catalysts was measured by nitrogen adsorption and desorption at 77 K using a Micromeritics ASAP 2020 volumetric adsorption analyser. Samples were degassed at 240 °C (ramp rate: 10 °C min^{-1}) for 2.5 h under dynamic vacuum before analysis. P/P_0 values between 0.05-0.25 were used in the BET calculation for evaluation of the surface area.

2.2.3.5 Fourier Transform infrared spectroscopy (FTIR)

The spectra of hydrotalcite precursors was recorded using a Perkin Elmer Frontier IR spectrometer in the wavenumber range of 4000-400 cm^{-1}.

2.2.3.6 TGA

TGA of aNib-P samples was carried to determine the change of structure with thermal treatment and therefore fix a calcination temperature. A Perkin Elmer TGA 8000 was used for the TGA experiment. A small quantity (~10 mg) of each sample was heated from room temperature to 900 °C at a rate of 10 °C min^{-1} in flowing air.

2.2.4 Aqueous phase reforming

Aqueous phase reforming was carried out in a batch autoclave reactor 300 mL EZE-Seal Reactor manufactured by Parker Autoclave engineers. The autoclave was a second-hand instrument and was re-commissioned after repairs. A good amount of time during this project was invested in fixing the reactor (leaks, stirring system, power supply to furnace) and attaching it to the auxiliaries (gas lines, cooling water). The autoclave vessel is a 300 mL steel cylindrical vessel (dead volume= 210 mL, due to the space occupied by stirrer and thermowell when mounted), which is attached to the main body by 6 bolts and metal-metal sealing is obtained using PTFE BS 220 O-rings. The main body has a thermowell which goes into the vessel when the vessel is mounted. In this thermowell, a K-type thermocouple is inserted. This thermocouple is attached to an Omega CN7500 temperature controller to control the temperature of the furnace. The furnace is jacketed around the vessel for heating. A paddle type stirrer is also mounted on a central rod and goes inside the vessel when the vessel is mounted. The stirrer is powered using a DC bench power system (TENMA, single output 0-3A/0-60V) and speed of rotation is observed on a tachometer. The voltage on the DC bench power system can be adjusted to increase/decrease the speed of rotation. An internal cooling coil is also provided with the autoclave to cool the content of the vessel but it was only used as a baffle in this work and no active cooling was employed. Nitrogen was filled into the reactor using a manifold system, which is connected to the gas cylinder via a ball valve and the manifold is connected to the reactor using another ball valve. Hence, to fill the reactor, first the ball valve between manifold and cylinder is opened to fill the manifold with nitrogen, and thereafter the valve is closed. Once the manifold is filled up, the valve between the manifold and reactor is opened to fill the autoclave up to the desired pressure. Argon was filled directly from the gas cylinder using a needle valve. Both Nitrogen and Argon are used as received from the vendor

without any purification. Two pressure gauges are mounted on the reactor, first a small one (0-40 bars) to accurately fill the gases in the reactor and a second one (0-300 bars) to increase the monitoring range of the pressure. The small gauge is closed using a needle valve once the gases are filled to avoid damage to the gauge when the pressure is above 40 bars. All the valves, connections and pressure fittings were procured from Swagelok or Ham-let.

In a typical APR experiment, catalyst and feed are charged into the autoclave vessel and the vessel is mounted on the body of the autoclave. Firstly, the reactor is vented 3 times with nitrogen to eliminate any oxygen or hydrogen in the system. Then 2 bars of argon are filled in the reactor by opening the needle valve. This argon is used as internal calibrant for analysis for hydrogen. After that the reactor is pressurized using nitrogen gas. Then the small gauge is cordoned off and the reactor is isolated from the gas supply using a ball valve. The furnace is jacketed around the vessel, before turning on heating and stirring. The autoclave was ramped from room temperature to reaction temperature at 5 °C min^{-1} and on reaching the set temperature the time of the reaction was started. Once the time of reaction is completed, the furnace is removed using heat-resistant gloves and the vessel is left to cool down. Once the vessel is cooled to room temperature, the gases were taken in a steel sampling vessel via a needle valve available on the reactor body. The sampling vessel has a pressure gauge mounted on it and was filled up to 5 bars of gas. The sampling vessel is taken for gas analysis. The rest of the gas is vented out and the autoclave vessel is unbolted. The liquid products (with catalyst inside) are taken in a centrifuge tube and centrifuged for 30 min at 8000 rpm. Once the solid-liquid is separated, the liquid is filtered using a syringe filter. The filtrate is used for liquid product analysis. The solid obtained from centrifugation, is dried overnight at 80 °C before vacuum drying at 120 °C. Once the catalyst is dried it is taken for further analysis or used again in the reaction.

2.2.4.1 Aqueous phase reforming of ethylene glycol (EG)

50 g of 6 wt.% ethylene glycol was used as a feed for aqueous phase reforming. In a typical experiment 750 mg (catalytic loading: 0.25 g of catalyst/g of substrate) was used, although it was varied (0.141 & 0.075) in a few cases where specified to study the effect of catalytic loading. Most of the reactions were carried out at 260 °C, however a few reactions were also carried out at 240 °C and 250 °C where specified to study the effect of temperature. The reactor was pressurized just above the bubble point of feed: 40 bar at 240 °C, 45 bar at 250 °C and 50

bar at 260 °C. Mostly the time of reaction was fixed as 2 h, some reactions where specified were carried out for 1 h to determine the effect of reaction time.

Analysis of gas products: For the analysis of the gas products, two GC's were connected in sequence to avoid any error due to pressure difference. Both GCs are equipped with 6-way sampling valves connected in series. The first GC is a Bruker 456-GC equipped with both a flame ionization (FID) and a thermal conductivity (TCD) detector. A Restek micropacked column (ShinCarbon ST 100/120, 2 m, 1 mm I.D., 1/16'' O.D., Silco) was used and hydrogen was used as carrier gas. The TCD was used to detected argon and nitrogen, while FID was used to detect CO, CO_2, and hydrocarbons (via a methaniser put after TCD. The methaniser using hydrogen and CO/CO_2 as reactants converted the CO/CO_2 into methanol/methane which could be then deteched by FID). The column oven temperature was 35 °C for 9 min and thereafter ramped to 60 °C (ramp rate 20 °C min^{-1}.) and held at 60 °C for 30 min. The injector was kept at 260 °C and the detectors were kept at 250 °C. The second GC was a Shimadzu GC-2014 gas chromatograph, equipped with a thermal conductivity (TCD) detector and was used for hydrogen analysis. The gas chromatograph was equipped with a micropacked column (Restek ShinCarbon ST 80/100, 2m, 2mm I.D., 1/8'' O.D. Silco) and nitrogen was used as carrier gas. The column oven temperature was kept at 60 °C, the temperature of injector was 210 °C, and the temperature of detector was 200 °C. A calibration plot of area of hydrogen/area of argon vs. molar ratio of H_2/Ar was made beforehand and was used to evaluate the concentration of hydrogen (see appendix 1).

Analysis of Liquid products: Before and after reaction samples were analysed using a GC equipped with FID. 1 mL of sample was diluted in 5 mL acetonitrile and 100 mg of 1,2 butadiene was added to be used as internal calibrant before injecting the samples in the GC. A HP 5890 GC equipped with 30m x 0.25mm x 0.25mm film thickness J&W CP52CB Carbowax column was used and hydrogen was used as carrier gas. The temperature of injector was 220 °C, detector was 300 °C, and initial oven temperature was 35 °C, held for 5 min and then ramped to 240 °C at 5 °C min^{-1}, and held at 240 °C for 10 min. The GC was injected manually using a Hamilton micro syringe (0-10 µL, 701) with 0.5 µL solution. A calibration plot of concentration of ethylene glycol vs. area of ethylene glycol/area of 1,2 Butadiene was made beforehand and used to evaluate concentration of ethylene glycol (see appendix 1).

Conversion and selectivity for hydrogen were calculated using Equations 11 and 12 respectively:

$$Conversion\ (\%) = \frac{Moles\ of\ EG\ before\ reaction - Moles\ of\ EG\ after\ reaction}{Moles\ of\ EG\ before\ reaction} \times 100$$

Equation 11: conversion of EG in APR

$$Selectivity\ (\%) = \frac{Moles\ of\ hydrogen}{(Moles\ of\ EG\ before\ reaction - Moles\ of\ EG\ after\ reaction)\ \times 5} \times 100$$

Equation 12: Selectivity for hydrogen in APR of EG

2.2.4.2 Aqueous phase reforming of Phenol

The aqueous phase reforming of phenol was carried out using 50 mL of 0.2 M phenol at 240 °C, 250 °C and 260 °C with pressure just above bubble point. 750 mg of catalyst was used. The reaction time was 2 h.

Analysis of gas products: The gases were analysed using the same setup as described in analysis of ethylene glycol products.

Analysis of liquid products: The samples before and after reaction were analysed using HPLC equipped with UV/Vis detector. First the samples were diluted 10 times and thereafter 0.5 mL of diluted sample was mixed with 0.5 mL of 0.01 M benzoic acid as internal calibrant. A Waters XBridge C18 column (100 x 4.6 mm, 3.5um) was used. For mobile phase, a gradient elution of 90% (0.1% formic acid in water), 10% Acetonitrile to 5% (0.1% formic acid in water), 95% Acetonitrile over 10 min was used. The chromatogram was extracted at 260 nm. A calibration plot of area of phenol/area of benzoic acid vs. concentration of phenol was made beforehand and used to evaluate concentration of phenol (see appendix 1).

The activity and selectivity of hydrogen were calculated using equations Equation 13 and Equation 14 respectively:

$$Conversion\ (\%) = \frac{Moles\ of\ phenol\ before\ reaction - Moles\ of\ phenol\ after\ reaction}{Moles\ of\ phenol\ before\ reaction} \times 100$$

Equation 13: Conversion for APR of phenol

$$Selectivity\ (\%) = \frac{Moles\ of\ hydrogen}{(Moles\ of\ phenol\ before\ reaction - Moles\ of\ phenol\ after\ reaction)\ \times 14} \times 100$$

Equation 14: Selectivity for hydrogen in APR of phenol

Chapter 3: Results and Discussion

3.1 Characterization of catalyst precursors and catalysts

This section describes the results of characterization techniques (namely: pXrd,, ICP-OES, BET, TGA, FTIR, TPR, TPD) for catalyst precursors and catalysts used in this project.

3.1.1 pXrd

The pXrd patterns (Figure 9) of precursor hydrotalcite with Ni loading: 5 wt.%, 10 wt.%, 15 wt.% and 20 wt.% and M2+/M3+ ratio: 2,3,6,8 showed reflections at 2Θ = 11.5°, 23.5°, 35°, 60.3° and 61.5° corresponding to the diffraction of X-rays on (003), (006),(009), (110) and (113) basal planes in the 3R rhombohedral lamellar structures, confirming the formation of hydrotalcite structure.[4,119] No additional phases were observed in any of the precursors, meaning Ni cations incorporated in the hydrotalcite have isomorphously replaced Mg cations in the hydrotalcite layers.

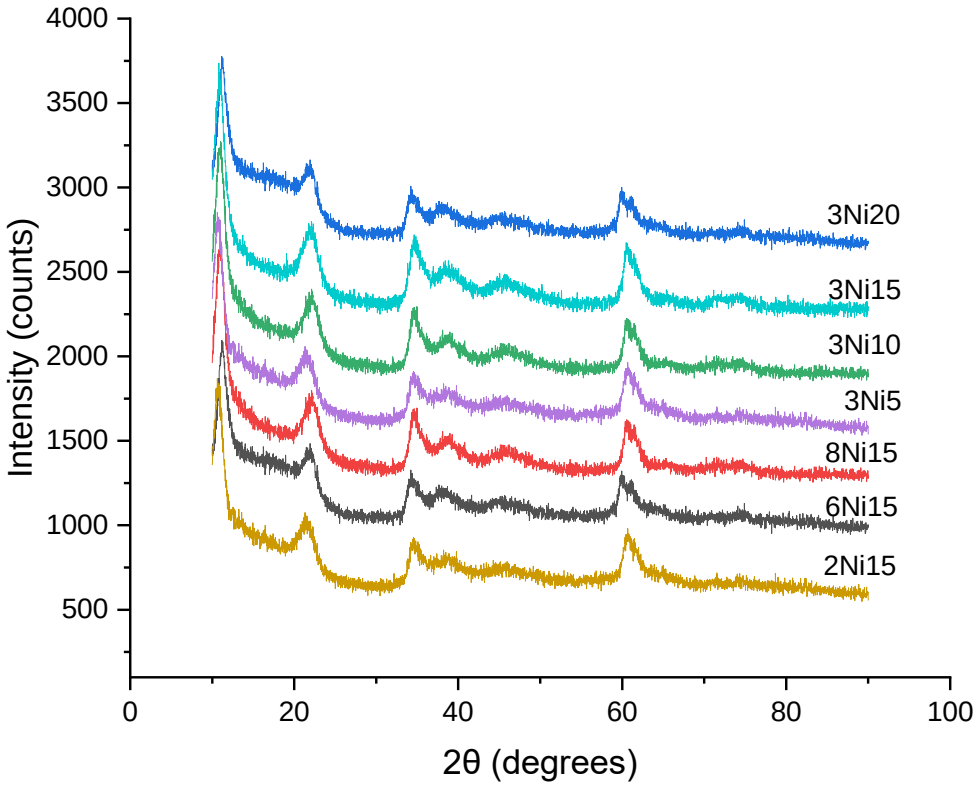

Figure 9: pXrd pattern of various Ni hydrotalcite precursors (patters are offset for clarity).

The pXrd pattern for the corresponding calcined hydrotalcite materials (Figure 10) have three reflections at 2Θ = 36°, 43.5°, 63°, 74.9° and 78.9° which are assigned to periclase-like structure of Ni-Mg-Al mixed oxides formed after calcination. The reflections are assigned to NiO and MgO periclase structures, indicating the formation of a NiO-MgO solid solution after calcination.[3-4]

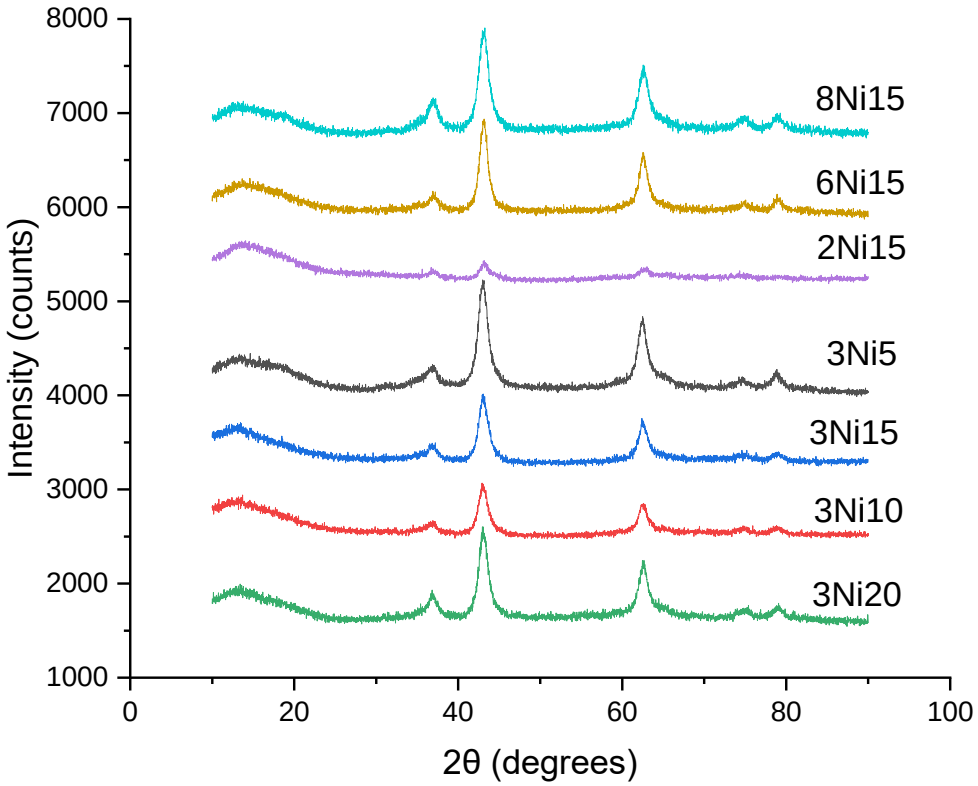

Figure 10: pXrd patterns of various calcined hydrotalcite materials (patterns offset for clarity).

Figure 11 shows the reduced Ni based catalysts. In the catalyst Ni/γ-Al_2O_3 the peaks at 2θ = 44.5° and 51.8° are associated with metallic f.c.c. Ni phase.[120] No reflections for NiO were observed after reduction at 800 °C. The other peaks observed were at 2θ = 37.5° and 65.6° are associated with $NiAl_2O_4$ spinel phase.[121] For the hydrotalcite derived catalysts, both f.c.c. Ni (2θ = 44.5°, 51.8°, 76.39°) and NiO (2θ = 37.2°, 43.2°, 62.8°) phases[120] appeared in the pXrd pattern. The Al and Mg oxide periclase diffraction was overshadowed by the diffraction of NiO at similar angles. The crystallite size of f.c.c. Ni was estimated for all the samples using the Scherrer equation at 2θ = 51.8° (Table 3). It was observed that crystallite size increased with the decrease in the Mg. The sample 3Ni15 (in calcined state) was reduced at 4 different

temperatures (650 °C, 700 °C, 750 °C, 800 °C). The pXrd patterns (Figure 12) showed peaks for metallic Ni (2θ = 44.5°, 51.8°) only at reduction temperatures of 750 °C and 800 °C. The intensity of reflections associated with metallic Ni were greater at a reduction temperature of 800 °C than 750 °C. The presence of metallic Ni was not detected in pXrd patterns of the same materials reduced at 650 °C or 700 °C, this might be because crystallite size of Ni at this temperature were less than 4 nm or because reduction had not occurred.

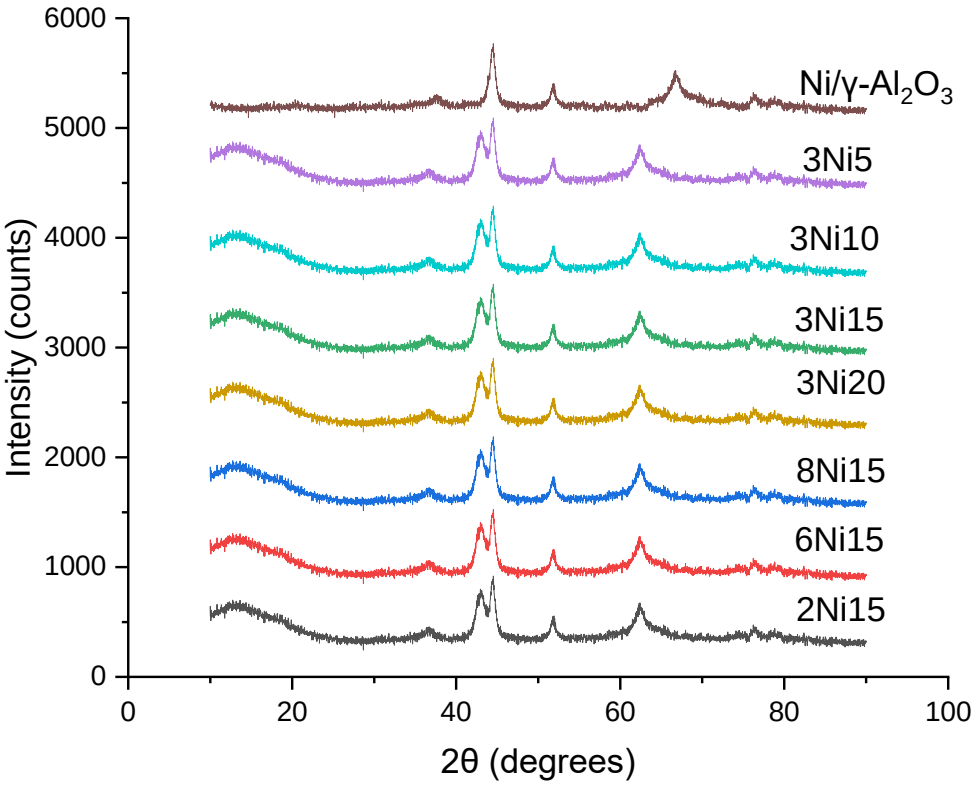

Figure 11: pXrd pattern of various reduced Ni based catalysts (patterns offset for clarity).

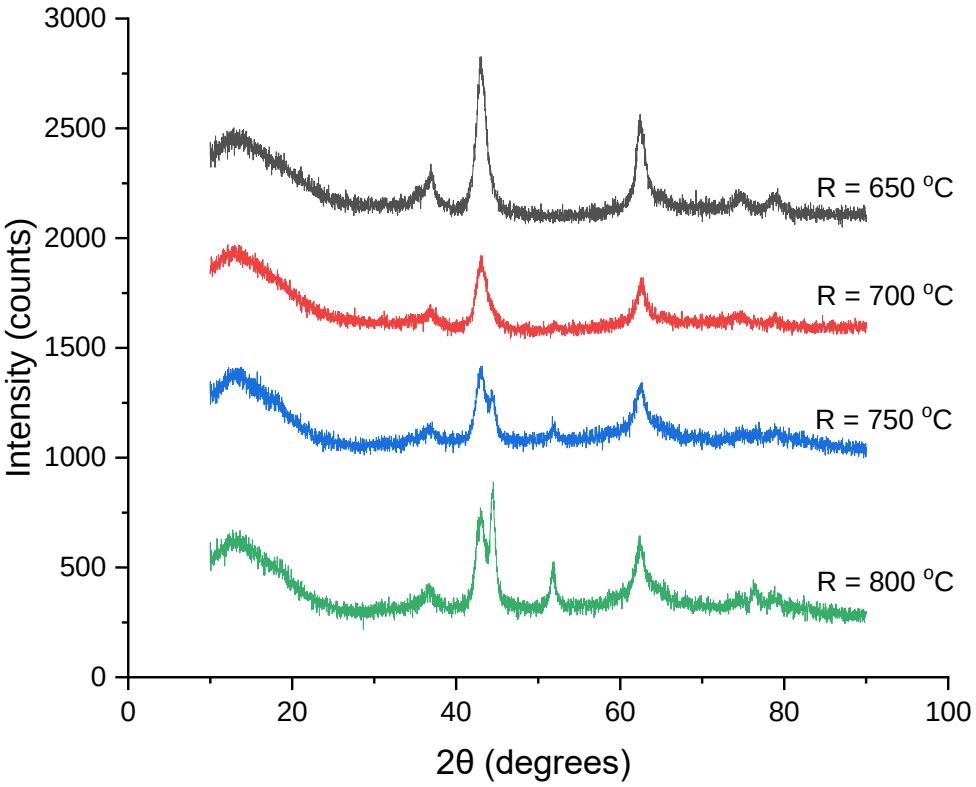

Figure 12: Reduction of calcined Ni hydrotalcites at different temperatures (sample: 3Ni15) ('R' in the image represents reduction temperatures). (Patterns offset for clarity).

Table 3: Estimated crystallite size of Ni based catalysts (reduced) based on using the Scherrer equation and the width of the reflection at 2θ = 51.8°. (The figures have an error bar of ±1.2 nm based on the error in calculation of FWMH)

Sample	Crystallite size (nm)
2Ni15	13
3Ni15	11
6Ni15	8
8Ni15	7
3Ni5	7
3Ni10	10
3Ni20	14
Ni/γ-Al_2O_3	27

3.1.2 ICP-OES, TGA, FTIR and BET of synthesized catalysts

ICP-OES of all in house synthesized catalysts was done to quatify the amount of each metal present. The results are shown in Table 4. Appropriate amounts of Ni, Mg and Al were found in all samples, just below the theoretical values, probably because a small amount of the metal was leached out during washing. However, the M^{2+}/M^{3+} ratios remained very close to the theoretical values. As seen from the table, with an increase in the M^{2+}/M^{3+}, the content of Mg increased and Al decreased. Also, with the increase in the Ni wt.% the amount of Mg decreased but amount of Al remained almost constant.

Table 4: ICP-OES results for Ni based catalysts (in calcined state). (As all the samples were done in duplicate, an error bar (deviation in two data) of ±0.4% was observed).

Sample	Ni Theoretical (%)	Ni Obtained (%)	Mg Theoretical (%)	Mg Obtained (%)	Al Theoretical (%)	Al Obtained (%)	Ni wt.%	M^{2+}/M^{3+}
3Ni5	5	4.89	39.11	38.76	15.24	15.03	4.89	3
3Ni10	10	9.2	35.79	34.23	14.78	14.32	9.2	3
3Ni15	15	14.21	32.48	32.30	14.32	13.43	14.21	3
3Ni20	20	18.52	29.17	28.77	13.86	12.44	18.52	3
2Ni15	15	13.98	27.48	27.29	18.70	18.3	13.98	2
6Ni15	15	14.16	39.21	37.89	8.40	8.10	14.16	6
8Ni15	15	14.55	41.28	40.41	6.59	6.38	14.55	8
Ni/γ-Al_2O_3	15	14.32	---	---	---	---	14.32	---

Figure 13 shows a typical TGA curve for one of the hydrotalcite precursors. The curve consists of a two-stage thermal decomposition, typical of hydrotalcite materials. The first step is observed around 100 C – 150 C corresponding to a weight loss of around 15%, which is due to the loss of water, of physisorbed carbon dioxide, and the release of interlayer water. No structural changes are observed at this point. The second step is observed between 300 °C – 500 °C correponding around 40% weight loss and is due to the dehydroxylation of the hydrotalcite-layered structure and to the decomposition of interlayer anions.[122] The calcination step should occur at a temperature over the second step to decompose the hydrotalcite structure and obtain a periclase like structre of incorporated metal oxides.

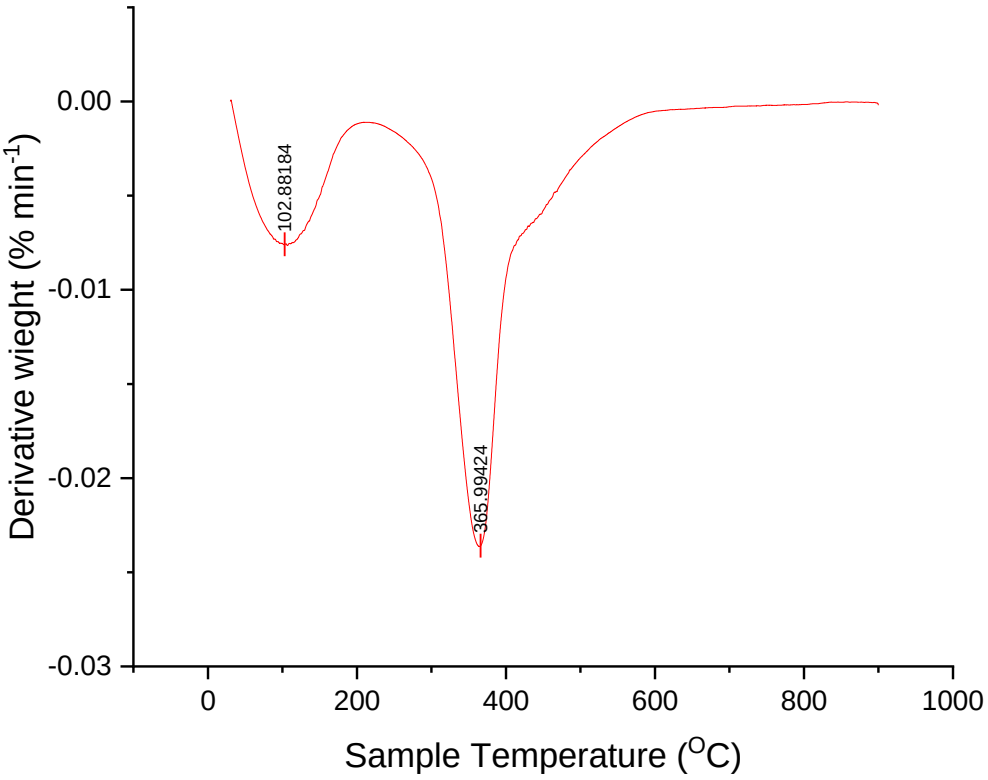

Figure 13: TGA (differentiated) curve of hydrotalcite precursor (sample shown: 3Ni15).

FTIR spectra of the hydrotalcite precursors (Figure 14) shows a broad band around 3500 cm^{-1} which is assigned to the O-H stretching vibration confirming the presence of hydroxyl groups in the hydroxide layer. The shoulder around 2800 cm^{-1} can be associated to the bridging hydroxyl interacting with carbonate ions in between the layers of the hydrotalcites. Bands around 1400 cm^{-1} are due to the disordered nature of interlayers or lowering of carbonate symmetry. Peaks below 1000cm^{-1} are assigned to the metal-OH bond stretching.[123]

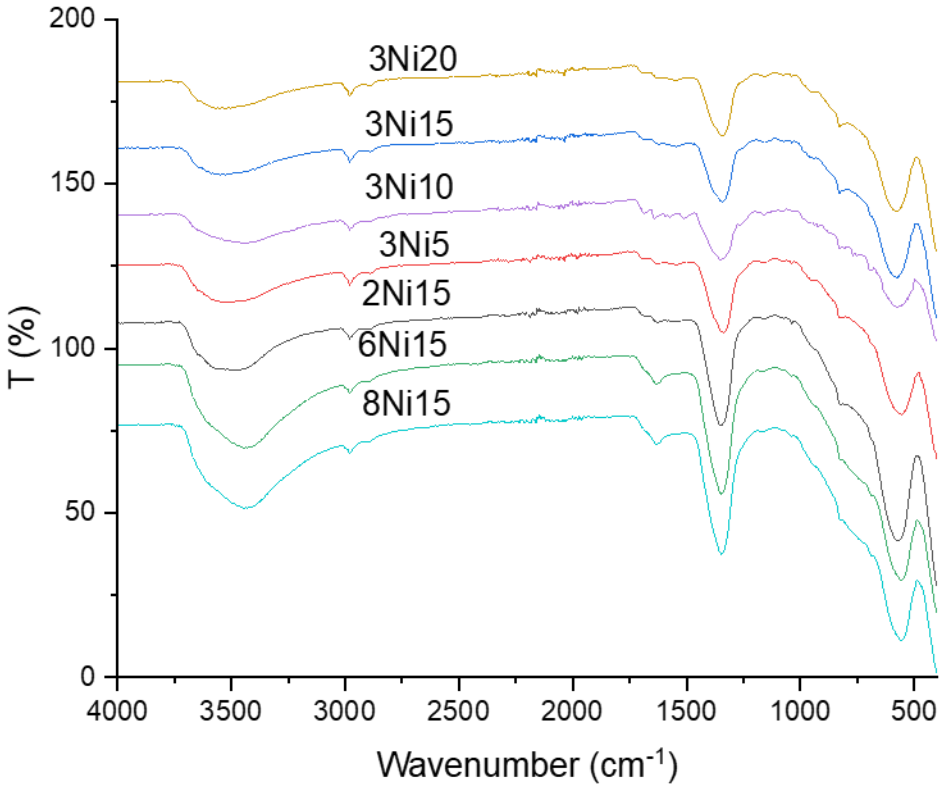

Figure 14: FTIR spectra of Ni hydrotalcite precursors. (Patterns are offset for clarity).

The BET surface area was calculated using the methodology described in section 2.1.2.2. The surface area was found to be between 110 $m^2 g^{-1}$ to 130$m^2 g^{-1}$ (Figure 15, Table 5), however, no systematic variation between samples was discerned. All the materials exhibited type IV isotherms with hysteresis loop type H1, a characteristic of an ordered mesoporous structure and having interparticle porosity in the material.[106]

Table 5: BET surface area of Ni hydrotalcite derived catalysts (Sample 3Ni15 and 6Ni15 were repeated twice to obtain an error bar of ±6 $m^2 g^{-1}$).

Sample	BET surface area ($m^2 g^{-1}$)
3Ni5	112
3Ni10	124
3Ni15	120
3Ni20	109
2Ni15	134

6Ni15	129
8Ni15	111

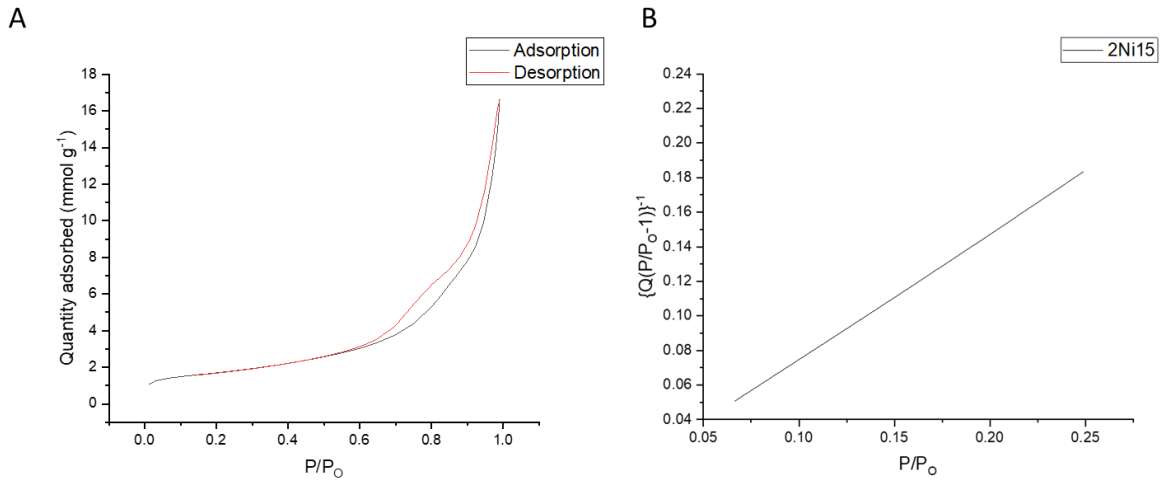

Figure 15: A) Adsorption/Desorption curves of reduced hydrotalcite derived catalysts. B) Plot of $\frac{1}{Q[\left(P_o/P\right)-1]}$ vs. $\left(P/P_o\right)$ for BET surface area (sample shown: 2Ni15, for other sample curves please see Appendix 2).

3.1.3 TPR and TPD of calcined hydrotalcites

After calcination, the TPR profiles (Figure 16) indicated that the centre of peak shifted towards higher reduction temperature with increase in M^{2+}/M^{3+} (keeping the Ni wt.% constant) i.e., with increase in the Mg amounts. Similarly, when Ni wt.% was increased (keeping M^{2+}/M^{3} constant) i.e., decrease in the Mg amount, the reduction temperature also decreased. Other authors have reported similar results.[3, 5] A few studies have indicated that in hydrotalcite derived materials, a MgO-NiO solid solution is formed which leads to a stronger interaction between Ni and Mg-Al oxide matrix.[122] The reduction of nickel oxide is only feasible in Ni-O-Ni species and not in Ni-O-Mg which means that Ni is first extracted from the solid solution of Ni-O-Mg and then reduced to Ni[124]. Hence, with the decrease in the Mg content, the interaction of Ni weakened with the other oxides and the reduction temperature decreases.

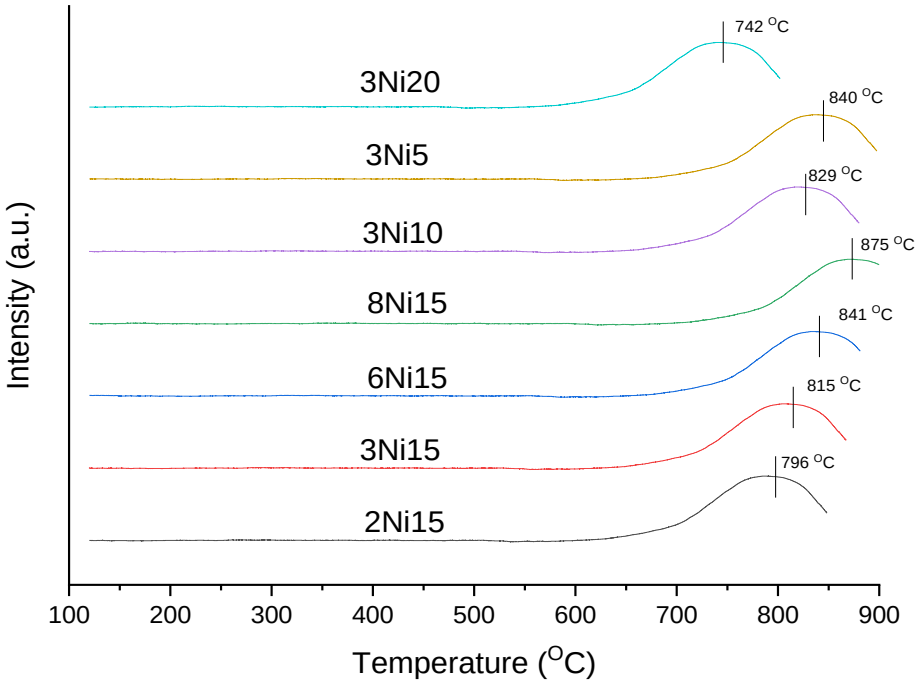

Figure 16: TPR curve for various calcined hydrotalcite derived materials (A linear baseline was subtracted from the curves due to a slightly sloping background during measurements).

The basicity of catalysts was determined using CO_2TPD (Figure 17). Previous reports identified three different types of basic sites associated with hydrotalcite derived materials: weak Bronsted OH groups, medium strength metal-oxygen Lew pairs and strong Lewis basic sites-oxygen anions.[88] The TPD profiles is overlapping of the desorption from three basic sites at peaks around temperature 100-150 C (weak basic sites), 150-250 C (medium basic sites) and 280-500 C (strong basic sites).[3]

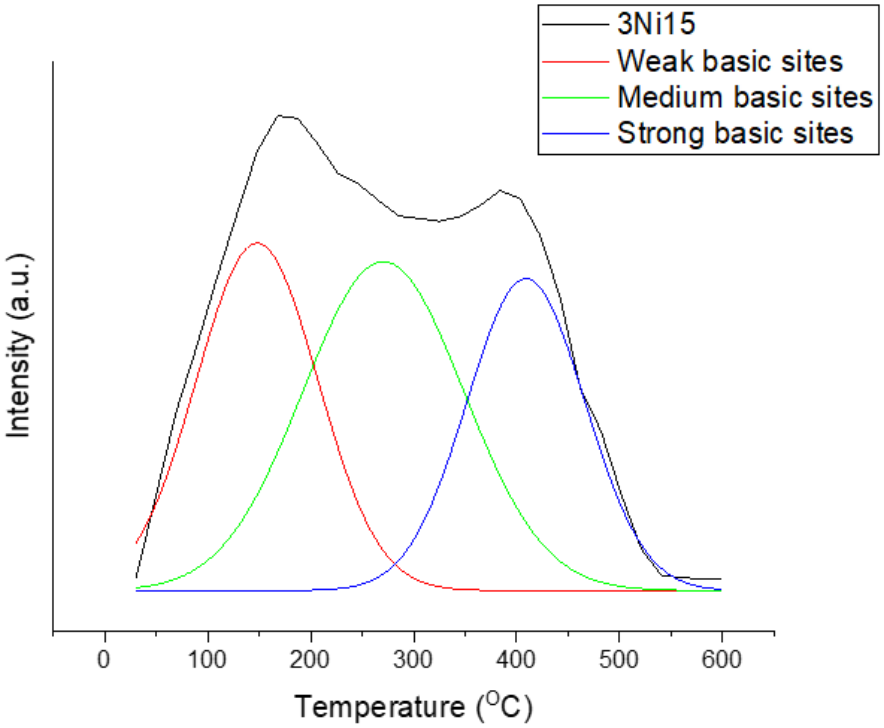

Figure 17: CO_2 TPD curves for calcined hydrotalcite material (the curve is de-convoluted into 3 curves as described in the experimental section).

The total basicity was calculated by integrating the area under the TPD curve and the TPD curve was deconvoluted into three Gaussian curves to determine each type of basicity. The total basicity increased with the increase in the M^{2+}/M^{3+} ratio and decreased with the increase in the Ni wt.%. Hence, the basicity was dependent upon Mg/Al ratio. Interestingly, it was also observed that with the increase in basicity, the strong basic sites increased, and medium basic sites decreased.

Table 6: Basicity of Ni hydrotalcite (in calcined state) determined by CO_2 TPD (The figures have an error bar of ±22 µmol CO_2 g^{-1} based on the error in area of fitted curves).

Sample	Weak basic sites (µmol CO_2 g^{-1})	Medium basic sites (µmol CO_2 g^{-1})	Strong basic sites (µmol CO_2 g^{-1})	Total basicity (µmol CO_2 g^{-1})
2Ni15	52	96	64	212
3Ni15	72	95	89	256
6Ni15	143	39	99	281
8Ni15	149	37	107	293
3Ni10	123	44	93	260

3Ni20	99	67	76	242

3.2 Aqueous phase reforming of ethylene glycol

APR of ethylene glycol was carried out in a batch autoclave reactor with 6 wt.% ethylene glycol at 260 °C (ramp rate = 5 °C min^{-1}) at 50 bar pressure for 2 h. Figure 18 shows conversion and selectivity of hydrogen obtained by all the fresh catalysts tested during this project. Samples 3Ni15, 2Ni15, 6Ni15, 3Ni20 were repeated thrice and the conversion and selectivity for hydrogen could be re-produced within a range of ±3%. This range was used as error bar in rest of the report. Hydrogen was counted as the main product, while the side products produced were CO_2, CO and CH_4 in the gaseous stream and ethanol and methanol in the liquid stream. No quantification was done for the side products. A commercial Pt/C catalyst demonstrated the best conversion and selectivity toward hydrogen in all catalysts. For nickel-based catalyst there was a trade-off between conversion and selectivity. Ni/γ-Al_2O_3 showed comparable conversion to Pt/C however, suffered from poor selectivity towards hydrogen. Hydrogen selectivity for hydrotalcite derived catalyst 8Ni15 was comparable to Pt/C but the conversion was significantly lower. Samples 2Ni15 and 3Ni20 exhibited a balance of conversion and selectivity to hydrogen. These samples represent a balance in amount of Mg and Al to be added in a Ni based catalyst to obtain appropriate conversion as well as hydrogen production. Also, as will be seen in a later section, sample 3Ni20 demonstrated least leaching of nickel (section 4.3.2).

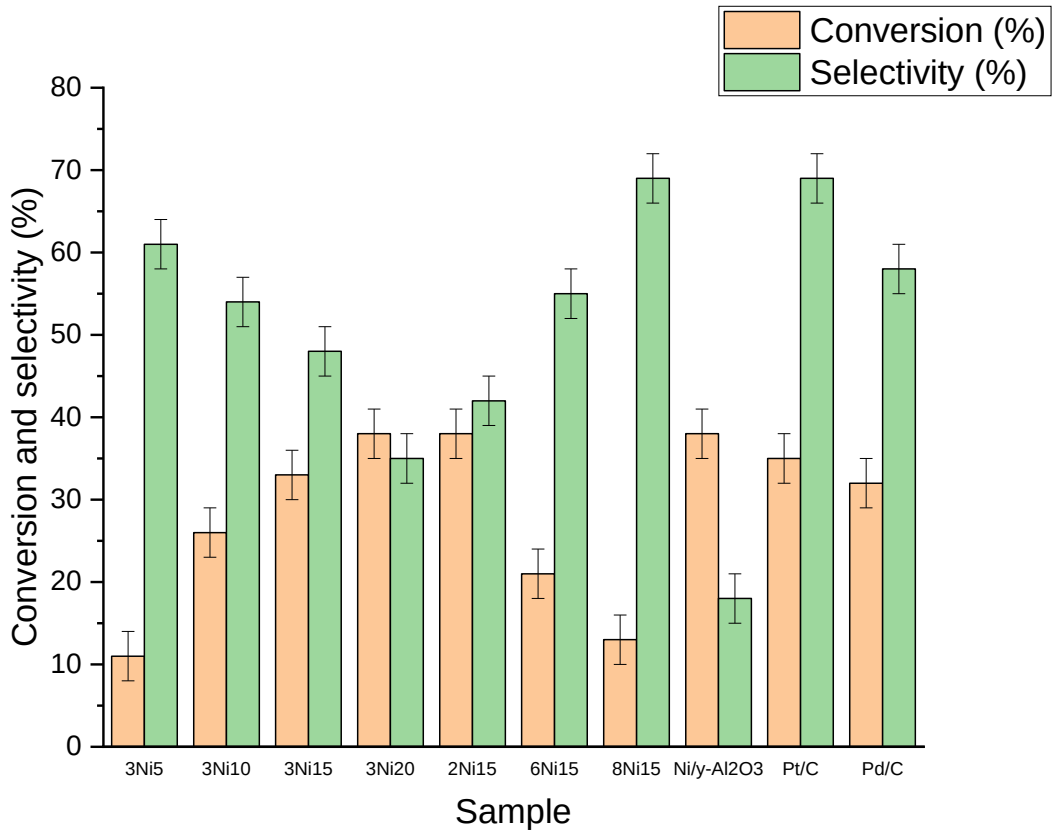

Figure 18: Conversion and selectivity for hydrogen in APR of ethylene glycol of all the fresh catalysts used in the project. (Reaction conditions: pressure 50 bar at 260 °C temperature, 750 mg catalyst and 2 h reaction time). (Error bar of ±3% for both conversion and selectivity based on repetition of 4 different samples thrice during this project).

3.2.1 Effect of Ni loading

Ni wt.% was varied from 5 to 20 wt.% keeping the M^{2+}/M^{3+} constant at 3 to evaluate the conversion and selectivity of hydrogen in APR of ethylene glycol as a function of changing Ni loading (Figure 19). With increase in the Ni loading, as might be expected, the conversion increased: 3Ni5 < 3Ni10 < 3Ni15 < 3Ni20. Higher nickel loading and decrease in the temperature of reduction with increase in loading (section 4.1.3, Figure 16), indicated the presence of more metallic Ni with increase in loading, hence higher conversion was obtained. However, the selectivity of hydrogen decreased with increase in the loading. This might be due to the larger Ni^0 crystallite size (section 4.1.1) and decrease in the basicity of the catalyst (section 4.1.3, Table 6) due to decrease in the Mg content as in the starting material the Ni replaces the Mg in the layers.

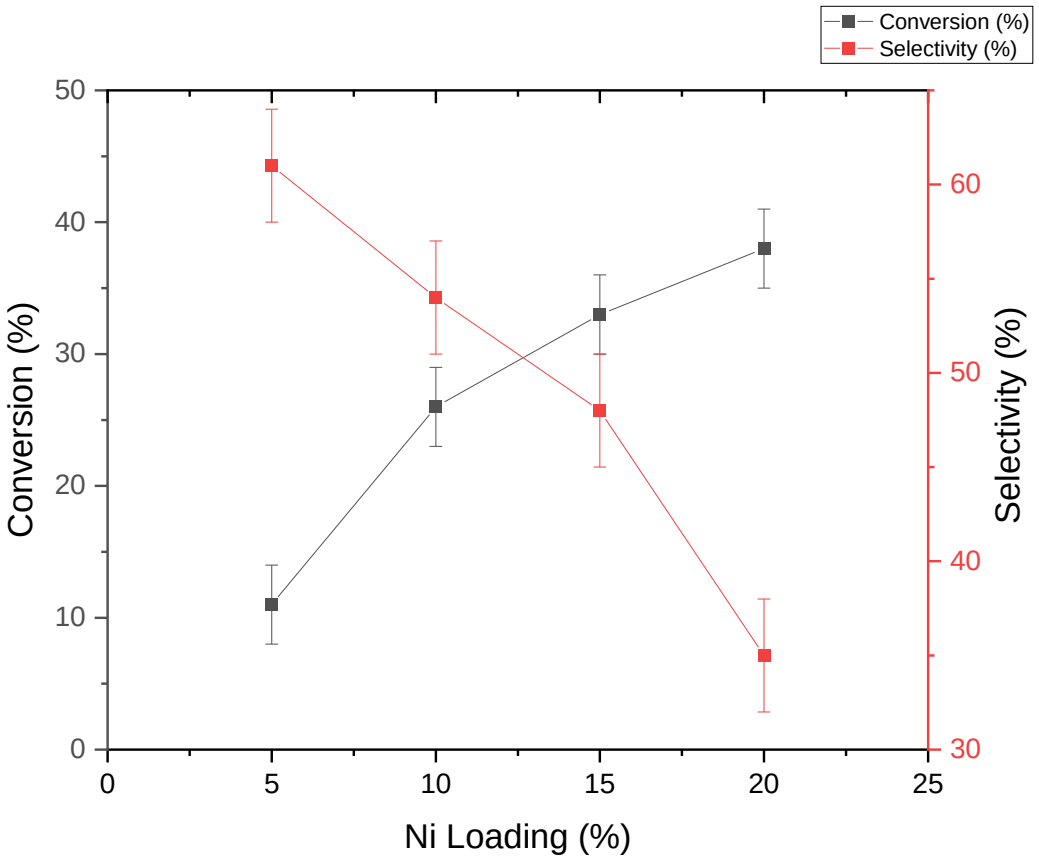

Figure 19: Effect of Ni loading (M^{2+}/M^{3+} ratio constant = 3) in hydrotalcite derived catalysts on conversion and selectivity for hydrogen. (Reaction conditions: pressure 50 bar at 260 °C temperature, 750 mg catalyst and 2 h reaction time). (Error bar of ±3% for both conversion and selectivity based on repetition of 4 different samples thrice during this project).

3.2.2 Effect of M^{2+}/M^{3+} ratio

The M^{2+}/M^{3+} ratio was varied as 2, 3, 6, 8 keeping the Ni loading as 15% in all cases, to evaluate the effect of bivalent to trivalent metal ratio in LHD based catalysts for APR of ethylene glycol (Figure 20). The trend observed for conversion was 2Ni15 > 3Ni15 > 6Ni15 > 8Ni15, while opposite trend was observed for selectivity (2Ni15 < 3Ni15 < 6Ni15 < 8Ni15). The reduction temperature increased with increase in the M^{2+}/M^{3+} ratio (Figure 16), meaning it is likely less metallic nickel was available for reaction due to sintering (and larger, lower Ni surface area catalysts) or incomplete reduction, hence the conversion decreased. The increase in basicity (Table 6) and decrease in Ni^0 crystallite size (section 4.1.1) increased the selectivity for hydrogen with increase in the M^{2+}/M^{3+} ratio.

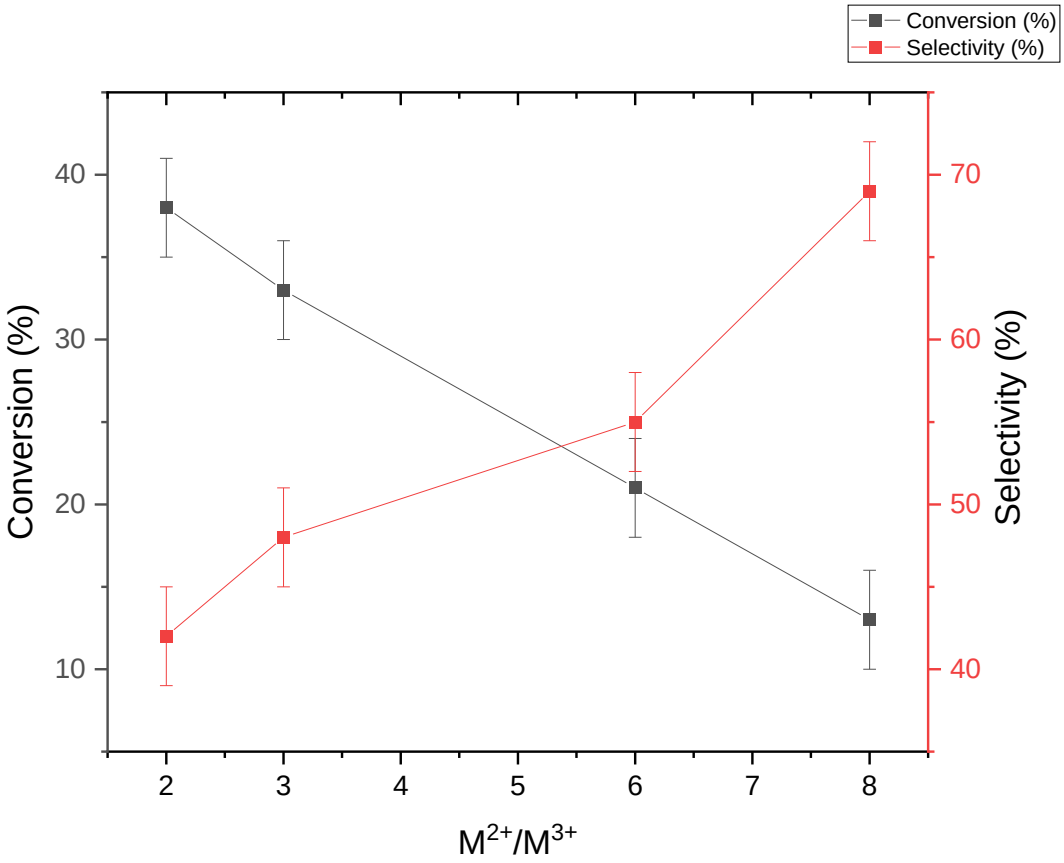

Figure 20: Effect of M^{2+}/M^{3+} (Ni loading constant = 15 wt.%) in hydrotalcite derived catalysts on conversion and selectivity for hydrogen (Reaction conditions: pressure 50 bar at 260 °C temperature, 750 mg catalyst and 2 h reaction time). (Error bar of ±3% for both conversion and selectivity based on repetition of 4 different samples thrice during this project).

3.2.3 Effect of reduction temperature

The sample 3Ni15 was reduced at 4 different temperatures: 650 °C, 700 °C, 750 °C, and 800 °C and tested in APR of ethylene glycol (Figure 21). The conversion increased with the increase in the reduction temperature due to the increase of metallic Ni at higher reduction temperature. Although no reflections for Ni^0 were seen in the pXRD pattern (Figure 12) in the case of 650 °C and 700 °C reduction temperature, these samples still have an conversion of 9% and 13% respectively. It is therefore likely that some metallic Ni was present in the sample, however the size of Ni crystals was smaller than 4 nm and were not detected by pXrd. The selectivity of hydrogen decreased with the increase in the reduction temperature. This is because of increase in the total pressure of the system as at higher conversion more hydrogen (+ CO_2) was produced and so may be more likely to be consumed in the side reactions.

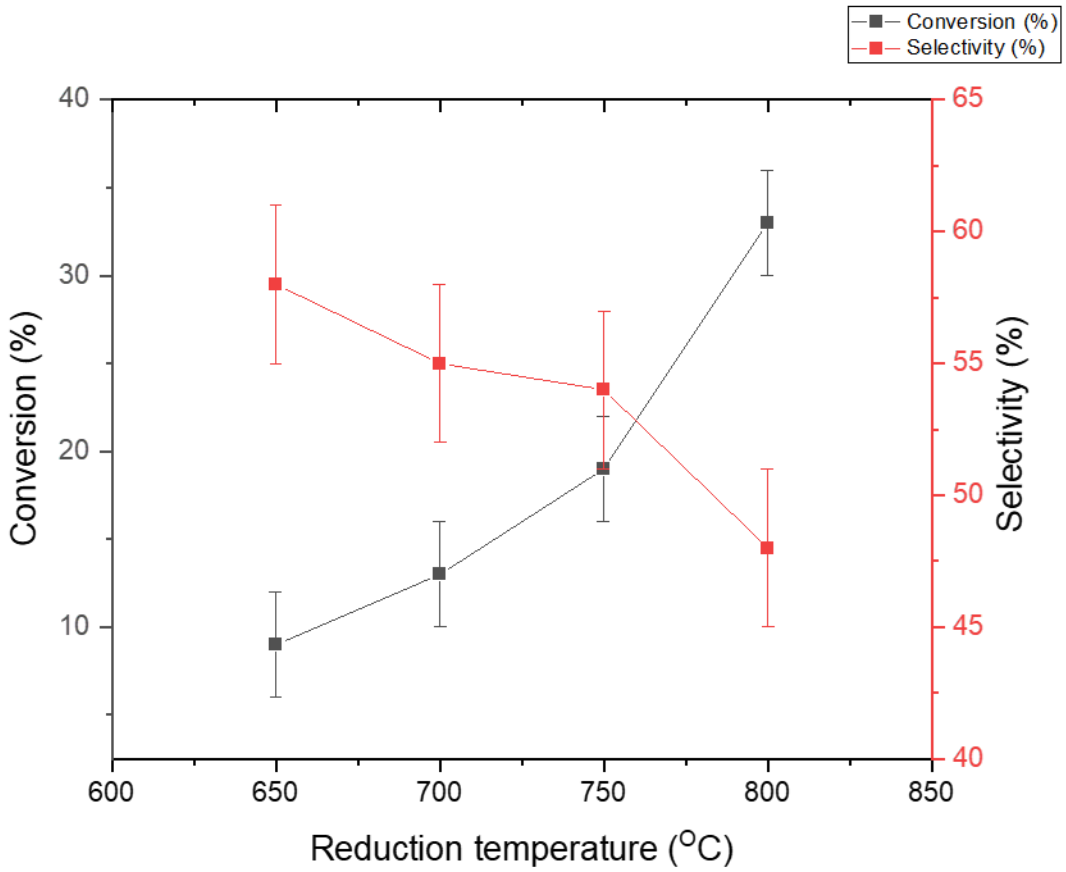

Figure 21: Effect of reduction temperature in hydrotalcite derived catalysts on conversion and selectivity of hydrogen. (Sample: 3Ni15R, reaction conditions: pressure 50 bar at 260 °C temperature, 750 mg catalyst and 2 h reaction time). (Error bar of ±3% for both conversion and selectivity based on repetition of 4 different samples thrice during this project).

3.2.4 Effect of time of reaction

The time of reaction was varied from 1 h to 2.5 h to determine the effect of reaction time (Figure 22). The conversion increased with the time but the conversion for the 0-60 min was more (20% vs 13% conversion) than the conversion for 60-120 min. This is because the catalyst was getting deactivated with the time. Due to the conversions being below 35%, it seems unlikely this substantial rate decrease is due to a decrease in the conversion of ethylene glycol by a factor of 0.8.

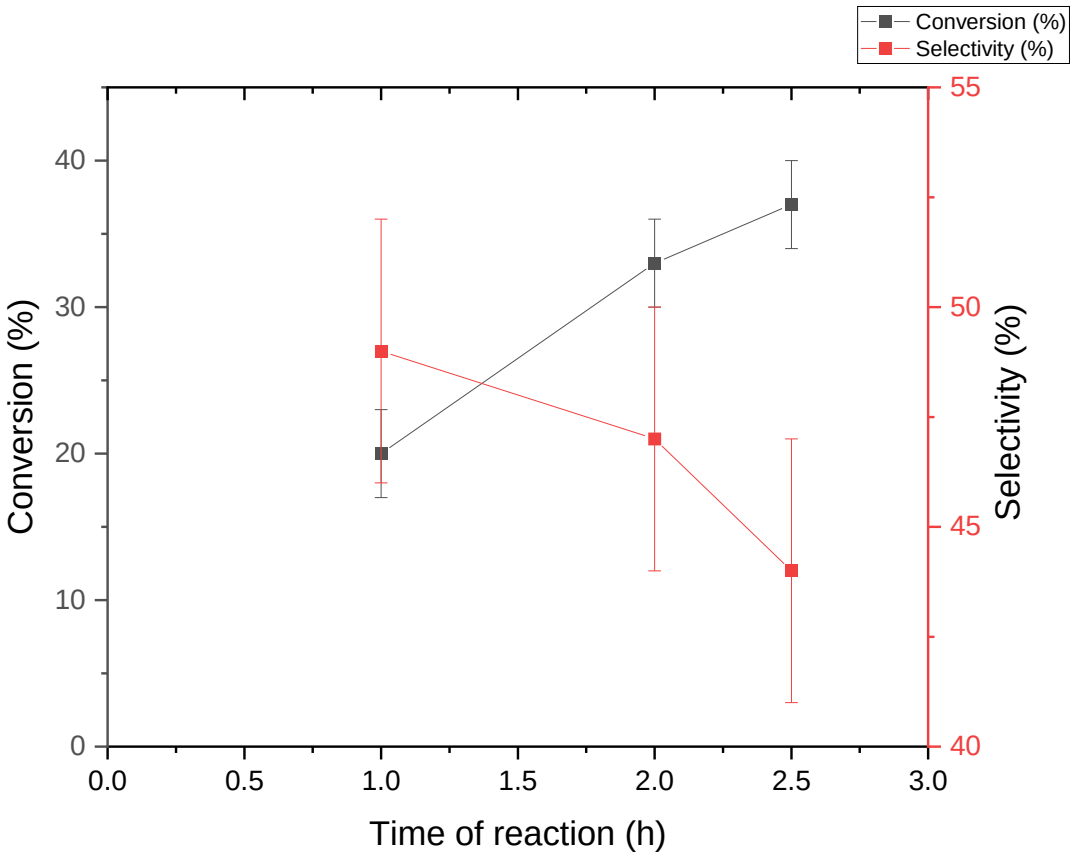

Figure 22: Effect of time of reaction in hydrotalcite derived catalysts on conversion and selectivity for hydrogen (Sample: 3Ni15R, reaction conditions: pressure 50 bar at 260 °C temperature, 750 mg catalyst) (Error bar of ±3% for both conversion and selectivity based on repetition of 4 different samples thrice during this project).

3.2.5 Effect of reaction temperature

The reaction temperature was increased, keeping the pressure just above the bubble point to stop the feed from evaporating. With the increase in the reaction temperature the conversion of ethylene glycol increased (Figure 23). It followed an expected rule of thumb in chemistry based on the exponential dependence of the Arrhenius equations, where for every 10 °C increment in the reaction temperature, the conversion almost doubled. The selectivity for hydrogen decreased with the increase in temperature. As before the decrease could be because at higher conversions there is more hydrogen (and a higher hydrogen pressure) to be converted in side reactions

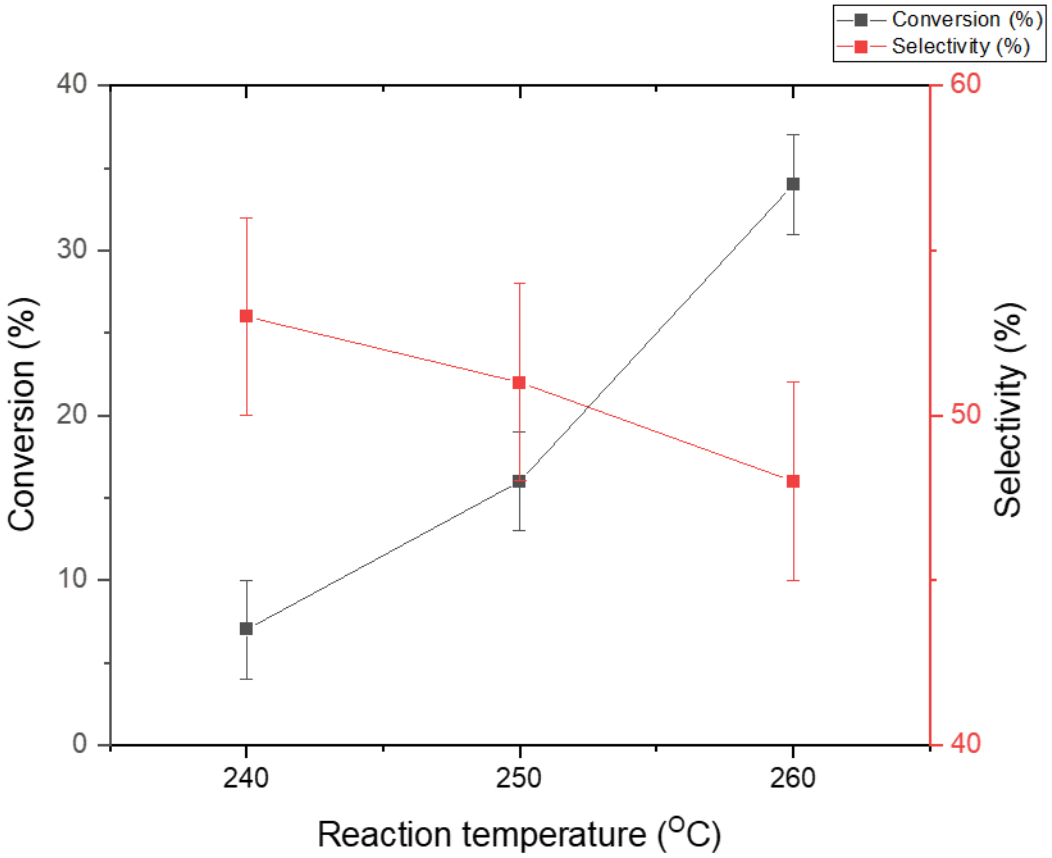

Figure 23: Effect of reaction temperature in hydrotalcite derived catalysts on conversion and selectivity of hydrogen. (Sample: 3Ni15R, reaction conditions: pressure 40 bars at 240 °C, 45 bars at 250 °C, 50 bar at 260 °C, 750 mg catalyst and 2 h reaction time). (Error bar of ±3% for both conversion and selectivity based on repetition of 4 different samples thrice during this project).

3.2.6 Effect of catalytic loading

The catalytic loading was varied from 0.075 to 0.25 g of catalyst per g of substrate to study the effect of catalyst amount on the aqueous phase reforming of ethylene glycol and look for possible mass transport issues. At 0.075 g/g of loading, no conversion was observed. Increasing the loading from 0.075 to 0.141 around 15% conversion was observed which reached 33% when loading was increased to 0.25 (Figure 24). Hence, for an increase of 43% in the loading, the conversion increased by 57%. This behaviour was not expected as usually, with conversion increase in same ratio as of loading. No concrete reasons could be attributed to no conversion at loading 0.075 g/g, but it is possible too much material is physically lost in dead zones of the reactor (or another external mass transport limit).

A hypothesis is the nickel is getting reduced in-situ. Since reduction was carried out ex-situ and metallic Ni was exposed to air before reaction, some surface oxidation must have taken place. The surface oxidation is reversible at relatively low temperature. Hence at 260 °C the initial hydrogen produced is used to reduce the nickel and with a greater number of metallic Ni sites available initially (at higher loading) more in situ reduction can take place. This gives higher conversion at higher loading. However, the transport of hydrogen from active site to the reduce site will be a diffusional challenge. Also, at 225 mg catalyst (0.075 g/g loading) of noble metals (Pt, Pd) which are resistant to surface oxidation, showed no conversion, indicating, in-situ reduction might not be responsible for the phenomenon observed.

Another hypothesis is some catalyst is getting stuck to the lower end corner of reactor vessel due to fast stirring (dead zone). The stuck catalyst will not be able to participate in the reaction, hence at lower loading (0.075 g/g) almost all catalyst went to the side of the reactor and gave no conversion.

However, in future more experimentations are required to understand the effect of catalytic loading and is currently, not being completely understood at the time of writing this thesis. The results reported in the rest of the report use the larger value of 0.25 g/g to be well away from this limit.

Another hydrotalcite dervied catalyst 6Ni15 (Figure 25) was also used to study the effect of catalytic loading, to verify the trend seen as a function of loading. Similar results were obtained, where at 0.075 g/g loading, no conversion was observed and for 0.141 to 0.25 (43% increase in loading) the conversion increased by 52%.

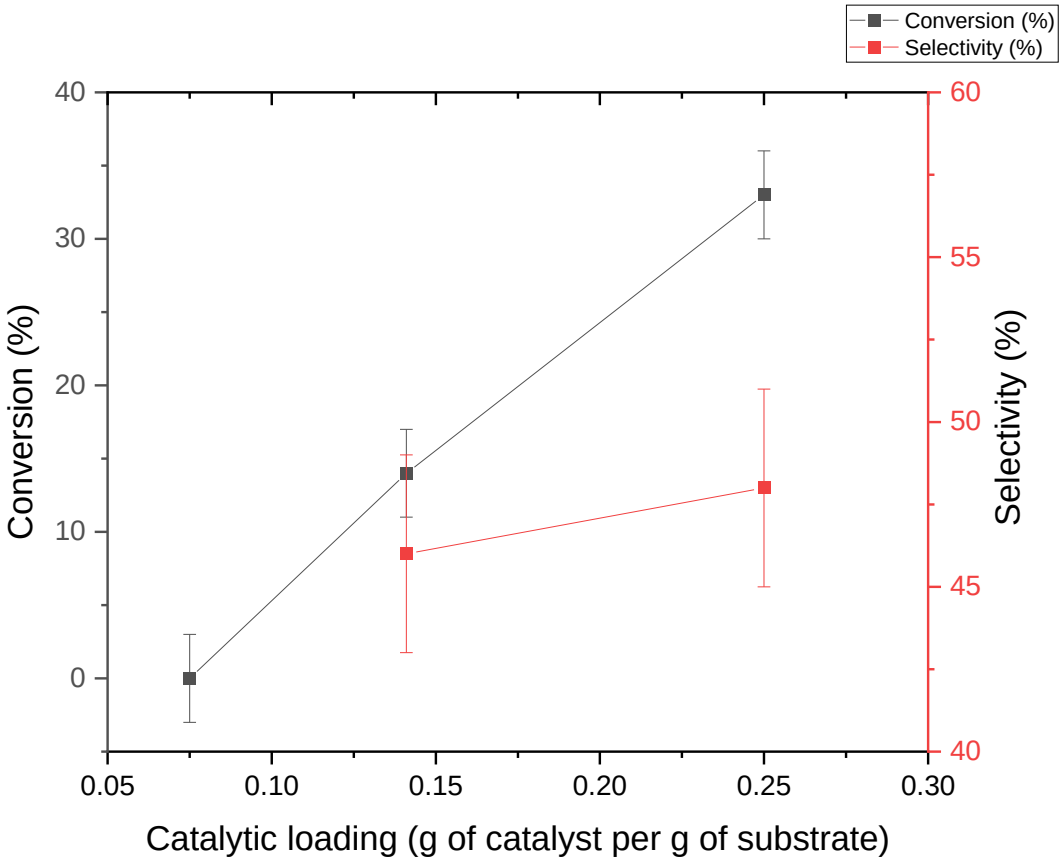

Figure 24: Effect of catalyst loading (g of catalyst per g of substrate) in hydrotalcite derived catalysts on activity and selectivity of hydrogen (Sample: 3Ni15, reaction conditions: pressure 50 bar at 260 °C temperature, catalyst amount: , 225 for 0.075 loading, 425 mg for 0.141 loading, 750 mg for 0.25 loading, and 2 h reaction time) (Error bar of ±3% for both conversion and selectivity based on repetition of 4 different samples thrice during this project).

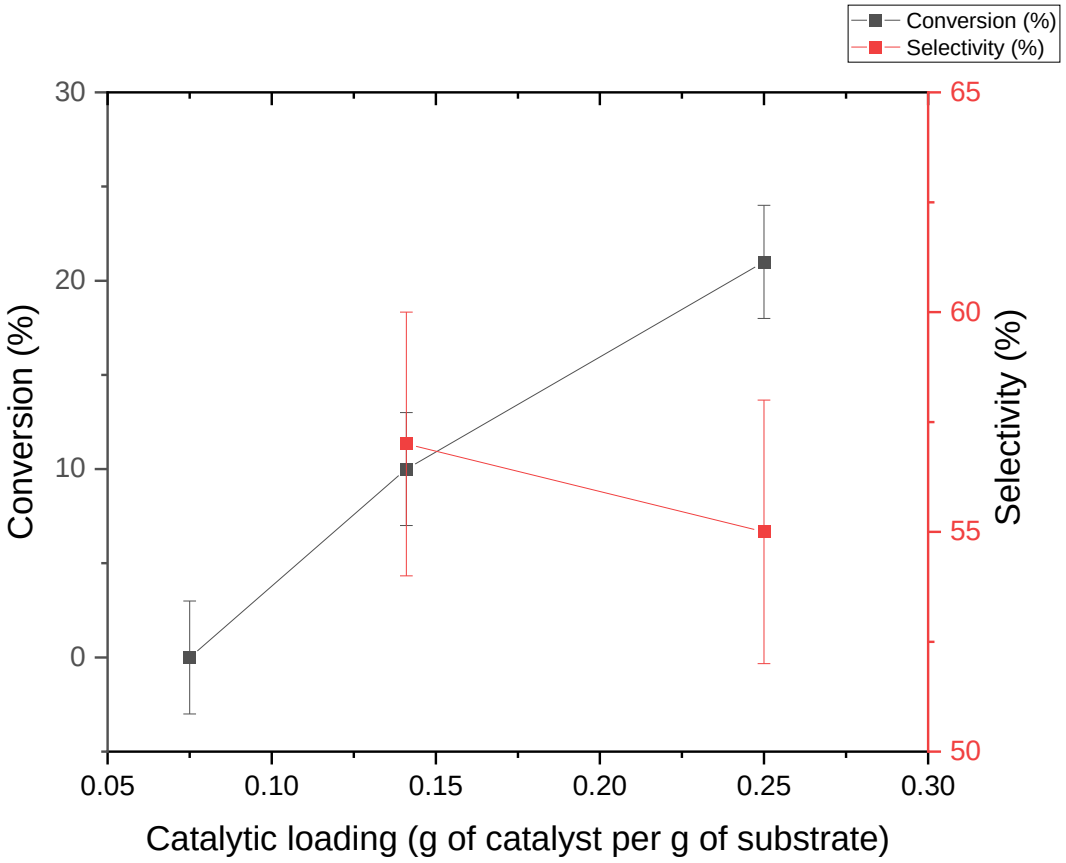

Figure 25: Effect of catalyst loading (g of catalyst per g of substrate) in hydrotalcite derived catalysts on activity and selectivity of hydrogen (Sample: 6Ni15, reaction conditions: pressure 50 bar at 260 °C temperature, catalyst amount: , 225 for 0.075 loading, 425 mg for 0.141 loading, 750 mg for 0.25 loading, and 2 h reaction time). (Error bar of ±3% for both conversion and selectivity based on repetition of 4 different samples thrice during this project).

3.3 Spent catalyst characterization

To try and rationalise some of the above trends, and in particular the deactivation seen as a function of time, and the suitability of nickel-based catalysts of this type for APR, characterisation of the post reaction samples was carried out.

3.3.1 pXrd

All the spent Ni catalyst were subjected to pxrd to identify any structural changes (Figure 26). The spent Ni/γ-Al_2O_3 pXrd pattern showed reflections at: 14.5°, 28.2°, 38.4°, 49.3°, 55.3°, 60.6°, 64.1°, 65.0°, 67.7°, 72.0° which can be assigned to the presence of a boehmite structure.[52] Hence, the gamma alumina structure has been changed to boehmite structure under hydrothermal conditions. Boehmite typically has less surface area than gamma phase alumina, and higher surface acidity.[52] It is also important to note that no peaks were observed for metallic

Ni or NiO, hence if they are present they will have crystallite sizes less than 4 nm and so cannot be detected in the pXrd pattern.

For hydrotalcite derived catalysts, the pXrd pattern had reflections at 2θ: 11.5°, 23°, 34.5°, 39.2°, 44.5°, 46.4°, 51.8°, 60.7°, 62°, 65.6°, 75°, 76.4° (except for the sample 3Ni5, where reflections at 44.5°, 51.8° and 76.4° were missing). The reflection at 2θ is 65.6° (plane (440)) is a characteristic peak for the formation of $NiAl_2O_4$ spinel.[121] No peak for NiO was not detected, probably, because of the smaller than detection limit (<4mn) size of any crystallites. In all samples other than 3Ni5, peaks at 44.5°, 51.8° and 76.4° were observed for metallic Ni. Hence the Ni in the hydrotalcite derived catalysts was not completely oxidized and the catalyst should still be active in the reaction. The spinel structure might affect conversion and selectivity for hydrogen in the APR reactions. The spinel cannot be turned back to hydrotalcites easily, however, they can be calcined and reduced (at higher temperature than hydrotalcites) to obtain more metallic nickel.[125] It is important to note here that reducing spinel at higher temperature will yield larger crystallite size, which can affect the selectivity of hydrogen in the APR.

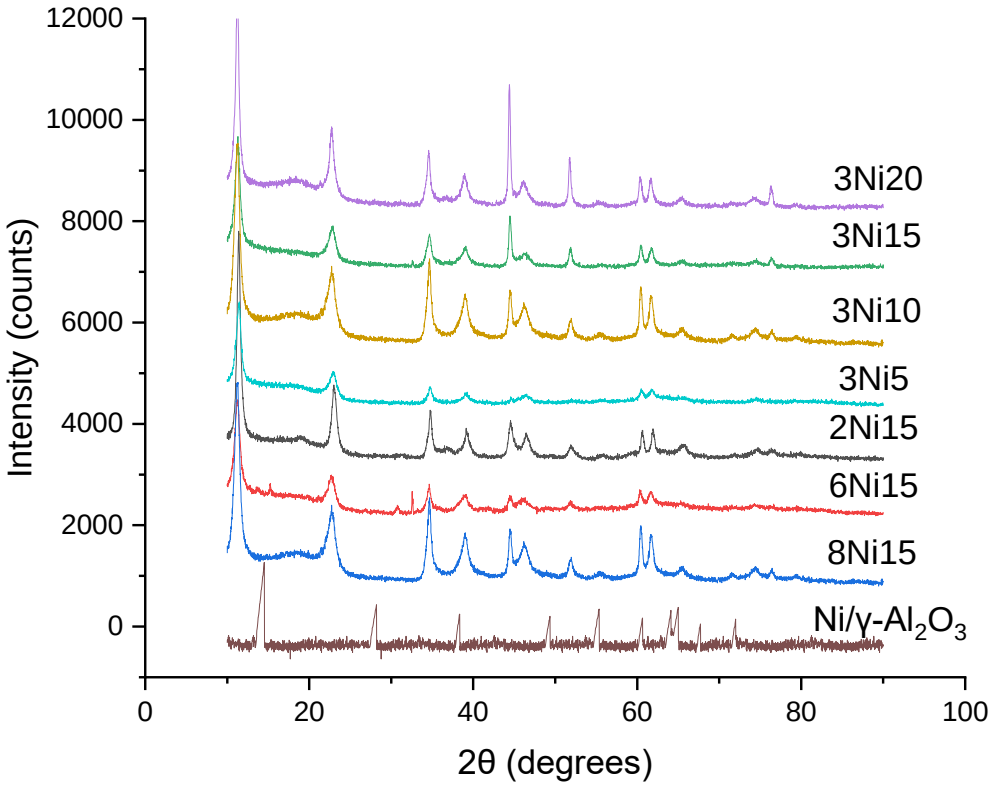

Figure 26: pXRd pattern for Ni based catalysts of different compositions after APR reaction of ethylene glycol (Reduction temperature: 800 °C, reaction conditions: pressure 50 bar at 260 °C temperature, 750 mg catalyst and 2 h reaction time)

3.3.2 ICP-OES

ICP-OES of the spent catalyst and spent reaction solution was done to calculate Ni leaching for the Ni based catalysts (Figure 27). The amount of Ni lost from the catalysts was confirmed by observing its presence in the product solution. Expect for the sample 8Ni15, leaching in hydrotalcite derived catalysts was observed to be significantly less than for Ni/γ-Al_2O_3, although no clear trends between samples of differing M^{2+}/M^{3+} ratio or Ni content were otherwise observed. For the sample with the highest M^{2+} content (8Ni15) the leaching was observed even more than Ni/γ-Al_2O_3, implying that magnesium/aluminium ratio over a certain value will affect the stability of the hydrotalcite derived catalysts. Hence the aluminium is needed in the catalytic system over a certain amount to provide stability to the catalyst. Therefore, from the reaction data and leaching studies, it can be concluded that there is a synergistic effect of both Mg and Al in Ni based catalysts for aqueous phase reforming, and there will be a trade of between conversion, selectivity and stability of catalysts depending upon the catalyst composition.

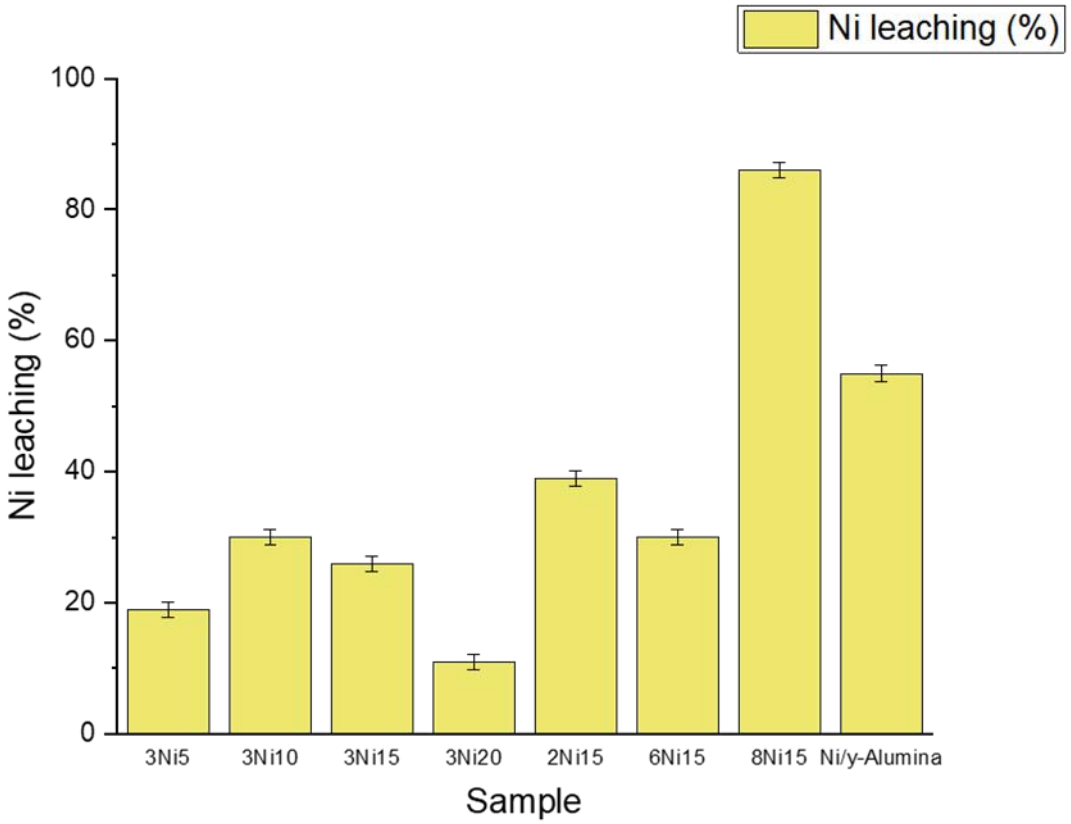

Figure 27: Leaching from Ni based catalysts (from ICP-OES of post-APR reaction catalyst materials). (As the samples were prepared in duplicate, an error bar (standard deviation in duplicates) of ±1.2% was obtained).

3.4 Aqueous phase reforming of ethylene glycol over spent catalysts

Three spent catalysts (one commercial and two in house synthesized hydrotalcite derived catalysts) were tested to in APR of ethylene glycol. It is important to note here that, since the catalysts recovery from spent solution was not 100% (due to catalyst sticking on syringe filter and a small portion of the catalyst having been used for characterization) two batches of spent catalysts were combined to give catalyst amount equal to 750mg/0.25 catalytic loading (equal to the loading of fresh catalyst testing). For the sample 3Ni20, the conversion dropped by 30% and selectivity dropped around 35% for spent catalyst as compared to fresh catalyst. For the sample 2Ni15, where leaching was much more than the sample 3Ni20 (around 30% more leaching) the conversion dropped significantly more (¬ 55%), however the drop in selectivity remained almost same (35%). Hence, the major reason for deactivation of catalyst is leaching. Some other factors responsible for deactivation are oxidation of Ni and change of structure from hydrotalcite to spinel. Comparing spent Ni hydrotalcite dervied catalyst to commercial

catalysts, the commercial catalyst Pd/C was much more stable and the drop in the conversion was only 14% and selectivity remained almost same.

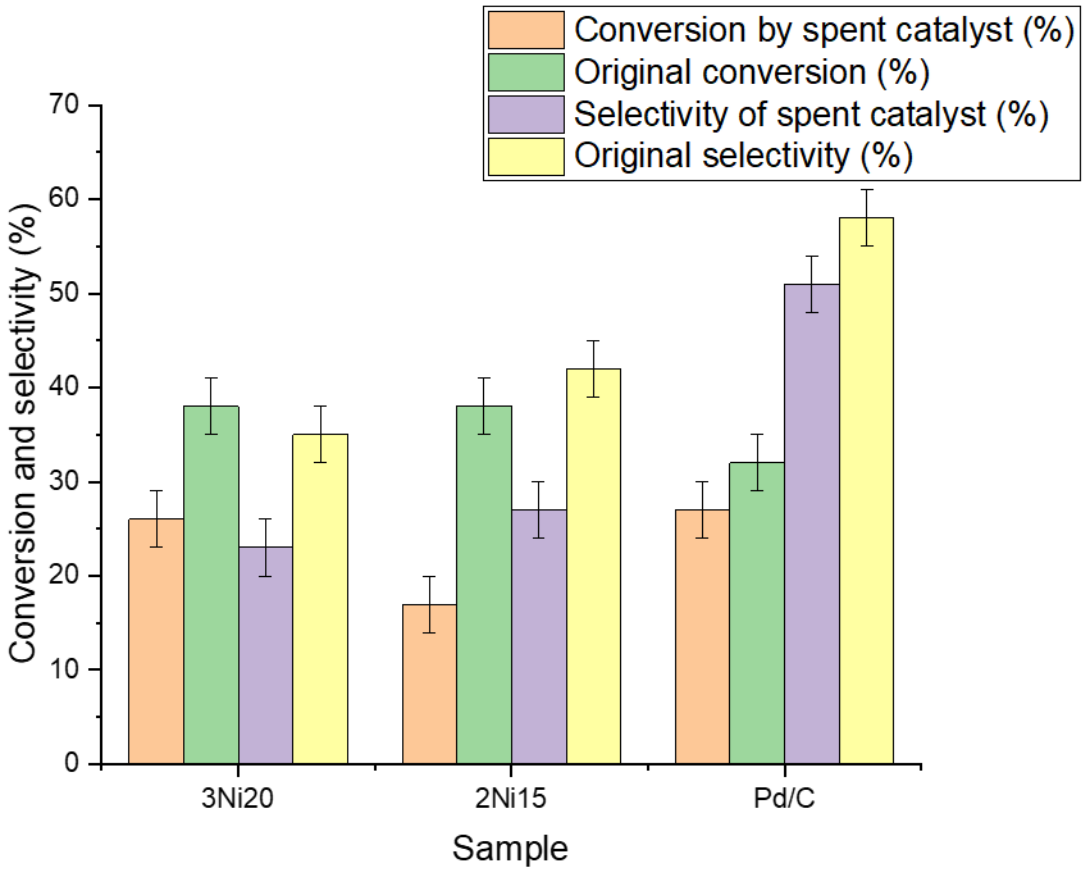

Figure 28:Comparison of APR of ethylene glycol over spent catalysts and original catalysts (Reaction conditions: pressure 50 bar at 260 °C temperature, 750 mg catalyst and 2 h reaction time). (Error bar of ±3% for both conversion and selectivity based on repetition of 4 different samples thrice during this project).

3.5 Aqueous phase reforming of phenol

Aqueous phase reforming of phenol was conducted in the same setup as ethylene glycol at same conditions due to literature reports of this process[91, 95]. However, no hydrogen production (confirmed by gas chromatography of gaseous products) or conversion of phenol (confirmed by HPLC of pre and post reaction solution) was observed. Commercial catalysts (Pt/C & Pd/C) and in house synthesized catalysts (Ni/γ-Al_2O_3, Pt/γ-Al_2O_3, hydrotalcite derived Ni/Mg/Al) both were tested at different temperatures (240 °C, 250 °C and 260 °C) with pressure just above bubble point, however, the initial and final concentration of phenol remained same and no peak for hydrogen was observed in the chromatograph. Evidently, concluding phenol does not reform at APR conditions and catalysts, as contrary to some recently published studies.[91, 96]

Chapter 4: Conclusions and future work

During this project, different hydrotalcite derived catalysts with varying Ni loading and M^{2+}/M^{3+} were synthesized using co-precipitation method and tested in a batch autoclave for aqueous phase reforming of ethylene glycol and phenol. The pXrd pattern of precursor showed no extra phase other than hydrotalcite, indicating the Ni has isomorphously replaced Mg in the layers. ICP-OES indicated that appropriate Ni, Mg, & Al metal concentrations were present in all the catalysts. With an increase in M^{2+}/M^{3+} ratio keeping the Ni loading constant, in other words, increasing the MgO content, both the temperature of reduction (by TPR curve) and basicity (by TPD curve) increased, and the Ni^0 crystallite size (estimated by Scherrer's equation) decreased. When the Ni loading was increased keeping the M^{2+}/M^{3+} constant, both the temperature of reduction and basicity decreased, but the Ni^0 crystallize size (estimated by Scherrer's equation) increased. These changes in the catalyst properties clearly effected the conversion and hydrogen selectivity in aqueous phase reforming of ethylene glycol. With the increase in basicity, the selectivity for hydrogen increased but since the amount of reduced nickel was comparatively less due to higher reduction temperature, conversion of ethylene glycol decreased. With the increase of reduction temperature, the conversion increased but the selectivity decreased. The selectivity for hydrogen of all hydrotalcite derived catalysts was more than selectivity for hydrogen observed in $Ni/\gamma\text{-}Al_2O_3$, which correlated with increased basicity and smaller crystallite size.

With the increase in reaction temperature at a pressure just above bubble point, higher conversions for ethylene glycol was achieved as expected. However, the selectivity was decreased, due to increase in total pressure enhancing side reactions, decreasing hydrogen selectivity.

An interesting phenomenon was observed when the catalytic loading was decreased from 0.25 to 0.141, the activity was expected to drop in the same ratio (43.6%). However, the activity dropped by 57%. This could be explained either by an induction type of behaviour in the kinetics or due to a dead zone in the reactor. However, there will be a need of future work in this area. The conversion obtained from time in the first hour of reaction was more than in the second hour, while the selectivity remained almost same. This meant the catalysts were getting deactivated with time.

Upon the characterization of spent catalyst, it was observed that the hydrotalcites are transformed to a spinel structure with some reduced Ni as compared to boehmite phase in Ni/γ-Al_2O_3 (which lead to decrease in basicity and surface area[52]). On the other hand, Ni based spinel catalysts are shown to be active and selective to hydrogen during APR in the literature[121], but the results are difficult to compare due to being in flow and reforming glycerol rather than ethylene glycol – this could be an area for future study.

Leaching was observed in LDH based catalysts but was to a lower extent than Ni/γ-Al_2O_3 in most cases. However, in 8Ni15 (the catalyst with highest MgO content) leaching was even more than Ni/γ-Al_2O_3. Upon re-testing the spent catalyst, conversion decreased by 60%, while selectivity remained the same. The decrease in activity is primarily due to leaching and possibly re-oxidation of Ni. The activity could be possibly further improved if that spent catalyst was calcined and reduced before reaction, however the spinel reduces at temperature high than hydrotalcites and will be expensive to reduce. The obtained Ni crystallite size from such higher temperature reductions might also increase and affect the selectivity after reduction.

In the APR of phenol, no catalytic activity, hydrogen production or side products were observed on any catalyst (including the commercial catalyst used in this project). As activity was observed for ethylene glycol in the same system, it is concluded that it is significantly harder to reform phenol directly into hydrogen by aqueous phase reforming, hence a pre-treatment such as catalytic oxidation of phenolic wastewater is needed before producing hydrogen via aqueous phase reforming.

Possible ideas for future work:

1) Study the kinetics of APR of ethylene glycol in a batch and fixed bed reactor to answer the questions about the induction period. Thus, answering the question why the decrease in activity is not in the same ratio as decrease on catalytic loading.
2) Study what factors effect the regeneration of the Ni/Mg/Al spinel and the impact on activity and selectivity of the catalyst.
3) Moving from a phenol type of structure to something more like a reduced sugar or a oxidation product of phenol and track how selectivity to hydrogen and conversion depends on substrate. This will help to develop an effective pre-treatment process for valorisation of phenolic wastewater to hydrogen.

References

1. Nikolaidis, P.; Poullikkas, A., A comparative overview of hydrogen production processes. *Renewable and Sustainable Energy Reviews* **2017,** *67*, 597-611.
2. Xu, M.; Wei, M., Layered Double Hydroxide-Based Catalysts: Recent Advances in Preparation, Structure, and Applications. *Advanced Functional Materials* **2018,** *28* (47), 1802943.
3. Dębek, R.; Motak, M.; Duraczyska, D.; Launay, F.; Galvez, M. E.; Grzybek, T.; Da Costa, P., Methane dry reforming over hydrotalcite-derived Ni–Mg–Al mixed oxides: the influence of Ni content on catalytic activity, selectivity and stability. *Catalysis Science & Technology* **2016,** *6* (17), 6705-6715.
4. Kalai, D. Y.; Stangeland, K.; Tucho, W. M.; Jin, Y.; Yu, Z., Biogas reforming on hydrotalcite-derived Ni-Mg-Al catalysts: the effect of Ni loading and Ce promotion. *Journal of CO2 Utilization* **2019,** *33*, 189-200.
5. Li, M.; Wang, X.; Li, S.; Wang, S.; Ma, X., Hydrogen production from ethanol steam reforming over nickel based catalyst derived from Ni/Mg/Al hydrotalcite-like compounds. *International Journal of Hydrogen Energy* **2010,** *35* (13), 6699-6708.
6. Chu, S.; Majumdar, A., Opportunities and challenges for a sustainable energy future. *Nature* **2012,** *488* (7411), 294-303.
7. Singh, S.; Jain, S.; Ps, V.; Tiwari, A. K.; Nouni, M. R.; Pandey, J. K.; Goel, S., Hydrogen: A sustainable fuel for future of the transport sector. *Renewable and Sustainable Energy Reviews* **2015,** *51*, 623-633.
8. Ball, M.; Wietschel, M., The future of hydrogen – opportunities and challenges. *International Journal of Hydrogen Energy* **2009,** *34* (2), 615-627.
9. Höök, M.; Tang, X., Depletion of fossil fuels and anthropogenic climate change—A review. *Energy Policy* **2013,** *52*, 797-809.
10. T.A. Boden, G. M., and R.J. Andres *Global, Regional, and National Fossil-Fuel CO2 Emissions*; Carbon Dioxide Information Analysis Center, Oak Ridge National Laboratory, U.S. Department of Energy, Oak Ridge,: Tenn., U.S.A., 2010.
11. Sartbaeva, A.; Kuznetsov, V. L.; Wells, S. A.; Edwards, P. P., Hydrogen nexus in a sustainable energy future. *Energy & Environmental Science* **2008,** *1* (1), 79-85.
12. Solomon, B. D.; Banerjee, A., A global survey of hydrogen energy research, development and policy. *Energy Policy* **2006,** *34* (7), 781-792.
13. Jain, I. P., Hydrogen the fuel for 21st century. *International Journal of Hydrogen Energy* **2009,** *34* (17), 7368-7378.
14. Barnoon, P.; Toghraie, D.; Mehmandoust, B.; Fazilati, M. A.; Eftekhari, S. A., Comprehensive study on hydrogen production via propane steam reforming inside a reactor. *Energy Reports* **2021,** *7*, 929-941.
15. Marquevich, M.; Sonnemann, G. W.; Castells, F.; Montané, D., Life cycle inventory analysis of hydrogen production by the steam-reforming process: comparison between vegetable oils and fossil fuels as feedstock. *Green Chemistry* **2002,** *4* (5), 414-423.
16. Sengodan, S.; Lan, R.; Humphreys, J.; Du, D.; Xu, W.; Wang, H.; Tao, S., Advances in reforming and partial oxidation of hydrocarbons for hydrogen production and fuel cell applications. *Renewable and Sustainable Energy Reviews* **2018,** *82*, 761-780.
17. Laidler, K. J., A glossary of terms used in chemical kinetics, including reaction dynamics (IUPAC Recommendations 1996). *Pure and Applied Chemistry* **1996,** *68* (1), 149-192.
18. Cordus, V., *Le guidon des apotiquaires. C'est à dire, la vraye forme et maniere de composer les médicamens ... / Traduite de latin en françoys, et repurgée*. Lyon: Cloquemin: 1575.
19. Davy, H., VIII. Some new experiments and observations on the combustion of gaseous mixtures, with an account of a method of preserving a continued light in mixtures of inflammable gases and air without flame. *Philosophical Transactions of the Royal Society of London* **1817,** *107*, 77-85.

20. Wisniak, J., The History of Catalysis. From the Beginning to Nobel Prizes. *Educación Química* **2010,** *21* (1), 60-69.
21. Leach, B. E., CHAPTER 1 - Industrial Catalysis: Chemistry Applied to Your Life-Style and Environment. In *Applied Industrial Catalysis*, Leach, B. E., Ed. Academic Press: 1983; pp 1-30.
22. Berzelius, J. J., *Årsberättelse om framstegen i fysik och kemi: 1835*. Norstedt: 1835.
23. Ranade, V. V.; Joshi, S. S., Chapter 1 - Catalysis and Catalytic Processes. In *Industrial Catalytic Processes for Fine and Specialty Chemicals*, Joshi, S. S.; Ranade, V. V., Eds. Elsevier: Amsterdam, 2016; pp 1-14.
24. Speight, J. G., Chapter 13 - Pharmaceuticals. In *Handbook of Industrial Hydrocarbon Processes (Second Edition)*, Speight, J. G., Ed. Gulf Professional Publishing: Boston, 2020; pp 553-595.
25. Introduction to Catalysis. In *Concepts of Modern Catalysis and Kinetics*, 2003; pp 1-21.
26. Kinetics. In *Concepts of Modern Catalysis and Kinetics*, 2003; pp 23-78.
27. Homogeneous Catalysis. In *Catalysis*, 2008; pp 77-125.
28. Herrmann, W. A.; Cornils, B., Introduction. In *Applied Homogeneous Catalysis with Organometallic Compounds*, 2017; pp 1-22.
29. de Jong, K. P., General Aspects. In *Synthesis of Solid Catalysts*, 2009; pp 1-11.
30. Thomas, J. M., Design, Synthesis, and In Situ Characterization of New Solid Catalysts. *Angewandte Chemie International Edition* **1999,** *38* (24), 3588-3628.
31. Coronado, I.; Stekrova, M.; Reinikainen, M.; Simell, P.; Lefferts, L.; Lehtonen, J., A review of catalytic aqueous-phase reforming of oxygenated hydrocarbons derived from biorefinery water fractions. *Int. J. Hydrogen Energy* **2016,** *41* (26), 11003-11032.
32. Cortright, R. D.; Davda, R. R.; Dumesic, J. A., Hydrogen from catalytic reforming of biomass-derived hydrocarbons in liquid water. *Nature* **2002,** *418* (6901), 964-967.
33. Davda, R. R.; Shabaker, J. W.; Huber, G. W.; Cortright, R. D.; Dumesic, J. A., A review of catalytic issues and process conditions for renewable hydrogen and alkanes by aqueous-phase reforming of oxygenated hydrocarbons over supported metal catalysts. *Appl. Catal., B* **2005,** *56* (1–2), 171-186.
34. Shahbudin, M. I.; Jacob, D. M.; Ameen, M.; Aqsha, A.; Azizan, M. T.; Yusoff, M. H. M.; Sher, F., Liquid value-added chemicals production from aqueous phase reforming of sorbitol and glycerol over sonosynthesized Ni-based catalyst. *Journal of Environmental Chemical Engineering* **2021,** *9* (4), 105766.
35. Zoppi, G.; Pipitone, G.; Pirone, R.; Bensaid, S., Aqueous phase reforming process for the valorization of wastewater streams: Application to different industrial scenarios. *Catalysis Today* **2022,** *387*, 224-236.
36. He, R.; Davda, R. R.; Dumesic, J. A., In Situ ATR-IR Spectroscopic and Reaction Kinetics Studies of Water−Gas Shift and Methanol Reforming on Pt/Al2O3 Catalysts in Vapor and Liquid Phases. *The Journal of Physical Chemistry B* **2005,** *109* (7), 2810-2820.
37. Roy, B.; Sullivan, H.; Leclerc, C. A., Effect of variable conditions on steam reforming and aqueous phase reforming of n-butanol over Ni/CeO2 and Ni/Al2O3 catalysts. *Journal of Power Sources* **2014,** *267*, 280-287.
38. Shabaker, J. W.; Huber, G. W.; Dumesic, J. A., Aqueous-phase reforming of oxygenated hydrocarbons over Sn-modified Ni catalysts. *Journal of Catalysis* **2004,** *222* (1), 180-191.
39. Davda, R. R.; Shabaker, J. W.; Huber, G. W.; Cortright, R. D.; Dumesic, J. A., Aqueous-phase reforming of ethylene glycol on silica-supported metal catalysts. *Applied Catalysis B: Environmental* **2003,** *43* (1), 13-26.
40. Shabaker, J. W.; Huber, G. W.; Davda, R. R.; Cortright, R. D.; Dumesic, J. A., Aqueous-Phase Reforming of Ethylene Glycol Over Supported Platinum Catalysts. *Catalysis Letters* **2003,** *88* (1), 1-8.
41. Tuza, P. V.; Manfro, R. L.; Ribeiro, N. F. P.; Souza, M. M. V. M., Production of renewable hydrogen by aqueous-phase reforming of glycerol over Ni–Cu catalysts derived from hydrotalcite precursors. *Renewable Energy* **2013,** *50*, 408-414.

42. Pendem, C.; Sarkar, B.; Siddiqui, N.; Konathala, L. N. S.; Baskar, C.; Bal, R., K-Promoted Pt-Hydrotalcite Catalyst for Production of H2 by Aqueous Phase Reforming of Glycerol. *ACS Sustainable Chemistry & Engineering* **2018,** *6* (2), 2122-2131.
43. Chen, G.; Xu, N.; Li, X.; Liu, Q.; Yang, H.; Li, W., Hydrogen production by aqueous-phase reforming of ethylene glycol over a Ni/Zn/Al derived hydrotalcite catalyst. *RSC Advances* **2015,** *5* (74), 60128-60134.
44. Cruz, I. O.; Ribeiro, N. F. P.; Aranda, D. A. G.; Souza, M. M. V. M., Hydrogen production by aqueous-phase reforming of ethanol over nickel catalysts prepared from hydrotalcite precursors. *Catalysis Communications* **2008,** *9* (15), 2606-2611.
45. Cesar, D. V.; Santori, G. F.; Pompeo, F.; Baldanza, M. A.; Henriques, C. A.; Lombardo, E.; Schmal, M.; Cornaglia, L.; Nichio, N. N., Hydrogen production from ethylene glycol reforming catalyzed by Ni and Ni–Pt hydrotalcite-derived catalysts. *International Journal of Hydrogen Energy* **2016,** *41* (47), 22000-22008.
46. Zhang, J.; Xu, N., Hydrogen Production from Ethylene Glycol Aqueous Phase Reforming over Ni–Al Layered Hydrotalcite-Derived Catalysts. *Catalysts* **2020,** *10* (1), 54.
47. Neira D'Angelo, M. F.; Ordomsky, V.; van der Schaaf, J.; Schouten, J. C.; Nijhuis, T. A., Aqueous phase reforming in a microchannel reactor: the effect of mass transfer on hydrogen selectivity. *Catalysis Science & Technology* **2013,** *3* (10), 2834-2842.
48. D'Angelo, M. F. N.; Ordomsky, V.; Paunovic, V.; van der Schaaf, J.; Schouten, J. C.; Nijhuis, T. A., Hydrogen Production through Aqueous-Phase Reforming of Ethylene Glycol in a Washcoated Microchannel. *ChemSusChem* **2013,** *6* (9), 1708-1716.
49. Neira D'Angelo, M. F.; Ordomsky, V.; van der Schaaf, J.; Schouten, J. C.; Nijhuis, T. A., Continuous hydrogen stripping during aqueous phase reforming of sorbitol in a washcoated microchannel reactor with a Pt–Ru bimetallic catalyst. *International Journal of Hydrogen Energy* **2014,** *39* (31), 18069-18076.
50. D'Angelo, M. F. N.; Ordomsky, V.; Schouten, J. C.; van der Schaaf, J.; Nijhuis, T. A., Carbon-Coated Ceramic Membrane Reactor for the Production of Hydrogen by Aqueous-Phase Reforming of Sorbitol. *ChemSusChem* **2014,** *7* (7), 2007-2015.
51. Jeon, S.; Ham, H.; Suh, Y.-W.; Bae, J. W., Aqueous phase reforming of ethylene glycol on Pt/CeO2–ZrO2: effects of cerium to zirconium molar ratio. *RSC Advances* **2015,** *5* (68), 54806-54815.
52. El Doukkali, M.; Iriondo, A.; Cambra, J. F.; Gandarias, I.; Jalowiecki-Duhamel, L.; Dumeignil, F.; Arias, P. L., Deactivation study of the Pt and/or Ni-based γ-Al2O3 catalysts used in the aqueous phase reforming of glycerol for H2 production. *Applied Catalysis A: General* **2014,** *472*, 80-91.
53. van Haasterecht, T.; Ludding, C. C. I.; de Jong, K. P.; Bitter, J. H., Toward stable nickel catalysts for aqueous phase reforming of biomass-derived feedstock under reducing and alkaline conditions. *Journal of Catalysis* **2014,** *319*, 27-35.
54. van Haasterecht, T.; Ludding, C. C. I.; de Jong, K. P.; Bitter, J. H., Stability and activity of carbon nanofiber-supported catalysts in the aqueous phase reforming of ethylene glycol. *Journal of Energy Chemistry* **2013,** *22* (2), 257-269.
55. Alonso, D. M.; Wettstein, S. G.; Dumesic, J. A., Bimetallic catalysts for upgrading of biomass to fuels and chemicals. *Chem. Soc. Rev.* **2012,** *41* (24), 8075-8098.
56. Huber, G. W.; Shabaker, J. W.; Evans, S. T.; Dumesic, J. A., Aqueous-phase reforming of ethylene glycol over supported Pt and Pd bimetallic catalysts. *Applied Catalysis B: Environmental* **2006,** *62* (3), 226-235.
57. Tanksale, A.; Zhou, C. H.; Beltramini, J. N.; Lu, G. Q., Hydrogen production by aqueous phase reforming of sorbitol using bimetallic Ni–Pt catalysts: metal support interaction. *Journal of Inclusion Phenomena and Macrocyclic Chemistry* **2009,** *65* (1), 83-88.
58. Kaya, B.; Irmak, S.; Hasanoğlu, A.; Erbatur, O., Developing Pt based bimetallic and trimetallic carbon supported catalysts for aqueous-phase reforming of biomass-derived compounds. *International Journal of Hydrogen Energy* **2015,** *40* (10), 3849-3858.

59. Shabaker, J. W.; Simonetti, D. A.; Cortright, R. D.; Dumesic, J. A., Sn-modified Ni catalysts for aqueous-phase reforming: Characterization and deactivation studies. *Journal of Catalysis* **2005,** *231* (1), 67-76.
60. Xie, F.; Chu, X.; Hu, H.; Qiao, M.; Yan, S.; Zhu, Y.; He, H.; Fan, K.; Li, H.; Zong, B.; Zhang, X., Characterization and catalytic properties of Sn-modified rapidly quenched skeletal Ni catalysts in aqueous-phase reforming of ethylene glycol. *Journal of Catalysis* **2006,** *241* (1), 211-220.
61. Zhu, L.-J.; Guo, P.-J.; Chu, X.-W.; Yan, S.-R.; Qiao, M.-H.; Fan, K.-N.; Zhang, X.-X.; Zong, B.-N., An environmentally benign and catalytically efficient non-pyrophoric Ni catalyst for aqueous-phase reforming of ethylene glycol. *Green Chemistry* **2008,** *10* (12), 1323-1330.
62. Guo, Y.; Liu, X.; Azmat, M. U.; Xu, W.; Ren, J.; Wang, Y.; Lu, G., Hydrogen production by aqueous-phase reforming of glycerol over Ni-B catalysts. *International Journal of Hydrogen Energy* **2012,** *37* (1), 227-234.
63. Iriondo, A.; Barrio, V. L.; Cambra, J. F.; Arias, P. L.; Güemez, M. B.; Navarro, R. M.; Sánchez-Sánchez, M. C.; Fierro, J. L. G., Hydrogen Production from Glycerol Over Nickel Catalysts Supported on Al2O3 Modified by Mg, Zr, Ce or La. *Topics in Catalysis* **2008,** *49* (1), 46.
64. Bastan, F.; Kazemeini, M.; Larimi, A. S., Aqueous-phase reforming of glycerol for production of alkanes over Ni/CexZr1-xO2 nano-catalyst: Effects of the support's composition. *Renewable Energy* **2017,** *108*, 417-424.
65. Stekrova, M.; Rinta-Paavola, A.; Karinen, R., Hydrogen production via aqueous-phase reforming of methanol over nickel modified Ce, Zr and La oxide supports. *Catalysis Today* **2018,** *304*, 143-152.
66. Rahman, M. M., Aqueous-Phase Reforming of Glycerol over Carbon-Nanotube-Supported Catalysts. *Catalysis Letters* **2020,** *150* (9), 2674-2687.
67. Park, Y. H.; Kim, J. Y.; Moon, D. J.; Park, N. C.; Kim, Y. C., Effect of LaAlO3-supported modified Ni-based catalysts on aqueous phase reforming of glycerol. *Research on Chemical Intermediates* **2015,** *41* (12), 9603-9614.
68. Coronado, I.; Stekrova, M.; García Moreno, L.; Reinikainen, M.; Simell, P.; Karinen, R.; Lehtonen, J., Aqueous-phase reforming of methanol over nickel-based catalysts for hydrogen production. *Biomass and Bioenergy* **2017,** *106*, 29-37.
69. Wu, K.; Dou, B.; Zhang, H.; Liu, D.; Chen, H.; Xu, Y., Aqueous phase reforming of biodiesel byproduct glycerol over mesoporous Ni-Cu/CeO2 for renewable hydrogen production. *Fuel* **2022,** *308*, 122014.
70. Guo, Y.; Azmat, M. U.; Liu, X.; Wang, Y.; Lu, G., Effect of support's basic properties on hydrogen production in aqueous-phase reforming of glycerol and correlation between WGS and APR. *Applied Energy* **2012,** *92*, 218-223.
71. He, L.; Huang, Y.; Wang, A.; Wang, X.; Chen, X.; Delgado, J. J.; Zhang, T., A Noble-Metal-Free Catalyst Derived from Ni-Al Hydrotalcite for Hydrogen Generation from N2H4.H2O Decomposition. *Angew. Chem., Int. Ed.* **2012,** *51*, 6191.
72. Pan, G.; Ni, Z.; Cao, F.; Li, X., Hydrogen production from aqueous-phase reforming of ethylene glycol over Ni/Sn/Al hydrotalcite derived catalysts. *Applied Clay Science* **2012,** *58*, 108-113.
73. Jirátová, K.; Čuba, P.; Kovanda, F.; Hilaire, L.; Pitchon, V., Preparation and characterisation of activated Ni (Mn)/Mg/Al hydrotalcites for combustion catalysis. *Catalysis Today* **2002,** *76* (1), 43-53.
74. Manfro, R. L.; Pires, T. P. M. D.; Ribeiro, N. F. P.; Souza, M. M. V. M., Aqueous-phase reforming of glycerol using Ni–Cu catalysts prepared from hydrotalcite-like precursors. *Catalysis Science & Technology* **2013,** *3* (5), 1278-1287.
75. de Souza, G.; Ruoso, C.; Marcilio, N. R.; Perez-Lopez, O. W., Dry Reforming of Methane over Mg-Co-Al Mixed-Oxides Catalysts: Effect of Mg Content and Reduction Conditions. *Chemical Engineering Communications* **2016,** *203* (6), 783-790.
76. Thao, N. T.; Trung, H. H., Selective oxidation of styrene over Mg–Co–Al hydrotalcite like-catalysts using air as oxidant. *Catalysis Communications* **2014,** *45*, 153-157.

77. Ohishi, Y.; Kawabata, T.; Shishido, T.; Takaki, K.; Zhang, Q.; Wang, Y.; Nomura, K.; Takehira, K., Mg–Fe–Al mixed oxides with mesoporous properties prepared from hydrotalcite as precursors: Catalytic behavior in ethylbenzene dehydrogenation. *Applied Catalysis A: General* **2005,** *288* (1), 220-231.
78. Zhang, J.-l.; Wang, X.; Ma, L.-p.; Yu, X.-f.; Ma, Q.-x.; Fan, S.-b.; Zhao, T.-s., Preparation of layered K/Mg-Fe-Al catalysts and its catalytic performances in CO hydrogenation. *Journal of Fuel Chemistry and Technology* **2017,** *45* (12), 1489-1498.
79. Polato, C. M. S.; Henriques, C. A.; Rodrigues, A. C. C.; Monteiro, J. L. F., De–SOx additives based on mixed oxides derived from Mg,Al-hydrotalcite-like compounds containing Fe, Cu, Co or Cr. *Catalysis Today* **2008,** *133-135*, 534-540.
80. Thao, N. T.; Kim Huyen, L. T., Enhanced catalytic performance of Cr-inserted hydrotalcites in the liquid oxidation of styrene. *Journal of Industrial and Engineering Chemistry* **2019,** *73*, 221-232.
81. Takehira, K., Recent development of layered double hydroxide-derived catalysts −Rehydration, reconstitution, and supporting, aiming at commercial application−. *Applied Clay Science* **2017,** *136*, 112-141.
82. Mokhtar, M.; Inayat, A.; Ofili, J.; Schwieger, W., Thermal decomposition, gas phase hydration and liquid phase reconstruction in the system Mg/Al hydrotalcite/mixed oxide: A comparative study. *Applied Clay Science* **2010,** *50* (2), 176-181.
83. Sato, T.; Wakabayashi, T.; Shimada, M., Adsorption of various anions by magnesium aluminum oxide of (Mg0.7Al0.3O1.15). *Industrial & Engineering Chemistry Product Research and Development* **1986,** *25* (1), 89-92.
84. Cavani, F.; Trifirò, F.; Vaccari, A., Hydrotalcite-type anionic clays: Preparatiòn, properties and applications. *Catal. Today* **1991,** *11* (2), 173-301.
85. Marchi, A. J.; Apesteguía, C. R., Impregnation-induced memory effect of thermally activated layered double hydroxides. *Applied Clay Science* **1998,** *13* (1), 35-48.
86. Rives, V.; Angeles Ulibarri, M. a., Layered double hydroxides (LDH) intercalated with metal coordination compounds and oxometalates. *Coordination Chemistry Reviews* **1999,** *181* (1), 61-120.
87. Allada, R. K.; Pless, J. D.; Nenoff, T. M.; Navrotsky, A., Thermochemistry of Hydrotalcite-like Phases Intercalated with CO32-, NO3-, Cl-, I-, and ReO4. *Chemistry of Materials* **2005,** *17* (9), 2455-2459.
88. Di Cosimo, J. I.; Díez, V. K.; Apesteguía, C. R., Synthesis of α,β-unsaturated ketones over thermally activated Mg–Al hydrotalcites. *Applied Clay Science* **1998,** *13* (5), 433-449.
89. Bastan, F.; Kazemeini, M., Renewable hydrogen production by aqueous-phase reforming of Glycerol using Ni/Al2O3-MgO nano-catalyst: effect of the Ni loading. *Biomass Conversion and Biorefinery* **2020**.
90. Boga, D. A.; Oord, R.; Beale, A. M.; Chung, Y.-M.; Bruijnincx, P. C. A.; Weckhuysen, B. M., Highly Selective Bimetallic Pt-Cu/Mg(Al)O Catalysts for the Aqueous-Phase Reforming of Glycerol. *ChemCatChem* **2013,** *5* (2), 529-537.
91. Li, X.; Zhang, J.; Xu, N.; Chen, G.; Yan, B., Aqueous-phase reforming of phenol over hydrotalcite-derived Ni/Zn/Al catalysts. *IET Renewable Power Generation* **2019,** *13* (10), 1641-1646.
92. Bastan, F.; Kazemeini, M.; Larimi, A.; Maleki, H., Production of renewable hydrogen through aqueous-phase reforming of glycerol over Ni/Al2O3MgO nano-catalyst. *International Journal of Hydrogen Energy* **2018,** *43* (2), 614-621.
93. Pipitone, G.; Zoppi, G.; Bocchini, S.; Rizzo, A. M.; Chiaramonti, D.; Pirone, R.; Bensaid, S., Aqueous phase reforming of the residual waters derived from lignin-rich hydrothermal liquefaction: investigation of representative organic compounds and actual biorefinery streams. *Catal. Today* **2020,** *345*, 237-250.
94. Zoppi, G.; Pipitone, G.; Galletti, C.; Rizzo, A. M.; Chiaramonti, D.; Pirone, R.; Bensaid, S., Aqueous phase reforming of lignin-rich hydrothermal liquefaction by-products: A study on catalyst deactivation. *Catalysis Today* **2021,** *365*, 206-213.

95. Yan, B.; Li, W.; Tao, J.; Xu, N.; Li, X.; Chen, G., Hydrogen production by aqueous phase reforming of phenol over Ni/ZSM-5 catalysts. *International Journal of Hydrogen Energy* **2017,** *42* (10), 6674-6682.
96. Li, X.; Yan, B.; Zhang, J.; Xu, N.; Tao, J.; Zhang, R.; Liu, B.; Sun, Z.; Chen, G., Hydrogen production by aqueous phase reforming of phenol derived from lignin pyrolysis over NiCe/ZSM-5 catalysts. *International Journal of Hydrogen Energy* **2018,** *43* (2), 649-658.
97. Putra, R. D. D.; Trajano, H. L.; Liu, S.; Lee, H.; Smith, K.; Kim, C. S., In-situ glycerol aqueous phase reforming and phenol hydrogenation over Raney Ni®. *Chemical Engineering Journal* **2018,** *350*, 181-191.
98. Xiang, Y.; Li, X.; Lu, C.; Ma, L.; Yuan, J.; Feng, F., Reaction Performance of Hydrogen from Aqueous-Phase Reforming of Methanol or Ethanol in Hydrogenation of Phenol. *Industrial & Engineering Chemistry Research* **2011,** *50* (6), 3139-3144.
99. Oliveira, A. S.; Baeza, J. A.; Saenz de Miera, B.; Calvo, L.; Rodriguez, J. J.; Gilarranz, M. A., Aqueous phase reforming coupled to catalytic wet air oxidation for the removal and valorisation of phenolic compounds in wastewater. *Journal of Environmental Management* **2020,** *274*, 111199.
100. Lok, M., Coprecipitation. In *Synthesis of Solid Catalysts*, 2009; pp 135-151.
101. Marceau, E.; Carrier, X.; Che, M., Impregnation and Drying. In *Synthesis of Solid Catalysts*, 2009; pp 59-82.
102. Introduction. In *Infrared Spectroscopy: Fundamentals and Applications*, 2004; pp 1-13.
103. Experimental Methods. In *Infrared Spectroscopy: Fundamentals and Applications*, 2004; pp 15-44.
104. Spectral Analysis. In *Infrared Spectroscopy: Fundamentals and Applications*, 2004; pp 45-70.
105. Llewellyn, P. L.; Bloch, E.; Bourrelly, S., Surface Area/Porosity, Adsorption, Diffusion. In *Characterization of Solid Materials and Heterogeneous Catalysts*, 2012; pp 853-879.
106. Thommes, M.; Kaneko, K.; Neimark, A. V.; Olivier, J. P.; Rodriguez-Reinoso, F.; Rouquerol, J.; Sing, K. S. W., Physisorption of gases, with special reference to the evaluation of surface area and pore size distribution (IUPAC Technical Report). *Pure and Applied Chemistry* **2015,** *87* (9-10), 1051-1069.
107. Catalyst Characterization. In *Concepts of Modern Catalysis and Kinetics*, 2003; pp 129-166.
108. Epp, J., 4 - X-ray diffraction (XRD) techniques for materials characterization. In *Materials Characterization Using Nondestructive Evaluation (NDE) Methods*, Hübschen, G.; Altpeter, I.; Tschuncky, R.; Herrmann, H.-G., Eds. Woodhead Publishing: 2016; pp 81-124.
109. Thompson, M.; Walsh, J. N., Introduction. In *Handbook of Inductively Coupled Plasma Spectrometry*, Thompson, M.; Walsh, J. N., Eds. Springer US: Boston, MA, 1989; pp 1-15.
110. Thompson, M.; Walsh, J. N., Instrumentation for ICP-AES. In *Handbook of Inductively Coupled Plasma Spectrometry*, Thompson, M.; Walsh, J. N., Eds. Springer US: Boston, MA, 1989; pp 43-92.
111. Pirola, C.; Galli, F.; Patience, G. S., Experimental methods in chemical engineering: Temperature programmed reduction—TPR. *The Canadian Journal of Chemical Engineering* **2018,** *96* (11), 2317-2320.
112. Ishii, T.; Kyotani, T., Chapter 14 - Temperature Programmed Desorption. In *Materials Science and Engineering of Carbon*, Inagaki, M.; Kang, F., Eds. Butterworth-Heinemann: 2016; pp 287-305.
113. Rajisha, K. R.; Deepa, B.; Pothan, L. A.; Thomas, S., 9 - Thermomechanical and spectroscopic characterization of natural fibre composites. In *Interface Engineering of Natural Fibre Composites for Maximum Performance*, Zafeiropoulos, N. E., Ed. Woodhead Publishing: 2011; pp 241-274.
114. Reactor Basics. In *Chemical Reactor Design and Control*, 2007; pp 1-30.
115. Worstell, J., Chapter 1 - Introduction. In *Batch and Semi-Batch Reactors*, Worstell, J., Ed. Butterworth-Heinemann: 2015; pp 1-6.
116. Robards, K.; Haddad, P. R.; Jackson, P. E., 1 - Introduction and Overview. In *Principles and Practice of Modern Chromatographic Methods*, Robards, K.; Haddad, P. R.; Jackson, P. E., Eds. Academic Press: Boston, 2004; pp 1-34.

117. Robards, K.; Haddad, P. R.; Jackson, P. E., 3 - Gas Chromatography. In *Principles and Practice of Modern Chromatographic Methods*, Robards, K.; Haddad, P. R.; Jackson, P. E., Eds. Academic Press: Boston, 2004; pp 75-177.
118. Robards, K.; Haddad, P. R.; Jackson, P. E., 5 - High-performance Liquid Chromatography—Instrumentation and Techniques. In *Principles and Practice of Modern Chromatographic Methods*, Robards, K.; Haddad, P. R.; Jackson, P. E., Eds. Academic Press: Boston, 2004; pp 227-303.
119. Seyed Dorraji, M. S.; Rasoulifard, M. H.; Daneshvar, H.; Vafa, A.; Amani-Ghadim, A. R., ZnS/ZnNiAl-LDH/GO nanocomposite as a visible-light photocatalyst: preparation, characterization and modeling. *Journal of Materials Science: Materials in Electronics* **2019,** *30* (13), 12152-12162.
120. Richardson, J. T.; Scates, R.; Twigg, M. V., X-ray diffraction study of nickel oxide reduction by hydrogen. *Applied Catalysis A: General* **2003,** *246* (1), 137-150.
121. Morales-Marín, A.; Ayastuy, J. L.; Iriarte-Velasco, U.; Gutiérrez-Ortiz, M. A., Biohydrogen production by glycerol Aqueous-Phase Reforming: Effect of promoters (Ce or Mg) in the NiAl2O4 spinel-derived catalysts. *Journal of Environmental Chemical Engineering* **2021,** *9* (6), 106433.
122. Daza, C. E.; Gallego, J.; Moreno, J. A.; Mondragón, F.; Moreno, S.; Molina, R., CO2 reforming of methane over Ni/Mg/Al/Ce mixed oxides. *Catalysis Today* **2008,** *133-135*, 357-366.
123. Sikander, U.; Sufian, S.; Salam, M. A., Synthesis and Structural Analysis of Double Layered Ni-Mg-Al Hydrotalcite Like Catalyst. *Procedia Engineering* **2016,** *148*, 261-267.
124. Daza, C. E.; Moreno, S.; Molina, R., Co-precipitated Ni–Mg–Al catalysts containing Ce for CO2 reforming of methane. *International Journal of Hydrogen Energy* **2011,** *36* (6), 3886-3894.
125. Morales-Marín, A.; Ayastuy, J. L.; Iriarte-Velasco, U.; Gutiérrez-Ortiz, M. A., Nickel aluminate spinel-derived catalysts for the aqueous phase reforming of glycerol: Effect of reduction temperature. *Applied Catalysis B: Environmental* **2019,** *244*, 931-945.

Appendix 1

This appendix shows graphs and equations of various calibration plots made and used during this project, and also explains the procedure used for calculating moles of different products.

Calibration plot for calculation of concentration of ethylene glycol

A calibration curve was made using 3 standard samples. Area ratio of ethylene glycol to internal calibrant was plotted against standard concentration (Figure 29). After a sample with ethylene glycol and internal standard (1,2 butadiene) was analysed by GC the area of the two peaks were integrated. Ratio of area of ethylene glycol to area of internal standard was calculated and using the equation in Figure 29 ethylene glycol wt.% was calculated. From ethylene glycol wt.%, mass of ethylene glycol is calculated using the weight of the total solution (50g). The obtained mass was divided with the molecular weight of ethylene glycol to calculate the moles of ethylene glycol. The procedure was repeated for both pre- and post-reaction samples. Finally, using Equation 11, conversion of ethylene glycol was calculated.

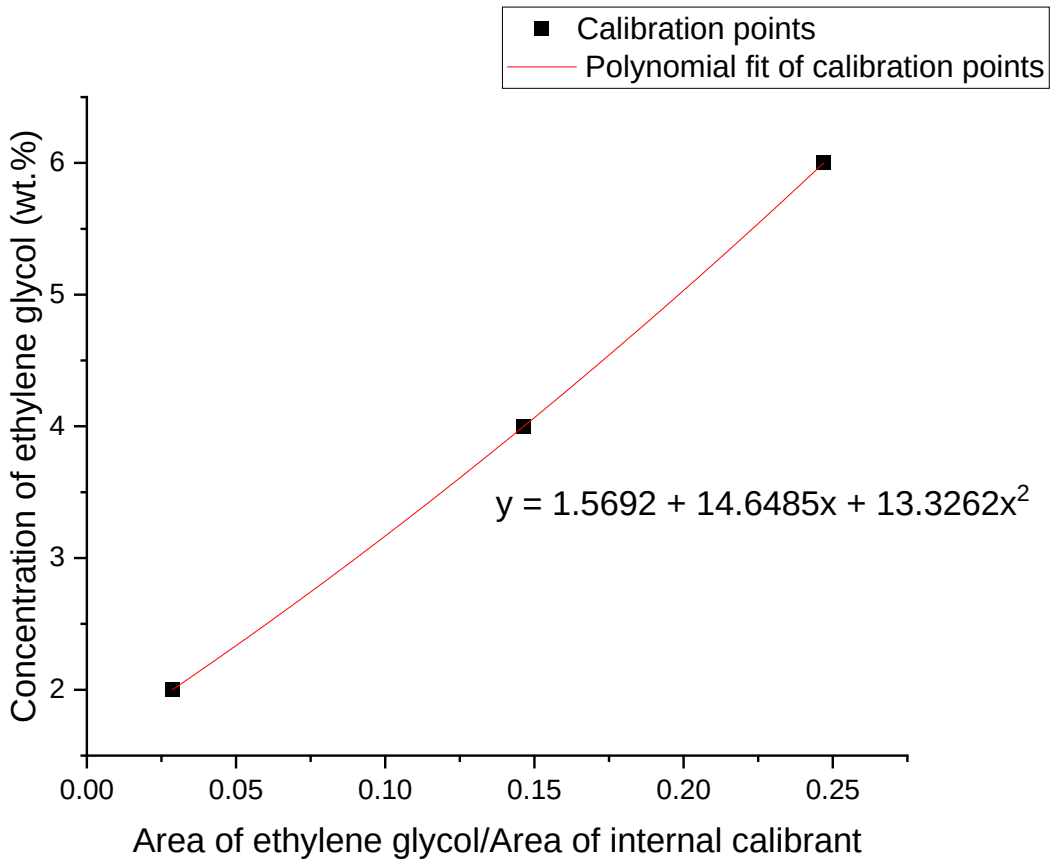

Figure 29: Calibration curve to determine the concentration of ethylene glycol. (The calibration points are an average of 3 different runs).

Calibration plot for determining the concentration of phenol

A calibration curve was made using 6 standard samples. Area ratio of phenol to internal calibrant was plotted against standard concentration (Figure 30). The peaks for phenol and internal calibrant (benzoic acid) in the chromatogram were integrated to obtain the area of the two peaks. The ratio of area of phenol to area of internal calibrant was calculated and using the equation in Figure 30 the concentration of phenol was calculated. This concentration was multiplied by 10 to obtain the real concentration (as the sample was diluted 10 times before running in HPLC). Moles of phenol was calculated using the molarity (moles = molarity × volume). The procedure was done for both pre- and post-reaction samples. Finally using Equation 13, conversion of phenol in aqueous phase reforming was calculated.

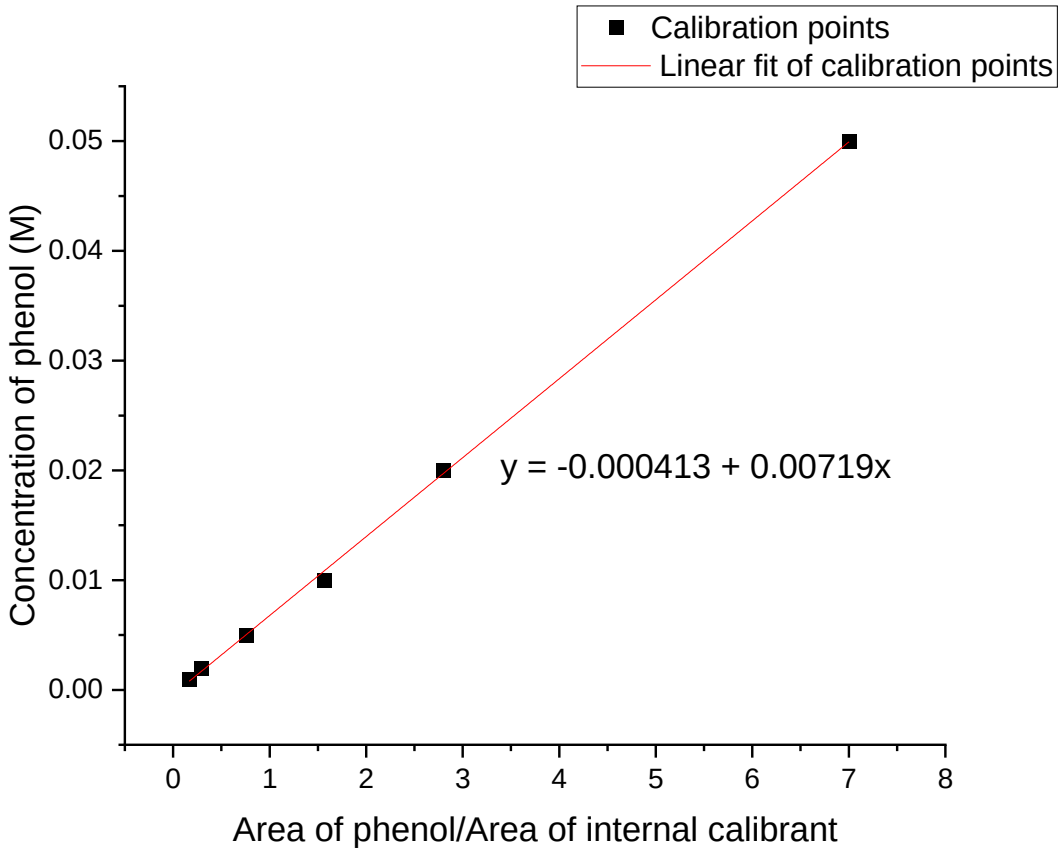

Figure 30: Calibration plot to determine the concentration of phenol. (Calibration points are an average of 3 runs).

Calibration plot for calculation of moles of hydrogen produced

A calibration curve was made using 5 standard samples. Area ratio of H_2 to Ar was plotted against H_2/Ar molar ratio (Figure 31). From the two different chromatograms, peaks for Ar and

H_2 were integrated separately to obtain their areas. Ratio of H_2 area to Ar area was calculated. Using the equation in Figure 31, H_2/Ar molar ratio was calculated. The moles of Ar was calculated using the ideal gas equation: PV=nRT, where P = 2 bar, V = 160 mL (dead volume of reactor (210 mL) – volume occupied by feed (50 mL)), n = moles of Ar, R is universal gas constant and T = room temperature (20 °C). Once the moles of Ar was obtained, the moles of hydrogen were calculated using the H_2/Ar molar ratio. Finally, Equation 12 and Equation 14 was used to calculate the selectivity towards hydrogen in aqueous phase reforming of ethylene glycol and phenol respectively.

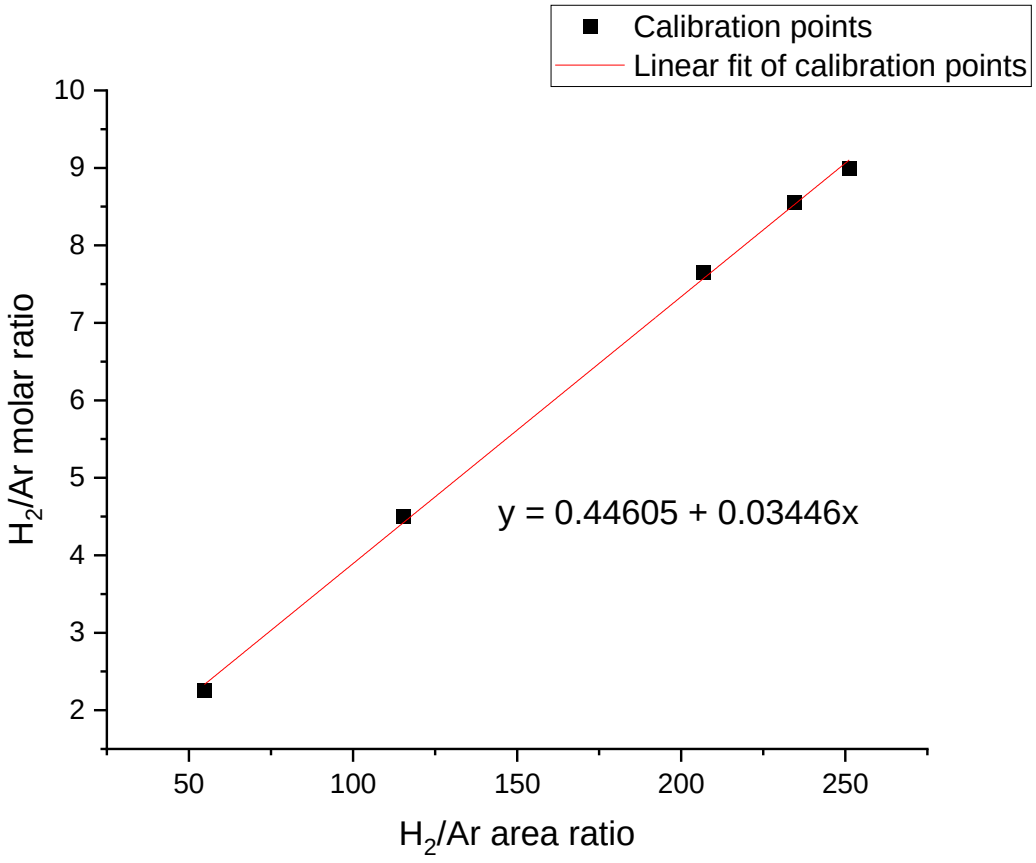

Figure 31: Calibration curve to determine the amount of hydrogen produced. (The calibration points were repeated twice, and an average was taken).

Appendix 2

This appendix shows BET curves and TPD curves of all the Ni hydrotalcite derived catalysts used in this project.

BET curves

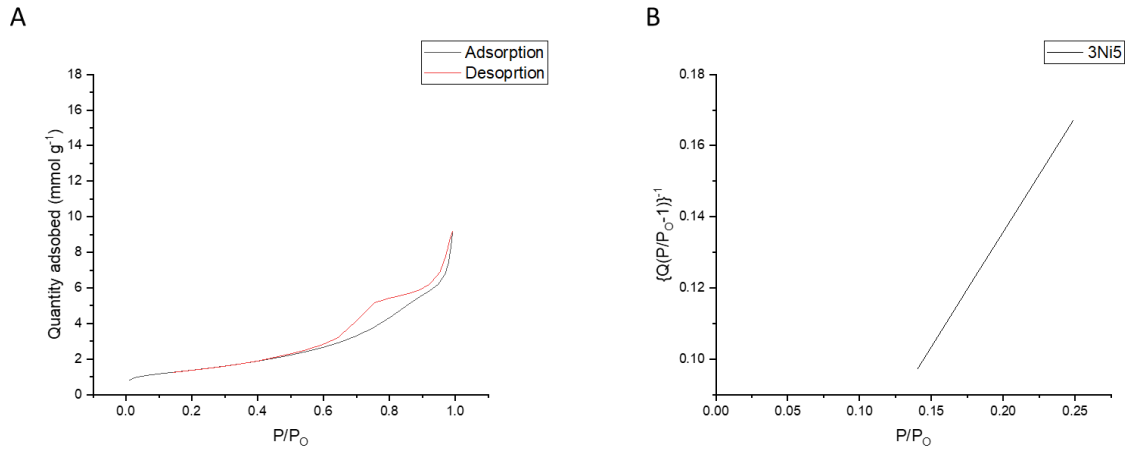

Figure 32: A) Adsorption/Desorption curves of reduced hydrotalcite derived catalysts. B) Plot of $\frac{1}{Q[(P_o/P)-1]}$ vs. $\left(P/P_o\right)$ for BET surface area. Sample: 3Ni5.

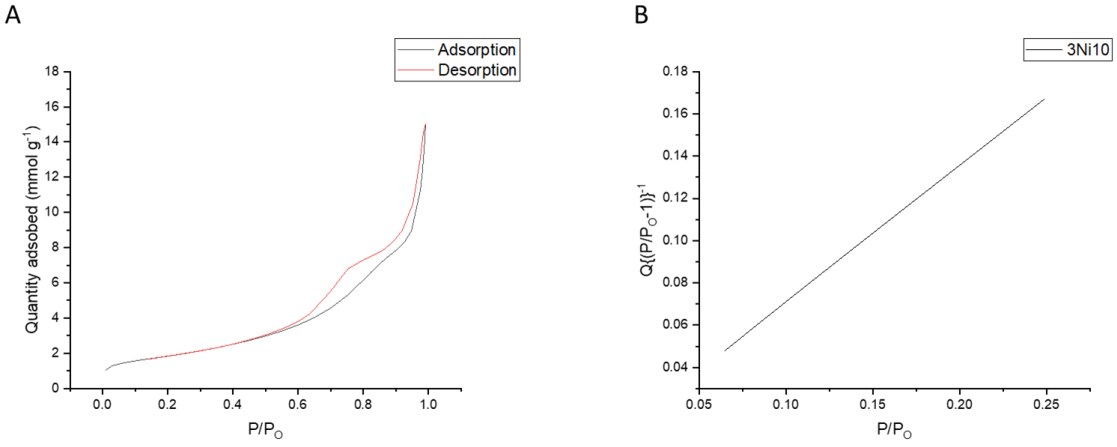

Figure 33: A) Adsorption/Desorption curves of reduced hydrotalcite derived catalysts. B) Plot of $\frac{1}{Q[(P_o/P)-1]}$ vs. $\left(P/P_o\right)$ for BET surface area. Sample: 3Ni10.

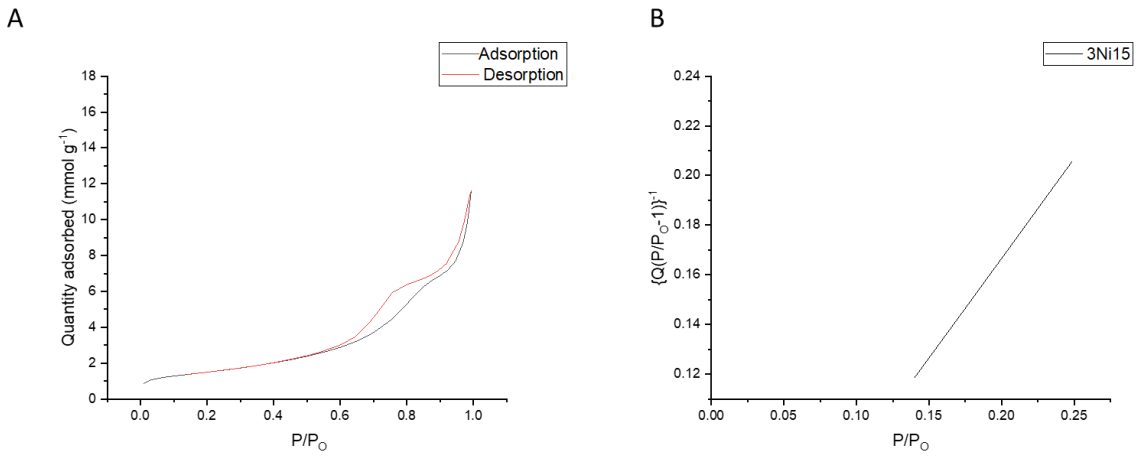

Figure 34: A) Adsorption/Desorption curves of reduced hydrotalcite derived catalysts. B) Plot of $\frac{1}{Q[\left({}^{P_o}/_{P}\right)-1]}$ vs. $\left({}^{P}/_{P_o}\right)$ for BET surface area. Sample: 3Ni15.

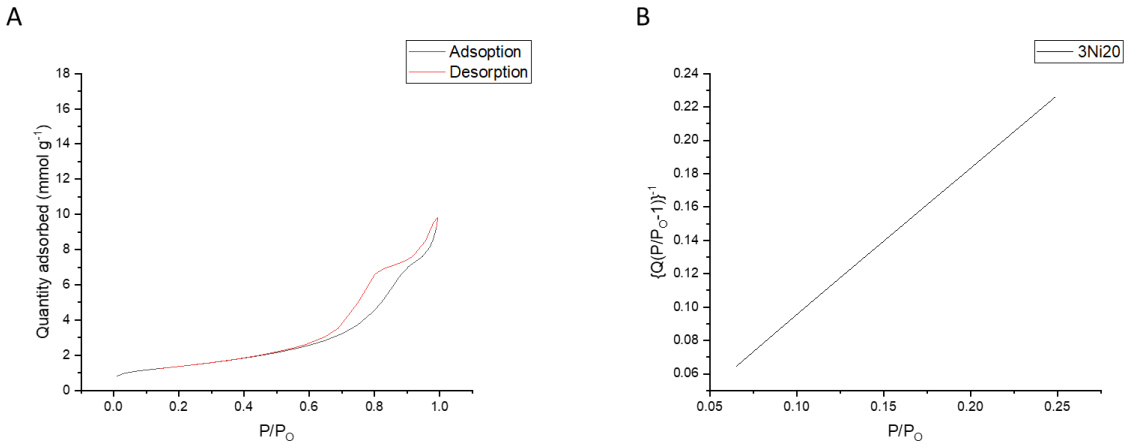

Figure 35: A) Adsorption/Desorption curves of reduced hydrotalcite derived catalysts. B) Plot of $\frac{1}{Q[\left({}^{P_o}/_{P}\right)-1]}$ vs. $\left({}^{P}/_{P_o}\right)$ for BET surface area. Sample: 3Ni20.

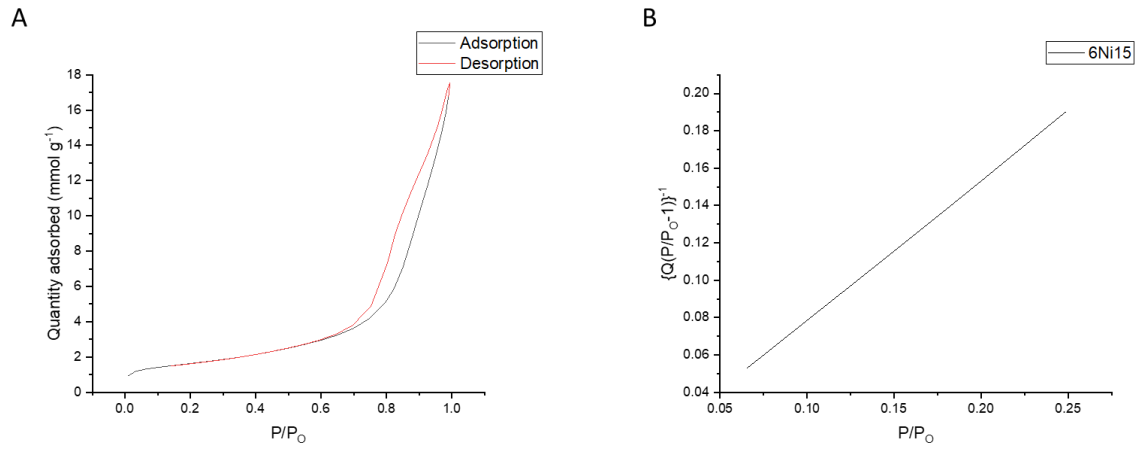

Figure 36: A) Adsorption/Desorption curves of reduced hydrotalcite derived catalysts. B) Plot of $\frac{1}{Q[(P_o/P)-1]}$ vs. $\left(P/P_o\right)$ for BET surface area. Sample: 6Ni15.

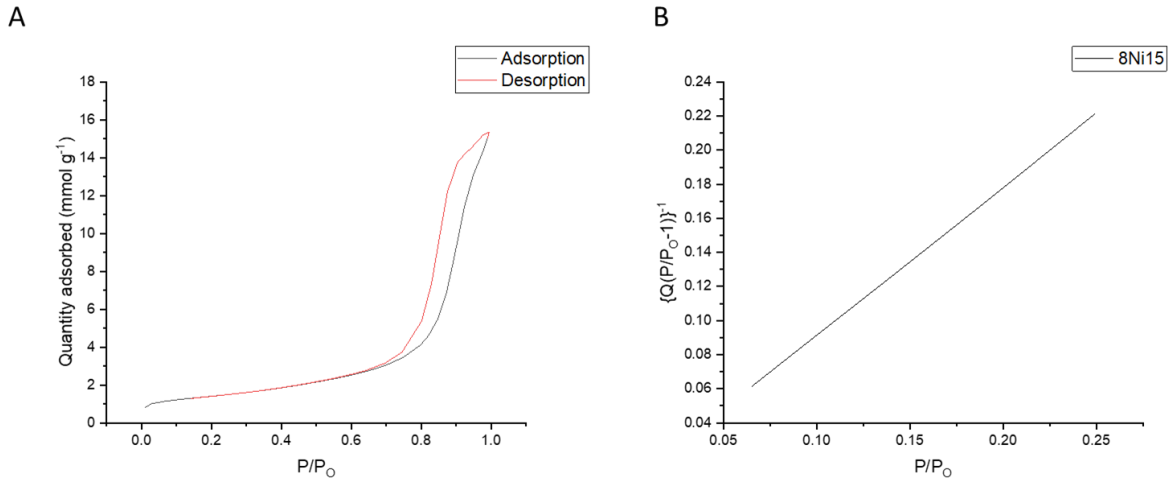

Figure 37: A) Adsorption/Desorption curves of reduced hydrotalcite derived catalysts. B) Plot of $\frac{1}{Q[(P_o/P)-1]}$ vs. $\left(P/P_o\right)$ for BET surface area. Sample: 8Ni5.

TPD Curves

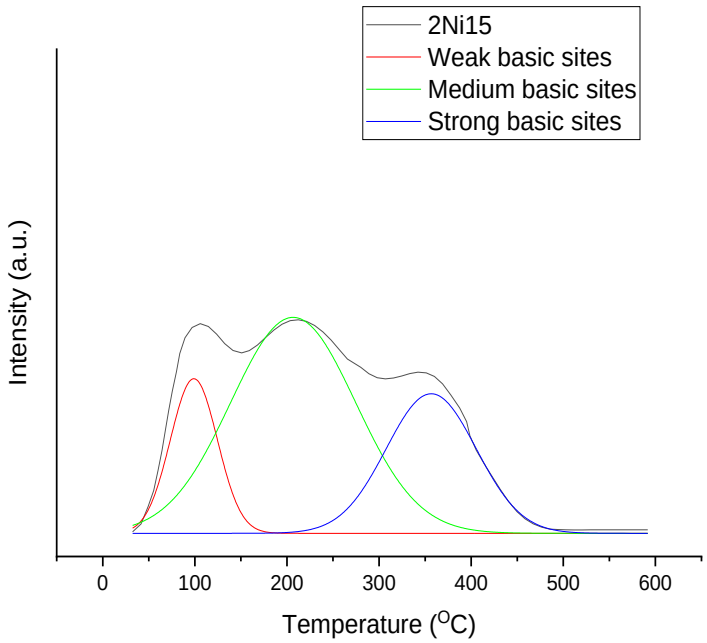

Figure 38: CO_2 TPD curves for 2Ni15 calcined hydrotalcite material (the curve is de-convoluted into 3 curves as described in the experimental section).

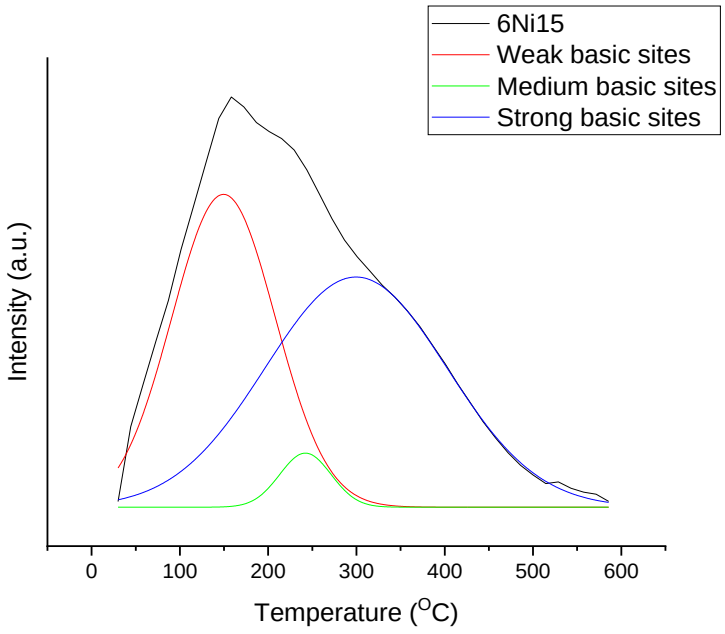

Figure 39: CO_2 TPD curves for 6Ni15 calcined hydrotalcite material (the curve is de-convoluted into 3 curves as described in the experimental section).

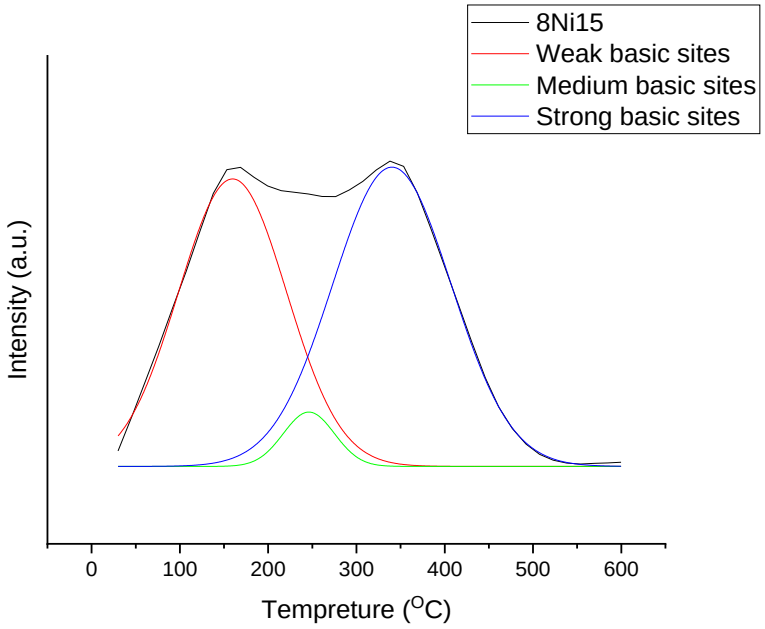

Figure 40: CO_2 TPD curves for 8Ni15calcined hydrotalcite material (the curve is de-convoluted into 3 curves as described in the experimental section).

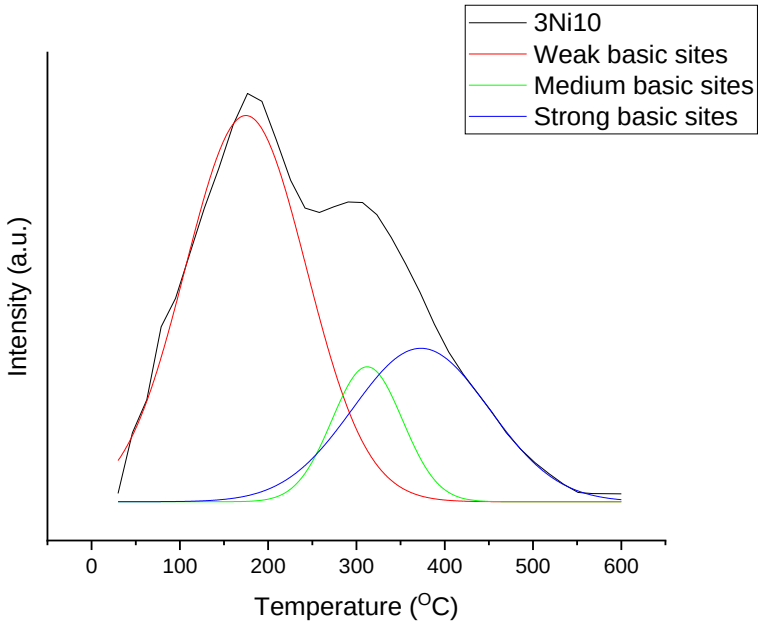

Figure 41: CO_2 TPD curves for 3Ni10 calcined hydrotalcite material (the curve is de-convoluted into 3 curves as described in the experimental section).

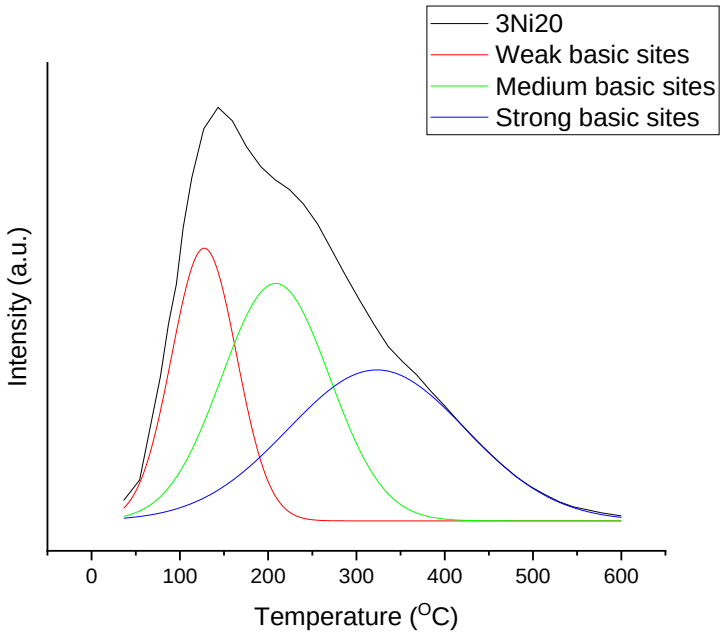

Figure 42: CO_2 TPD curves for 3Ni20 calcined hydrotalcite material (the curve is de-convoluted into 3 curves as described in the experimental section).